UNIVERSITAT DE BARCELONA

Delivery of SN-38 in pediatric solid tumors

Carles Monterrubio Martínez

UNIVERSITY OF BARCELONA

DELIVERY OF SN-38 IN PEDIATRIC SOLID TUMORS

Carles Monterrubio, 2016

UNIVERSITY OF BARCELONA
Pharmacy School
Research, Development and
Control of drugs doctorate program

DELIVERY OF SN-38 IN PEDIATRIC SOLID TUMORS

Report submitted by Carles Monterrubio Martinez to be eligible to the Doctor degree by the University of Barcelona

Director:
ÁNGEL MONTERO CARCABOSO

Ph.D. student:
CARLES MONTERRUBIO MARTINEZ

Tutor:
MARÍA LUISA GARCÍA LOPEZ

Carles Monterrubio, 2016.

One sometimes finds what
one is not looking for

Alexander Fleming

Acknowledgements

Working at the Developmental Tumor Biology Laboratory at Sant Joan de Deu Barcelona Hospital has been an honor and a privilege that I strongly thank to Angel Montero Carcaboso, my thesis director, who embraced me when I finished my graduate studies in Biology. He taught me new techniques, but he also taught me to be patient, to appreciate my own work and to be more confident and rely on the strength of my skills and results. I'm grateful to him for the chance he gave me to grow as a scientist, but also as a person. I want to thank also to all the lab mates from laboratory their support during this period.

I am also grateful to Alejandro Sosnik (and his family) for having hosted me at the Pharmaceutical Nanomaterials Laboratory at the Technion – Israel Institute of Technology. I thank him helping me in my last stage of the thesis and I would like him to know that I really appreciate his effort to make me feel valuable and comfortable in his laboratory. I want to thank also to Alex Buckchin and Inbar Schlachet for making me feel part of their group during my visit. We all shared both scientific and personal experiences that for sure we will remember.

I would like to thank also to Romina Glisoni her collaboration and support when I was learning from her at the University of Buenos Aires and also for showing me some hidden gems in the city of Buenos Aires.

Last but not least, I'm grateful with my family for encouraging me and I want to specially thank my wife her unconditional support for these more than four years of thesis that we both experienced together at the same time.

Thank you to you all that made possible such an important achievement.

Abbreviations

AUC	Area under the curve
CPT	Camptothecin
CPT-11	Irinotecan
CSC	Cancer stem cells
DDS	Drug delivery system
DIPG	Diffuse intrinsic pontine glioma
DLS	Dynamic Light Scattering
DMF	N,N-dimethylformamide
DMSO	dimethyl sulfoxide
ECF	Extracellular fluid
EDC	1-Ethyl-3-[3-dimethylaminopropyl]carbodiimide hydrochloride
EPR	Enhanced permeability and retention
ER	Enhanced recovery
ES	Ewing sarcoma
EtOAc	Ethyl acetate
f	Enhancement factor
FBS	Fetal Bovine Serum
FEP	Fluorinated ethylene propylene
FITC	fluorescein isothiocyanate
GPC	Gel permeation chromatography
HPBCD	2-hydroxypropyl-beta-cyclodextrin
HPLC	High performance liquid chromatography
HSDJ	Hospital Sant Joan de Deu
IF	Immunofluorescence
INSS	International Neuroblastoma Staging System
IRB	Biomedical Research Institute
IRN	Irinotecan
L.O.Q.	Limiot of quantification
MDR	Multidrug resistance
MES	2-(N-morpholino)ethanesulfonic acid
MSC	Mesenchymal stem cells
NB	Neuroblastoma

NHS	N-hydroxysulfosuccinimide
NIH	National Institutes of Health
NPs	Nanoparticles
NTA	Nanoparticle tracking analysis
o/w	Oil in water
PB	Protein binding
PBS	Phosphate buffered saline
PDI	Polydispersion index
PDX	Patient-derived xenograft
PEG	Polyethylene glycol
P-gp	P-glycoprotein
PK	Pharmacokinetic
PLA	Poly(lactic) acid
PLGA	Poly(lactic-co-glycolic) acid
PVA	Polyvinyl alcohol
QC	Quality control
RMS	Rhabdomyosarcoma
ROI	Region of interest
RR	Relative recovery
RT	Radiation therapy
s.c.	Subcutaneous
SD	Standard deviation
SEM	Scanning Electron Microscopy
SN-38	7-ethyl-10-hydroxycamptothecin
SN-38C	SN-38 Carboxylate
SN-38L	SN-38 Lactone
STD	Standard
TEA	Triethylamine
tECF	Tumor extracellular fluid
THF	Tetrahydrofuran
TPT	Topotecan
ZFR	Zero flow rate
ZNF	Zero net flux

Index

INTRODUCTION

1 Pediatric solid tumors

When talking about pediatrics, the range of age involved as “pediatric age” is not always clear. Biologically speaking, young adults may also present pediatric tumors and thus, be considered as pediatric cancer patients. It is increasingly accepted that pediatric cancer is a disease related to the phenomenon of development and growth [1], which involves many processes. From a single fertilized cell, there are roughly 2 x 10^{12} cells in the adult. Taking into account that in each cell division there is some chance of errors in nucleotide incorporation, that the average net mutation rate is 10^{-9} for single base changes per replicative cycle and that breaks in the double-stranded DNA occur spontaneously 50 times per cycle [2, 3], it seems that there are enough chances for a cell to undergo some mutations during the fetal development that could lead to developmental tumors.

1.1 Neuroblastoma

Neuroblastoma is the most common extracraneal solid tumor of the childhood. These tumors are a kind of developmental tumors because they are originated from undifferentiated cells of the neural crest during fetus development [4]. Due to its embryonic origin, neuroblastomas can be virtually found in any part of the sympathetic nervous system [4, 5], but the most common localization of the locoregional disease is on the adrenal gland (44%) (see Figure 1) [6].

The estimated incidence of this disease is about 1 in every 7000 alive newborns [5], which represents 50-70 new cases per year in Spain [7] and about 40% of the solid tumors in children above 4 years of age [8, 9] and the 15% of deaths by cancer in children under 15 years of age [5].

The clinical appearance is heterogeneous. Different locations, genetics and pathology change from one patient to another and the stage of the tumor and the age of the patient at diagnosis will dramatically change the prognoses of the disease. Classification of neuroblastoma tumors is made in stages according to the International Neuroblastoma Staging System (INSS)

[10]. The stratification of neuroblastoma stages by the COG group is represented in Table 1.

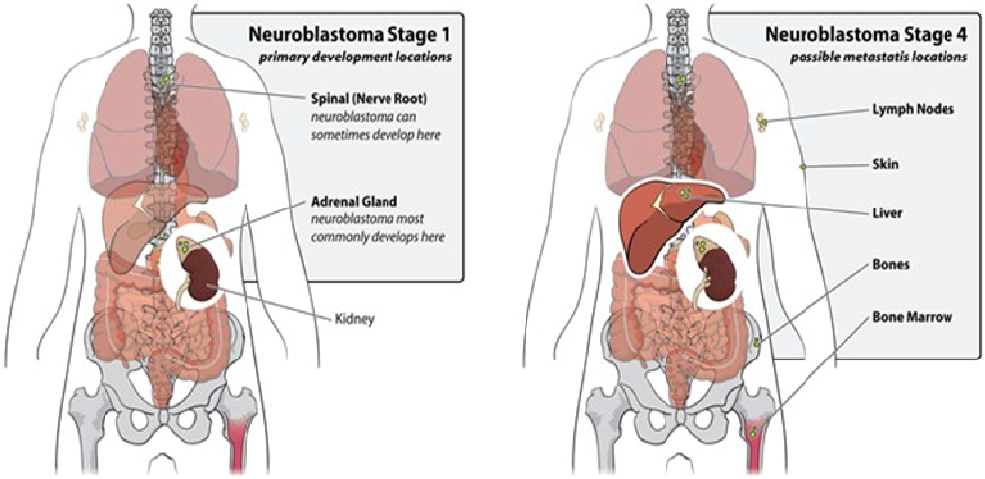

Figure 1. Most common localization of neuroblastoma in patients with stage 1 (left) and stage 4 (right) neuroblastoma. Primary stage 1 neuroblastomas are commonly found over the adrenal gland while stage 4 neuroblastomas can be virtually found anywhere in the sympathetic nervous system. Image from http://pedsurg.ucsf.edu

Locoregional or localized neuroblastoma usually requires only surgery and disseminated stage “4s” neuroblastomas (that appear only in newborns and infants until one year of age) are limited to skin, liver and bone marrow and regress spontaneously [11, 12]. Children under 18 months of age at diagnosis have better outcome than those diagnosed with neuroblastoma at a more advanced age. Some of these small children undergo spontaneous regression of their tumors. For stage 4 neuroblastoma, the most aggressive stage (with survival of around 30-40%), the best outcome is for those patients diagnosed before 18 months of age [13].

Children between 1.5-6 years of age at diagnosis still can still be cured with conventional treatments, but their probability of survival decreases when they are diagnosed with metastatic disease (stage 4 neuroblastoma). About 50% of the newly diagnosed patients already present metastasis to bone (60%), bone marrow (50%), lymph nodes (42%) and/or liver (15%) [10, 14, 15] and need intensive chemotherapy treatment, surgery and radiotherapy [13], but their survival remains poor and few advances have been made over the last decades. In contrast, patients diagnosed with locoregional tumors, or

those with stage 4s neuroblastoma without MYCN gene amplification (an indicator of poor prognoses) usually have good prognoses [16, 17]. MYCN gene is amplified in 25% of the patients [18, 19].

Table 1. Neuroblastoma stratification proposed by the Children's Oncology Group. Modified from Maris et al. 2007 [7].

Stage and definition		Age (d)	MYCN	Ploidy	Histology	Other	Risk group
1	Localized tumor with macroscopic total resection. Microscopically negative ipsilateral and contralateral lymph nodes						Low
2A	Localized tumor with incomplete resection. Microscopically negative ipsilateral and contralateral lymph nodes		Not amplified			>50% resection	Low
			Not amplified			<50% resection	Intermediate
2B	Localized tumor with or without complete resection. Microscopically positive ipsilateral lymph nodes and negative contralateral lymph nodes		Not amplified			Biopsy only	Intermediate
			Amplified				High
3	Unresectable localized unilateral tumor infiltrating across the midline; or localized tumor with involvement of the contralateral regional lymph node; or midline tumor with bilateral extension by infiltration or by lymph node involvement	<547	Not amplified				Intermediate
		≥547	Not amplified		Favorable		Intermediate
			Amplified				High
		≥547	Not amplified		Unfavorable		High
4	Primary tumor with dissemination to lymph nodes, bone, bone marrow, liver, skin, or other organs (except as defined by stage 4S)	<365	Amplified				High
		<365	Not amplified				Intermediate
		365-547	Amplified				High
		365-547		DI=1			High
		365-547			Unfavorable		High
		365-547	Not amplified	DI>1	Favorable		Intermediate
		≥547					High
4s	Localized primary tumor in patients up to 1 year of age with dissemination limited to skin, liver, or bone marrow (<10% malignant cells)	<365	Not amplified	DI>1	Favorable	No symptomatic	Low
		<365	Not amplified	DI=1			Intermediate
		<365	Missing	Missing	Missing		Intermediate
		<365	Not amplified			Symptomatic	Intermediate
		<365	Not amplified		Unfavorable		Intermediate
		<365	Amplified				High

1.1.1 Treatment of neuroblastoma

Conventional drug treatments for neuroblastoma need to be improved. Combinations of conventional drugs such as doxorubicin, cyclophosphamide, etoposide, cisplatin and vincristine are the most used for the induction phase of the treatment [20] and after progression or relapse the conventional treatment is usually carried out with combinations of irinotecan with temozolamide [21] or topotecan with cyclophosphamide [22-24]. Stage 4 neuroblastomas can initially respond to treatment but then they relapse and become resistant to the standard therapy. Then patients receive new treatments that, depending on the host clinical institution, involve retinoic acid for differentiation of tissues [25], anti-GD2 immunotherapy [26] or autologous bone marrow transplant [27].

The reason for the poor outcome of patients with stage 4 neuroblastoma, (as well for patients with other pediatric solid tumors such as high-risk Ewing sarcoma and rhabdomyosarcomas) is the development of resistance to conventional treatments, but the mechanisms of chemoresistance are poorly understood. Chemoresistance of neuroblastoma is usually attributed to biological reasons such as MYCN amplification [28], chromosomes 1p and 11q alterations [29], inactivation of the p53 pathway [30] or overexpression of multidrug resistance proteins [31]. It is not clearly understood if the insufficient drug distribution into the tumor tissue might lead to treatment failure and chemoresistance observed in tumors in late stages.

Despite the observed preclinical activity of novel candidates for the treatment of neuroblastoma such as anti-MDM2 [32], anti-TKR [33], anti-AKT [34] or anti-proteasome [35] their clinical efficacy has not been strongly proved yet [36, 37].

Most of the current research about chemoresistance in neuroblastoma is based on the study of overexpression of multidrug resistance proteins, p53 mutations or amplification of MYCN gene. Recently, molecular strategies have been also studied in neuroblastoma [18, 32, 35, 38-40]. By molecularly targeting drugs it is possible to specifically carry drugs to tumor tissues, increasing drug concentration at the required site of action while reducing

systemic toxicities responsible of very usual secondary malignances such as neutropenia or diarrhea. Increased activity of MDM2 [38] and the abnormal activity of the tyrosine kinase receptors RET (25) and ALK (24) are part of the most studied molecular pathways.

The inadequate penetration of drugs to the tumor tissue might play an important role on the acquired chemoresistance in neuroblastoma and other pediatric solid tumors [41] [42]. However, this field has not been thoroughly investigated yet. Thus, we propose the study of the tumor drug distribution to evaluate its role in resistance to chemotherapy.

1.2 Ewing sarcoma

Described first by James Stephen Ewing on 1921 [43], Ewing sarcoma (ES) tumor belongs to a bigger group of sarcomas that includes also extraosseous ES, peripheral primitive neuroectodermal tumor and Askin's tumor. ES can be a very aggressive kind of tumor and can be virtually found in any individual of any age but is most common in teenagers and young adults with a median age of presentation at 15 years and a slight tendency for presentation in male patients [44]. Moreover, 25% of the patients present metastatic disease at diagnosis [45].

ES belongs to the wide group of small round-cell tumors poorly differentiated, whose origin is not clear yet despite many different theories. However, it has been lately believed to have its origin on the mesenchymal stem cells (MSC) [46, 47].

The incidence of these tumors in the United States has been the same for over 3 decades [45]. From a total of 1631 diagnosed cases between 1973 and 2005 in US (about 45-50 cases a year in Spain), more than 75% were pediatric patients, i.e, infants, children, teenagers and young adults [48], and the 5-year survival is less than 30% for the metastatic disease (Source: St Jude Children's Hospital, Memphis, TN).

For the bone disease the primary tumor presentation is mostly in lower extremity (41%) and pelvis (26%) [49]. A representation of the most common localizations for ES is depicted in figure 2.

1.2.1 Treatment of Ewing sarcoma

Despite 70% of children with ES are cured thanks to the improvements in chemotherapy over the last 30 years [50], those patients with diagnosed ES aged above 15 years have a poor survival rate of about 50%, and those diagnosed with metastases have a mortality rate of about 70%.

Chemotherapy continues being the key in the standard of care of these patients together with a great importance of local control (surgery/radiotherapy) to secure more probabilities of curability [51, 52]. Current treatment from Euro Ewing 99 trial for non-metastatic ES includes combinations of vincristine, etoposide, doxorubicin and ifosfamide for 42 weeks and local control at week 15 [53]. Nevertheless, about 1 out of 4 patients already present metastasis at the moment of diagnosis. Table 2 shows the staging system for ES. Patients who respond to treatment undergo local control and consolidation phase with chemotherapy with combinations of different agents [54]. However, acute and long-term toxicities are also associated with the chemotherapeutic treatment while survival of patients with aggressive ES remains poor. Thus, new strategies are needed to overcome these limitations. Some chemotherapy trials for low- and high-risk ES are shown in Table 3.

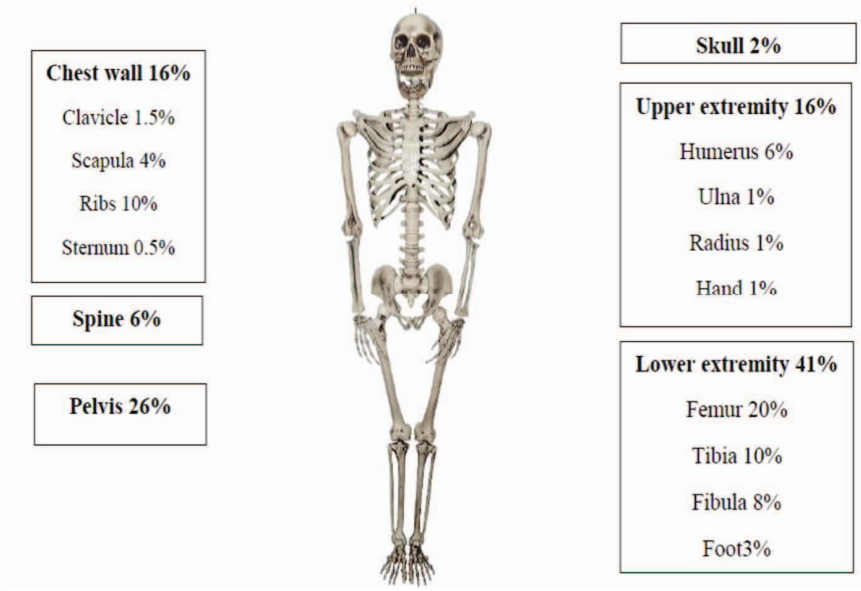

Figure 2. Most common distribution of Ewing sarcoma tumors. Extracted from the book of Valvi S & Kellie SJ [49].

Table 2. Staging system of the Ewing sarcoma. Adapted from the American Joint Committee on Cancer (AJCC).

Stage	Grade	Tumor size	Depth	Node	Metastasis	5 year survival
IA	Low grade	<8 cm	Any	None	None	98%
IB	Low grade	>8 cm			None	
IIA	High grade	<8 cm	Any	None	None	82%
IIB	High grade	>8 cm	Superficial	None	None	82%
III	Any	Discontinuous lesion	Deep	None	None	52%
IVA	Any	Any	Any	None	Lung	
IVB	Any	Any	Any	Present	Other than lung	30%

Table 3. Chemotherapy trials for standard risk and high risk ES. *%EFS or %OS at 5 year. Extracted from the book of Valvi S & Kellie SJ [49]. V = Vincristine; A = Actinomycin D; C = Cyclophosphamide; D = Doxorubicin; I = Ifosfamide; E = Etoposide.

Study	Duration	Randomization	Number of patients	Treatment	%EFS at 3 years	% OS at 3 years
EICESS-92 (79)	1992-1999	Yes	155	VAID	74	86
				VACD	73	90
EURO-EWING99-R1 (80)	2000-2010	Yes	856	VAI	78.2	85.5
				VAC	75.4	85.9
INT-0154/CCG7942/POG9354 (81)	1995-1998	Yes	478	VCD+IE Standard	72.1*	80.5*
				VCD+IE Intensified	70.1*	77*
AEWS0031/CCG7983 (82)	2001-2005	Yes	568	VCD+IE 3 weeks	65*	83*
				VCD+IE 2 weeks	73*	77*
EICESS-92 (79)	1992-1999	Yes	492	VAID	47	59
				EVAID	52	62
EWING99-R3 (24)	1999-2005	No	281	High dose therapy	27	34

1.3 Rhabdomyosarcoma

Rhabdomyosarcoma (RMS) is also a small round-cell childhood tumor. It is clinically presented with a wide variation of symptoms depending on the localization of the tumor, the presence or absence of metastases and the age of the patient.

With an incidence of 4 to 7 per million of children up to 15 years old, RMS is the third most common extracraneal childhood solid tumor after neuroblastoma and Wilm's tumor [55] and more than a half are diagnosed in children before 10 years of age with a slightly higher number of male patients [56, 57].

Common sites of primary presentation are head and neck, genitourinary tract and extremities (figure 3) [57]. While head and neck presentation is most commonly found in young children, RMS in adolescents is mostly present in extremities. Furthermore, the disease has been associated to familiar syndromes such as Li-Fraumeni or neurofibromatosis.

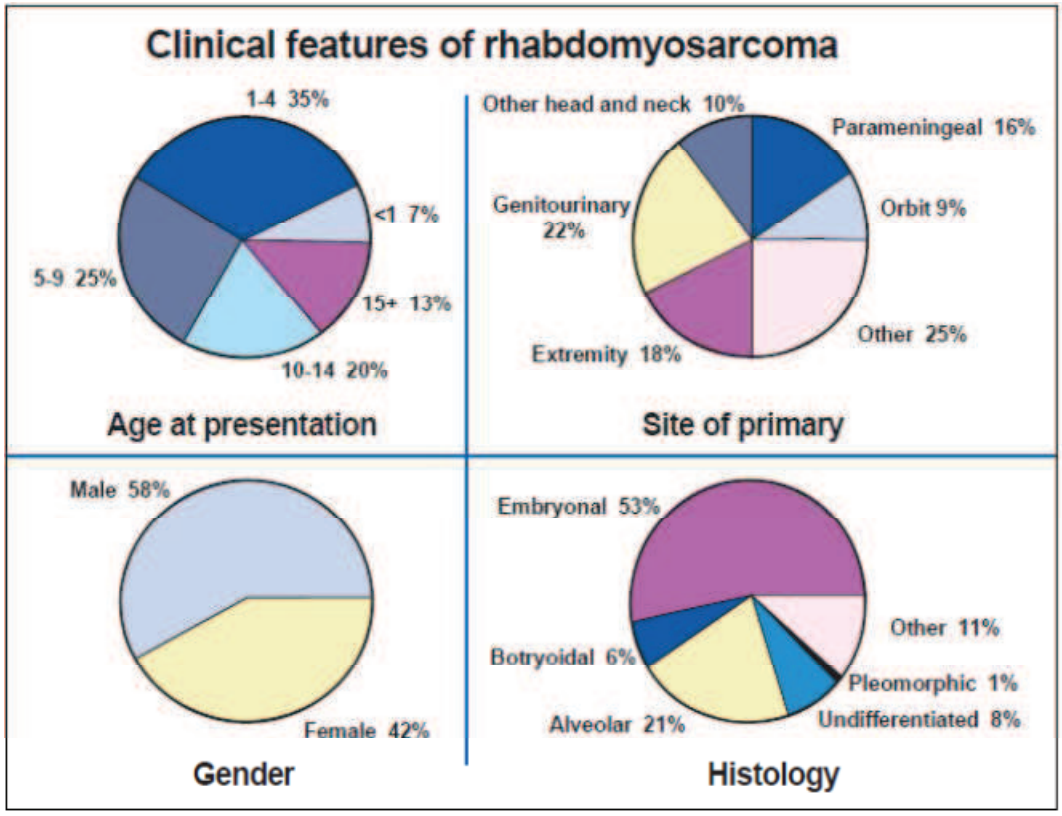

Figure 3. Clinical features of rhabdomyosarcoma tumors in children. From Dagher and Helman, The Oncologist. 1999.

1.3.1 Treatment of rhabdomyosarcoma

Current treatment of RMS recommends complete resection of the tumor whenever it is possible. Radiation plays an important role on fighting macro and microscopic residues after surgery but also on the treatment of those distant metastases localized in anatomic places of difficult resection. The use of radiation in certain areas of the body might be of concern because of the radiation doses might damage healthy tissues. On this line, in small RMS tumors located in areas such as head, vagina or prostate one of the best options for radiation delivery is the use of local implants to restrict delivery of radiation [58, 59]. Adjuvant and neoadjuvant chemotherapy is useful for the control of localized disease with or without micrometastatic disease. Common agents used in the treatment of childhood RMS include the same agents used for Ewing sarcoma (ifosfamide, etoposide, doxorubicin and vincristine) and also cyclophosphamide and actinomycin D. The standard of care at some institutions includes vincristine, actinomycin D and cyclophosphamide, which have resulted in good outcome for most patients with RMS.

Children diagnosed with localized disease present around 70% survival rates, but the 5-year survival rate is much lower (about 20-40%) for those with high-risk disseminated RMS (Source www.cancer.org). Thus, there is still much to do on the treatment of RMS to improve the survival rates of these patients.

Table 4. Rhabdomyosarcoma staging and risk. Adapted from Dagher and Helman, 1999 [57].

Stage	Localization	Size	Lymph node affectation	Metastasis
I	Localized or infiltrated	Any	Yes / No / Unknown	No distant metastasis
II	Localized or infiltrated	<5 cm	Unknown / not involved	No distant metastasis
III	Localized or infiltrated	<5 cm	Yes	No distant metastasis
		≥5 cm	Any	
IV	Localized or infiltrated	Any	Yes / No	Distant metastasis

2 Tumor drug chemoresistance

Tumors are not static systems since they can evolve towards more resistant phenotypes due to clonal evolution or acquisition of new mutations, becoming more aggressive.

There are two possible scenarios regarding tumor chemoresistance. There are tumors that respond upon first treatment and relapse is shown afterwards, and others are chemoresistant from diagnosis. Those tumors that undergo remission upon treatment and then relapse after some months, or even years, do not respond anymore to conventional treatment, thus new therapies are needed to overcome this situation.

Experimental studies about acquired tumor resistance to anticancer drugs after treatment are scarce. For instance, inhibition of tumor angiogenesis with anti-VEGFR2 therapy in a mouse model of pancreatic islet carcinogenesis led to marked activity against early-stage tumors, but late-stage tumors showed no response to the same treatment [60]. Tumors were able to escape from the effects of anti-VEGFR2 treatment by upregulation of other proangiogenic factors that are capable to stimulate again tumor angiogenesis independently from VEGF. Another example is provided by the acquired resistance to sunitinib in U87MG subcutaneous xenograft model, likely due to upregulation of BCRP expression in tumors that underwent treatment [61]. The authors of the study suggested that tumor resistance to chemotherapy may be due to low intracellular drug exposure caused by altered drug transport through the cellular membrane. Multidrug resistance (MDR) proteins like BCRP are known to be responsible of the active efflux of anticancer drugs from tumor cells [62]. In pediatric oncology the expression of MDR proteins have been widely studied, and the family of ATP-binding cassette (ABC) transporters is well studied [31, 63-68]. ABC transporters pump drugs outside the cell decreasing their intracellular concentration. Two MDR-associated proteins that are well known are permeability-glycoprotein 1 (P-gp) and MDR-associated protein 1 (MRP1). High-level of MRP1 expression has been associated with poor prognosis in primary neuroblastoma [31] and soft tissue sarcomas [69]. P-gp expression has been also correlated with poor prognosis in high-grade soft tissue sarcomas [67]

and the co-expression of MRP1 and MDR3 has been also shown in these kind of tumors [70]. Citti *et al*. demonstrated that the expression of MDR proteins was either induced or increased after chemotherapy [70]. However, it is still unclear if the increase in the expression of MDR proteins is mainly due to a clonal selection of tumor cells (Figure 4) expressing MDR proteins, upregulation of MDR proteins or both. Nevertheless what seems to be clear is that MDR proteins have an important role in tumor acquired chemoresistance.

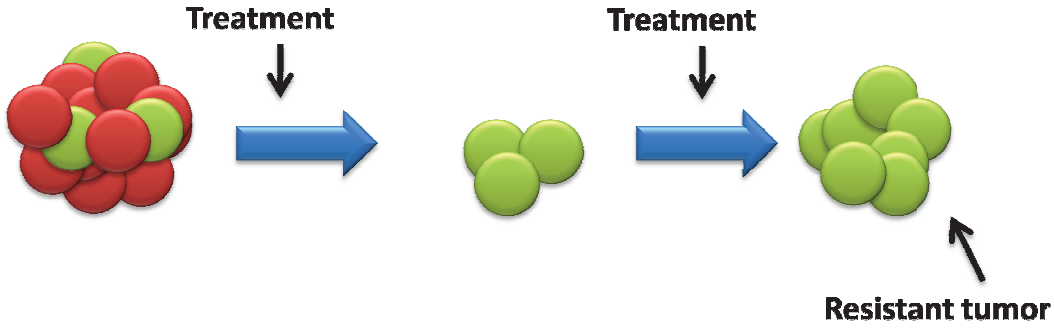

Figure 4. Tumor acquired resistance model by clonal selection of resistant cells upon treatment.

3 The patient-derived model for the study of drug resistance and delivery in oncology

Preclinical models used for pharmacological studies must represent faithfully the disease in the patients. Preestablished tumor cells lines are widely used for pharmacological studies [32, 33, 35, 71]. However, despite they can provide some powerful information and fast drug screening, long term culture selects for cells that show genetic changes as compared to the primary tumor [72, 73]. Some studies suggest that cells that have been grown *in vitro* have adapted to growth in conditions that differ from the natural tumor microenvironment [74]. It seems that gene expression can change *in vitro* and that this differential expression is not restored when growing again these cell lines *in vivo* [74]. Moreover, preestablished tumor cell lines demonstrated poor prediction of clinical efficacy of anticancer agents [75]. Preclinical studies have been performed using animal models for years to test novel anticancer drugs as well as to evaluate response and resistance proteins in preclinical research demonstrating to be a useful and reliable platform [76, 77].

Since the preclinical model must be representative of the clinical tumor, patient-derived xenograft (PDX) models have recently become the preferred option to reproduce the genetics and the structural microenvironment properties of the tumor in humans. It is widely accepted that transplanting a fresh fragment of a primary human tumor to immunodeficient mice keeps similarities with the genetics and genomics, histology, protein expression and tumor biomarkers of the original tumor even after several generations of the xenograft [74, 78-81]. Neale et al. showed how main genes kept their expression in xenografts established from fresh fragments of primary pediatric solid tumors subcutaneously implanted [82].

The establishment of tumor xenografts requires fresh tumor tissue from a biopsy (or a tumor resection) from a patient, followed by subcutaneous or orthotopic implantation of such human tissue into the flank of immunodeficient rodents [77, 83, 84]. Not all the tumors will engraft in a mouse model. In our experience, only about 30% of the transplanted tumors

grow in immunodeficient mice. Moreover, the amount of time that tumors need to grow is variable between different tumor models and also depends on the viability of the fresh tumor tissue directly obtained from the patient. Some tumors that may not grow in some immunodeficient mouse strains like athymic nude (which do not have T lymphocytes), and might be able to grow in nod-scid mice because they lack of T cells, B cells and their innate immunity is also diminished [85].

Since PDX models have been already applied to drug development studies in oncology [76, 86, 87], thus we proposed the use of PDX models obtained from fresh tumor biopsies from pediatric patients from Sant Joan de Deu Barcelona Hospital (Esplugues de Llobregat, Barcelona, Spain) for our drug delivery and efficacy studies. Figure 5 depicts the use of PDX models in oncology preclinical research.

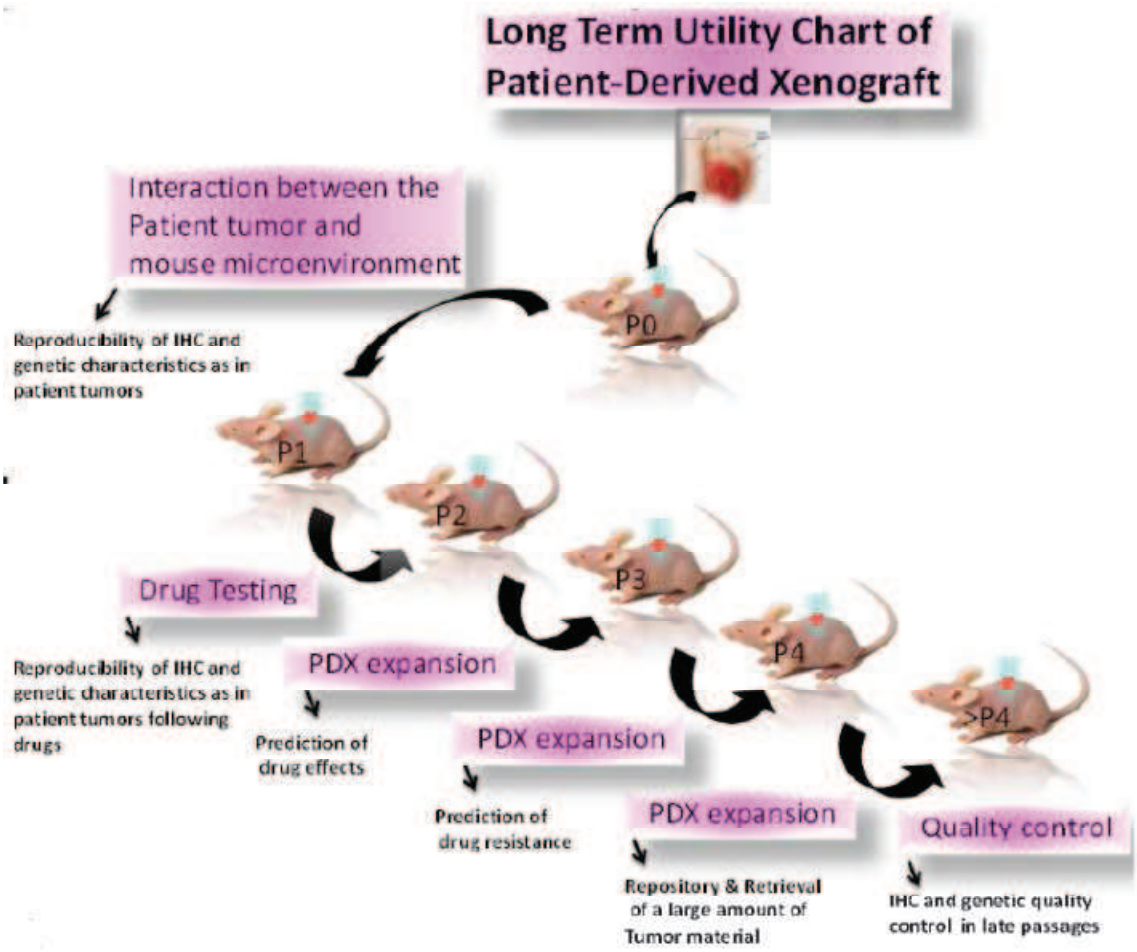

Figure 5. Usefulness of PDX models in oncology. The model reproduces with fidelity the original tumor in the patient through successive passages in contrast with what is observed in cell cultures. Those models serve as a platform to the study of drug interactions and effects. Figure extracted bfrom Dey *et al*. [88].

4 Camptothecins as model anticancer drugs

Camptothecins (CPT) are a family of topoisomerase-I inhibitor molecules. Its name comes from the Chinese bush named *Camptotheca acuminata*, the plant from which the classic CPT was obtained from the first time on 1966 [89]. However it wasn't until 1985 [90] that the activity against topoisomerase-I was known. The mechanism of action of CPT is by binding to topoisomerase-I forming a complex that impedes DNA replication. This CPT – Topoisomerase-I – DNA complex leads to single strand breaks that can be repaired when the CPT is removed [91]. However, when the replication fork meets the complex it leads to double-strand breaks that are not reparable and accumulate in the cell. If CPT are not removed from the cell, double-strand breaks accumulate leading to cell death [92].

Originally CPT was first administered as a soluble sodium salt but only 11.5% was present as lactone (less soluble) form *in vivo* [93]. The poor solubility of the CPT is due to the nitrogen atom in the quinoleine subunit which causes basicity of the molecule, and this hydrophobicity is much higher for the lactone form, but CPT lactone is also 10-fold more active than the carboxylate (soluble) counterpart [94]. This poor solubility was the reason why the first clinical trials were done using the carboxylate form, but poor activity with high toxicity was observed [93, 95]. The chemical structure of the classic CPT includes 5 rings with a quinoleine subunit fused to an α-hidroxy-δ-lactone terminal ring with a chiral center in carbon C-20 (see Figure 6). CPTs are presented in two alternative chemical forms in pH-dependent reversible equilibrium, lactone and carboxylate, being the first one the most active against tumor cells. The proportion of one or another counterpart depends on the pH, thus, the lactone form can be hydrolyzed spontaneously to carboxylate when the molecule is in basic or neutral (physiologic) pH, while in acid pH the lactone counterpart is predominant [96]. Moreover, protein binding affects to the proportion of both counterparts as well [97] and this proportion can be different from proteins of different species as the affinity protein-CPT can be modified [98]. It is currently possible to determine the concentration of carboxylate and lactone separately in a given sample, though HPLC [99-101].

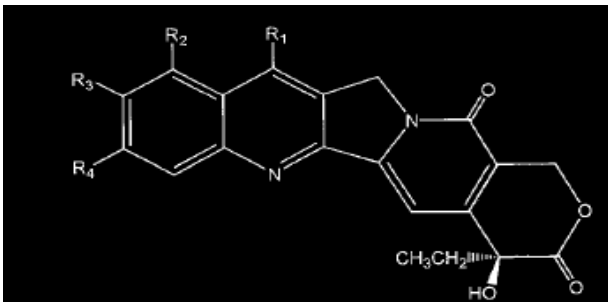

Figure 6. Chemical structure of a camptothecin. Modified from García-Carbonero [92].

Modifications on carbons C-9 and C-10 of the A aromatic ring of the quinoleine subunit have incremented the power of the CPT by improving its solubility with the aim of obtaining CPT derivates such as topotecan (TPT), with a basic group N-N-dimethylaminomethyl on C-9 (Figure 7), or irinotecan (IRN or CPT-11), with a dibasic bispiperidine on C-10 (Figure 8), both FDA-approved for chemotherapeutic use in cancer treatment [102]. Comercial TPT has to be formulated with dextrose [103] or tartaric acid [104] otherwise it would rapidly turn to its carboxylate form upon resuspension with saline solution before administration. Upon administration of TPT, its main clearance pathway is through its conversion to the carboxylate form, followed by renal excretion.

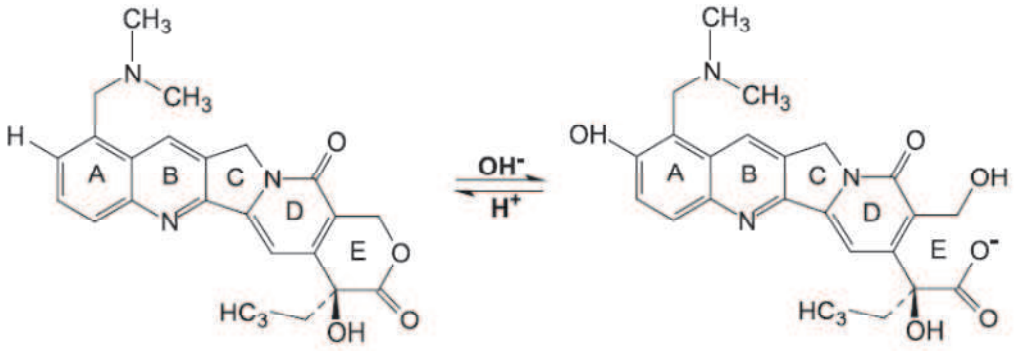

Figure 7. Chemical structure of topotecan. Lactone (active) and carboxylate forms at left and right, respectively. Extracted from Abraham [105].

IRN is the soluble prodrug of the active metabolite 7-ethyl-10-hydroxycamptothecin (SN-38) which is highly hydrophobic (insoluble in water) but very active, especially the lactone form (SN-38L), while the carboxylate form (SN-38C) presents high aqueous solubility. The bispiperidine group on the IRN molecule is cleaved by enzymatic excision

because of the carboxylesterases [106] and the final molecule is the active SN-38, which is 1000-fold more active than IRN. The process is briefly depicted in Figure 8. Although only about 4% of the administered IRN is converted to SN-38 in humans [107], the half-life of the lactone form (SN-38L) is above 11 hours, much higher than the one of the TPT. The reason for this seems to be the high affinity between SN-38 or IRN lactones and albumin. Such protein binding increases the half-life of drugs in the organism.

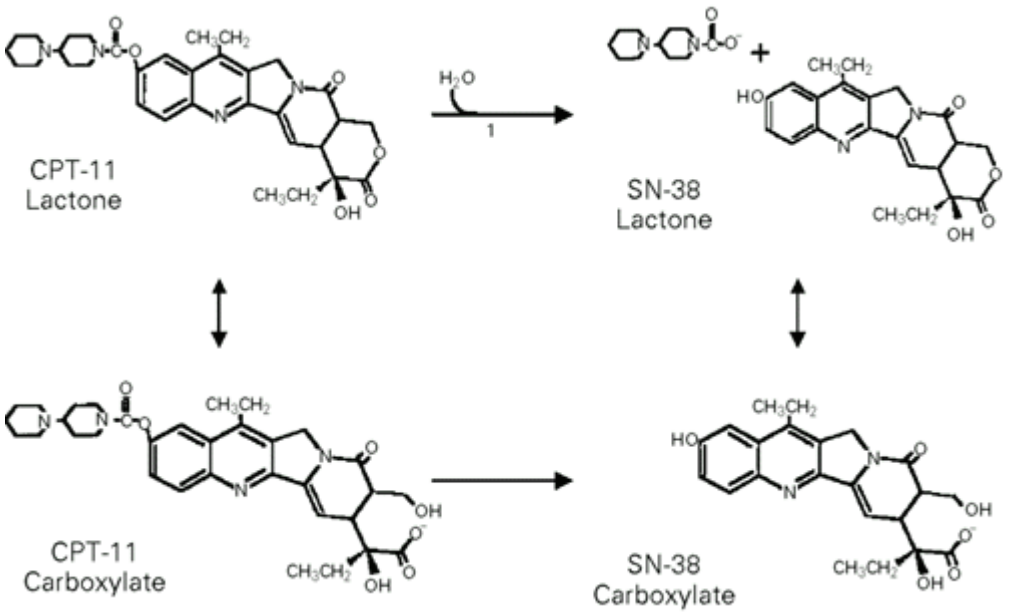

Figure 8. Metabolic conversion from irinotecan (left side) to SN-38 (right side) by carboxylesterases. Under acid pH conditions lactone forms are predominant (above) while carboxylate forms are predominant under neutral or basic pH (below). From Grivicich [108].

Although in preclinical assays SN-38 is highly active against solid tumors [109], it cannot be directly administered because of its poor solubility. Moreover, due to the poor conversion rate from IRN to SN-38 the distribution of SN-38 in the tumor stroma might be hindered [110]. Furthermore, IRN can be highly toxic at the concentration that it might be required to achieve activity, causing severe diarrhea [111].

While TPT has shown remarkable activity both in preclinical [112] studies as well as in patients [113] the high activity observed for IRN in preclinical models in resistant neuroblastomas [114, 115] has not been reproduced in refractory patients [21]. This lack of clinical activity could be correlated with higher activity of the carboxylesterases in murine models, with the

subsequent conversion from IRN to SN-38 in mice, up to 70%, as compared to 4-10% in humans [116].

Currently there are many research projects ongoing to develop new nanoparticulate formulations of SN-38 that have shown to be more active against several solid tumors [116-119] with less toxicity on the intestinal mucosa [120, 121]. Such new formulations allow the direct administration of SN-38 and overcome the problem of the poor conversion rate from IRN. Thus, we believe that using new drug delivery systems (DDS) for SN-38 delivery will be a good alternative for the treatment of chemoresistant aggressive pediatric solid tumors.

5 Drug distribution in solid tumors

5.1 Determination of compartmental drug distribution *in vivo*

The relationship between tissue drug concentration and efficacy of anticancer drugs has been shown in several studies [112, 122, 123]. Assays with animals, rats and mice mostly, have been useful to demonstrate the feasibility of microdialysis techniques for the measurement of the active metabolites of chemotherapeutic drugs into tumor tissue to characterize their pharmacodynamic (PD) and PK profiles not only in the tumor microenvironment but also in other parts of the organism distant from tumor.

Microdialysis is a minimally invasive technique [124-126] that allows continuous sampling of analytes from tissue interstitial fluids *in vivo*, and it may be used for sampling both exogenous and endogenous small molecules. The *in vivo* microdialysis technique consists on the insertion of a dialysis probe into a target tissue to sample the extracellular fluid, as depicted in figure 9 [127-129]. This technique allows continuous sampling in awake animals for PK and PD studies *in vivo* without the need of sacrificing large series of animals [130, 131]. Furthermore, improved restraining methods allow free-mobility of individuals used in the studies [127, 132-135].

Microdialysis was originally developed to measure concentrations of endogenous compounds in the extracellular fluid (ECF) as neurotransmitters [136-139]. This technique is based on the free diffusion of the analytes through a semi-permeable membrane due to a concentration gradient between the ECF and the perfusion fluid flowing inside the probe lumen [140, 141], thus enabling to assess the concentration of analytes in the ECF *in vivo.* Since the perfusate is being continuously pumped through the inlet tubing of the probe to the outlet tubing, and finally driven out of the probe, the complete equilibrium of concentrations between both sides of the membrane is never reached [142]. This is the principle of the microdialysis. This continuous traffic of analytes through the membrane is known as relative recovery (RR) and it is used, together with a calibration method, to know the real concentration of an analyte in a target tissue.

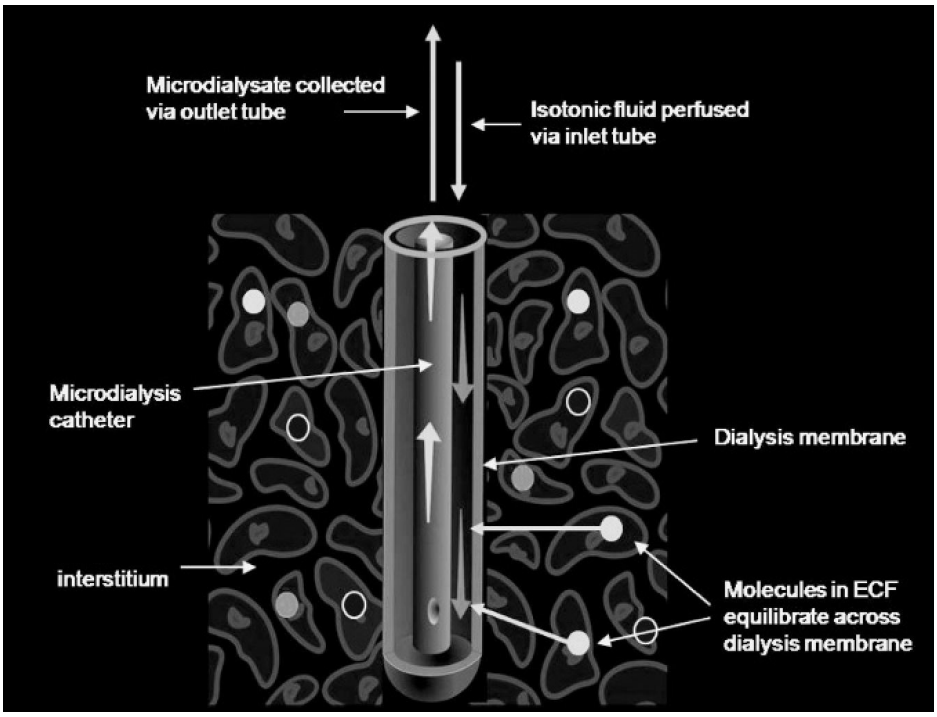

Figure 9. Example of extracellular fluid sampling by inserting a microdialysis probe in a tissue. ECF means 'extracellular fluid'. Adapted from Tisdall and Smith [143].

Under identical experimental conditions results for recovery and delivery experiments (when the traced analyte is within the perfusate) should be the same, but several factors may affect the RR of the probe including perfusate flow rate and composition [144-146], microdialysis device characteristics as membrane length or diameter cut-off, tube material and diameter, which could non-specifically interact with dialyzed compounds, analytes physicochemical properties such as solubility, temperature, tissue properties such as ECF pressure or metabolic processes, and the interaction between the analyte of interest and the tissue to be sampled [147-150]. Diverse *in vivo* calibration methods have been used to assess RR. Among those established methods the easiest and the most commonly used is retrodialysis [151]. There are also other calibration methods such as the zero net flux (ZNF) and the zero flow rate (ZFR) that might be more suitable in specific conditions, specifically when sampling hydrophobic compounds using solubilizer agents in the perfusion fluid, as we will detail in Chapter 1 of this thesis.

Lipophilic compounds generally result in low and usually non-reproducible RR due to non-specific binding to the microdialysis device. Several different approaches have been reported for enhancing microdialysis

RR for lipophilic compounds [141, 144, 152-156] adding different compounds such as polysorbate [157] or cyclodextrins [141, 152, 155, 158] to the perfusate in order to solubilize these drugs and to avoid the non-specific binding to the microdialysis system. In the same way, the addition of dextran has been reported to enhance the RR of large molecules [159-161]. Loos *et al*. showed how docetaxel, an anti-mitotic chemotherapeutic drug, was non-specifically bound to the microdialysis device in *in vitro* experiments [157]. Polysorbate 80 added to the perfusate overcame the problem to some (limited) extent but they could not obtain reproducible results and ruled out docetaxel for further microdialysis studies. Whitaker *et al*. encountered the same problem sampling doxorubicin (see figure 10), a compound used in chemotherapy because it inhibits replication of cells by stabilizing the topoisomerase-II [162]. These two studies are examples of possible troubles when trying to microdialyze lipophilic compounds. One commonly proposed solution is the use of mathematical models to correct the results [146] but the validation of results is difficult since many variables that could affect the RR must be considered.

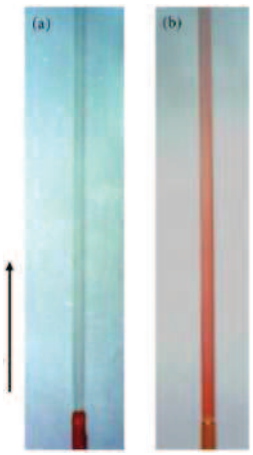

Figure 10. Images of probe membranes perfused with (a) Ringer's solution (control) and (b) antipyrine and doxorubicin (10 μM each). Arrow indicates flow direction. Doxorubicin shows strong adhesion (red staining) to the internal surface. Image adapted from Whitaker *et al.* [162]

When combined with tumor homogenates and blood samples, microdialysis is a useful technique to accurately determine the compartmental (vascular, extra- and intracellular) drug distribution in a specific tissue, which is of high importance to know whether the drug reaches the desired target at relevant active concentrations or not [127, 163]. The relationship between tissue drug disposition and treatment efficacy has been

explored by inserting microdialysis probes in some solid tumors to sample chemotherapeutic drugs such as cisplatin [164] and topotecan [165]. Microenvironment of a tumor tissue is significantly different from that in healthy tissue. Many factors such as heterogeneous tumor blood flow, abnormal vascular permeability, and cell density, as well as increased interstitial pressure, may impede penetration and delivery of drugs from blood into the tumor and disturb drug distribution within the tumor. Furthermore, the study of tumor homogenates provides information regarding total concentration of drug in the tumor bulk, both intra- and extracellular, as well as in the vascular compartment. The use of microdialysis allows to fully determine the penetration and distribution of drugs used in anticancer treatments and to know whether the lack of penetration and/or distribution could be a reason of treatment failure.

Microdialysis probes have been inserted in many types of tumors in order to understand the PD and PK not only into the tumor tissue but also in peripheral tissues, even at the same time using dual- or multi-probe systems, in order to observe the differences between the composition of the tumor ECF and the ECF in other parts of the body in the same individual at the same time. Sziraki *et al.* performed dual- and triple-probe microdialysis assays to determine drug-drug interactions with Pg-p in mice [166]. The authors employed quinidine and PSC-833 as P-gp substrate and inhibitor, respectively, to determine interactions with P-gp at the blood-brain barrier and the vascular compartment. A dose-dependent relation was seen in the penetration of quinidine into the brain. It was demonstrated that dual-probe microdialysis approach is an effective tool to design PK and PD studies *in vivo* in two different places simultaneously in the same organism [166].

In this thesis work, microdialysis has been used together with tumor homogenates to determine the compartmental distribution of the chemotherapeutic drug SN-38 in PDX models of neuroblastoma, Ewing sarcoma and rhabdomyosarcoma when given as either its prodrug formulation irinotecan (Chapter 2). Additionally, microdialysis was also useful to characterize newly developed polymeric DDS *in vivo* (Chapters 3 and 4).

5.2 Improving drug distribution within pediatric solid tumors

Pediatric solid tumors are treated by combined therapies that include radiation, surgery and chemotherapy based on the type, stage and localization of the tumor, but these approaches are not enough to eradicate all kind of tumors, because some of them have a high recurrence rate and develop resistance against chemotherapeutic drugs used as the standard of care. Thus, alternative drug treatments are needed for these patients. However, many of the new chemotherapeutic drugs have short half-live in the organism and others are too hydrophobic to be suitable for systemic administration *in vivo* despite their remarkable *in vitro* activity. Others are excessively toxic at the systemic concentrations needed to exert a therapeutic effect. New DDS, many of them based on biocompatible polymeric devices or liposomal formulations are being developed in order to overcome these limitations. Body fluids can penetrate through the pores on the surface of polymeric DDS with the subsequent gradual diffusion of the hydrophobic drugs entrapped inside these structures [167]. Furthermore, biocompatible polymer degradation may also release the drug that is still entrapped in the system.

New strategies to improve drug delivery in pediatric solid tumors could take advantage of unique features such as gene translocations like EWS/FLI1 in most Ewing sarcomas [168], highly expressed membrane gangliosides like GD2 in most neuroblastomas [169], and homogeneous mutations like K27M in H3 histones that is common to more than 80% of diffuse intrinsic pontine gliomas (DIPG) [170]. Those are homogenous targets found in most tumors of each type and could be used as special targets for drug delivery.

SN-38 and its water-soluble prodrug IRN are good models for the study of the limited drug distribution in chemoresistant pediatric solid tumors and to determine whether new drug formulations improve intratumoral drug distribution. As mentioned before, with around 1000-fold more activity than IRN [171], the high hydrophobicity of SN-38 precludes its systemic administration. To overcome this limitation IRN was developed but the high activity observed against neuroblastoma in preclinical murine models was not

reproduced in patients, probably due to the reduced activity of the human carboxylesterases, as compared to the mouse enzymes.

Encapsulation of SN-38 into polymeric NPs could overcome the limitation of the conversion rate from IRN by directly administering the active metabolite SN-38. One of such formulations of polymeric NPs could include surface modifications, such as polyethylene glycol (PEG), which allows increasing the half-life of the NPs in the organism before clearance [172-175]. Other surface modifications could address to targeted therapy by attaching antibodies against antigens overexpressed in some tissues, reducing systemic exposure and increasing local efficacy [176].

The enhanced permeability and retention (EPR) effect based on the vascular abnormality of the tumor tissue allows NPs to be retained for a longer period of time in the tumor microenvironment with a local-based effect [177-180]. A relevant nanodrug that has proved activity against pediatric tumors like Ewing sarcoma is nab-paclitaxel (Abraxane), which has been already approved by the FDA for adult refractory breast cancer [181], gastric cancer [182] and metastatic pancreatic cancer [183] and has been studied in rhabdomyosarcoma, osteosarcoma and neuroblastoma [184]. Some preclinical studies with nab-paclitaxel in pediatric tumors showed high activity against Ewing sarcoma, rhabdomyosarcoma, osteosarcoma and several pediatric tumor cell lines [184-186]. Clinical trials in pediatric patients with recurrent or refractory solid tumors [187] and malignant germ cells [188] are still ongoing and no results are published yet. A new preclinical study evaluated its activity against several pediatric solid tumors [185]. Abraxane was well tolerated and showed significant increase in event free survival as compared to control treatment. In Ewing sarcoma models, 5 out of 8 underwent complete responses as well as 6 out of 8 rhabdomyosarcomas, but response was not observed neither in neuroblastoma nor in osteosarcoma xenografts. Doxorubicin has been also highly studied in clinical trials. A nanodrug with proven activity is the PEGylated liposomal formulation of doxorubicin, known as Doxil, which has been already demonstrated active in adult cancer and it has been approved for its use by the FDA [189]. Munoz *et al*. determined the efficacy of the formulation in children with advanced sarcoma and they observed that patients who

previously underwent treatment with free doxorubicin experienced tumor response to the liposomal formulation [190], which is in contradiction with other previous results [191]. Upon its proven efficacy, some groups have investigated combinations of the liposomal formulation with other agents.

The use of polymeric nanofiber matrices as a platform for local release with increased local activity and minimum systemic effect has gained interest lately as well [192]. Body fluids can penetrate into the nanofiber matrices structure due to their high porosity and wide surface leading to diffusion of the entrapped drug. Chemotherapeutic agents have already been loaded into the polymer matrix of these structures [193-195]. Paclitaxel-loaded films have been tested against Lewis Lung Carcinoma cell line showing an increased survival of those mice treated with this new DDS compared with the administration of systemic or local free paclitaxel in a formulation of cremophor/ethanol [196]. The same group also tested paclitaxel-loaded films against CS-1 human chondrosarcoma, a model of locoregional recurrent sarcoma, showing promising results again [197]. Other drugs more similar to SN-38 have been also loaded into polymeric films showing promising antitumor activity. Hydroxycamptothecin is an analogue of the CPT that has been loaded into polymer films for the *in vivo* assessment of the antitumor efficacy over the Lewis Lung Carcinoma cell line [198]. This DDS showed a controlled release of the drug that lasted over a month leading to a significant tumor growth delay as compared to treatment with free systemic hydroxycamptothecin. Because of its high versatility, reproducibility and easy manipulation, polymeric nanofibers are being considered one of the best platforms for the local administration of chemotherapeutic drugs [199].

OBJECTIVES

Objectives

Successful drug distribution in solid tumors is essential for an efficient treatment since all tumor cells must be exposed to relevant cytotoxic concentration of the anticancer drug. However, drug penetration might be impeded in chemoresistant solid tumors [165]. Inadequate distribution of chemotherapeutic drugs into the solid tumor tissue could be related to treatment failure, but the mechanisms that limit drug distribution in solid tumors are not completely understood [41]. Drug penetration to the cancer cells might be impeded by several microenvironmental factors, like the abnormal phenotype of the tumor vasculature, which leads to areas of hypoxia, high interstitial pressure in the tissue, or vasculature leaks limiting drug delivery to these areas [200, 201]. We believe that a better understanding of the *in vivo* drug distribution in pediatric solid tumors might help us predict whether drugs that are active in *in vitro* models will have a clinical activity, and to propose new pharmaceutical strategies to improve drug distribution in solid tumors.

We used SN-38, the active metabolite of IRN, as a model drug because of its remarkable activity against different cell lines and PDX models generated from tumor biopsies or resections from patients at our institution. We took advantage of the low solubility of SN-38 to load it in different DDS that would release the drug in the targeted tissues. One of such DDS consisted in a local nanofiber matrix for local SN-38 release in the surgical bed after tumor resection surgery. The second DDS was a GD2-targeted nanoparticle formulation for neuroblastoma treatment.

Our overall hypothesis was that systemic drug delivery is limited in chemoresistant pediatric solid tumors and that in such cases, drug delivery could be improved by the mentioned pharmacological approaches. We used immunodeficient mice to establish PDX models in which we performed all the *in vivo* experiments to:

1. Develop a microdialysis method for continuous sampling of SN-38 from the tumor extracellular fluid *in vivo*. The developed methodology had to

be carefully validated as it was the basic technique for all the studies of SN-38 distribution included in this work.

2. Study the distribution of the highly active SN-38 within the tumor bulk of patient-derived xenografts of highly aggressive pediatric solid tumors generated from paired biopsies of pediatric solid tumor patients obtained at different stages during treatment. This work would allow us to determine whether tumor evolution –due to treatment pressure- towards a more chemoresistant phenotype leads to limited intratumor drug distribution.

3. Develop and characterize new nanofiber matrices loaded with SN-38, for local control of pediatric solid tumors after subtotal resection surgery. This work would include a precise characterization of local SN-38 distribution in the surgical bed and in pediatric solid tumors, in order to select the candidate patients that would benefit from this new delivery system.

4. To develop and characterize SN-38-loaded, GD2-targeted systemic NPs for the treatment of neuroblastoma. To achieve this goal, we evaluated the long term SN-38 distribution and efficacy achieved by the GD2-targeted nanoparticles in the tumor tissue, as compared to control (non-targeted) formulations or to the prodrug (IRN).

RESULTS

Chapter 1:

Combined Microdialysis-Tumor Homogenate Method for the Study of the Steady State Compartmental Distribution of a Hydrophobic Anticancer Drug in Patient-Derived Xenografts

Here we developed and validated a microdialysis method useful to sample, detect and quantify SN-38, a potent topoisomerase-I inhibitor, from dialysates and to determine the unbound SN-38 volume of distribution (i.e., the volume of drug in the intracellular compartment) in the PDX models when combined with terminal tumor homogenates and blood samples. The microdialysis technique described on the following published work was essential for all the other works developed in this thesis, as it will be explained on the upcoming chapters. This is the first time that it is possible to study the compartmental SN-38 distribution in PDX models in alive animals being able to distinguish between the two counterparts of the SN-38 molecule, the active and highly hydrophobic lactone and the carboxylate.

Pharm Res (2015) 32:2889–2900
DOI 10.1007/s11095-015-1671-9

RESEARCH PAPER

Combined Microdialysis-Tumor Homogenate Method for the Study of the Steady State Compartmental Distribution of a Hydrophobic Anticancer Drug in Patient-Derived Xenografts

Carles Monterrubio • Sonia Paco • Monica Vila-Ubach • Eva Rodríguez • Romina Glisoni • Cinzia Lavarino • Paula Schaiquevich • Alejandro Sosnik • Jaume Mora • Angel M. Carcaboso

Received: 22 December 2014 / Accepted: 6 March 2015 / Published online: 14 March 2015

ABSTRACT

Purpose To develop a reproducible microdialysis-tumor homogenate method for the study of the intratumor distribution of a highly hydrophobic anticancer drug (SN-38; 7-ethyl-10-hydroxycamptothecin) in neuroblastoma patient-derived xenografts.

Methods We studied the nonspecific binding of SN-38 to the microdialysis tubing in the presence of 2-hydroxypropyl-beta-cyclodextrin (HPBCD) in the perfusate. We calibrated the microdialysis probes by the zero flow rate (ZFR) method and calculated the enhancement factor (*f* = extrapolated SN-38 concentration at the ZFR / SN-38 concentration in the dialysed solution) of HPBCD. We characterized the extravasation of HPBCD to tumors engrafted in mice. *In vivo* microdialysis and terminal homogenate data at the steady state (subcutaneous pump infusions) were used to calculate the volume of distribution of unbound SN-38 ($V_{u,tumor}$) in neuroblastoma.

Results HPBCD (10%*w/v*) in the perfusate prevented the nonspecific binding of SN-38 to the microdialysis probe and enhanced SN-38 recovery (*f* = 1.86). The extravasation of HPBCD in the tumor during microdialysis was lower than 1%. $V_{u,tumor}$ values were above 3 mL/g tumor for both neuroblastoma models and suggested efficient cellular penetration of SN-38.

Conclusions The method contributes to overcome the limitations of the microdialysis technique in hydrophobic drugs and provides a powerful tool to characterize compartmental anticancer drug distribution in xenografts.

KEY WORDS drug distribution · drug penetration · hydrophobic anticancer drugs · microdialysis · neuroblastoma · patient-derived xenograft (PDX) · SN-38 · solid tumor · steady state · tumor homogenate · tumor microenvironment

ABBREVIATIONS

ECF	Extracellular fluid
ER	Enhanced recovery
f	Enhancement factor
FEP	Fluorinated ethylene propylene
HPBCD	2-hydroxypropyl-beta-cyclodextrin
PDX	Patient-derived xenograft
RR	Relative recovery
SN-38 C	SN-38 Carboxylate
SN-38 L	SN-38 Lactone
tECF	Tumor extracellular fluid
ZFR	Zero flow rate

Electronic supplementary material The online version of this article (doi:10.1007/s11095-015-1671-9) contains supplementary material, which is available to authorized users.

C. Monterrubio • S. Paco • M. Vila-Ubach • E. Rodríguez • C. Lavarino • J. Mora • A. M. Carcaboso
Department of Pediatric Hematology and Oncology,
Hospital Sant Joan de Déu Barcelona,
Esplugues de Llobregat, Spain

C. Monterrubio • S. Paco • M. Vila-Ubach • E. Rodríguez • C. Lavarino • J. Mora • A. M. Carcaboso (✉)
Preclinical Therapeutics and Drug Delivery Research Program,
Developmental Tumor Biology Laboratory,
Fundació Sant Joan de Déu, Santa Rosa, 39-57,
Esplugues de Llobregat, Barcelona, Spain
e-mail: amontero@fsjd.org

R. Glisoni
CONICET-Department of Pharmaceutical Technology, Faculty of Pharmacy and Biochemistry, Universidad de Buenos Aires, Buenos Aires, Argentina

P. Schaiquevich
CONICET-Clinical Pharmacokinetics Unit, Hospital de Pediatria JP Garrahan, Buenos Aires, Argentina

A. Sosnik
Department of Materials Science and Engineering, Technion-Israel Institute of Technology, Haifa, Israel

INTRODUCTION

Many potentially active anticancer agents are poorly distributed in tumors or display excessive systemic toxicity at concentrations required to achieve their pharmacological effect at the tumor cell level (1, 2). Thus, optimization of chemotherapeutic drug delivery to the solid tumor microenvironment has become one of the most studied fields in cancer research (3). Drug penetration of solid tumors might be improved by concomitant treatments targeting biological and physical properties of the tumor stroma (4), active transport at the tumor cells (5), or *via* new drug delivery systems (6). All these approaches require an accurate evaluation of the pursued pharmacokinetic effects, *i.e.*, accumulation of the drug in the tumor cell to increase therapeutic efficacy and, ideally, low systemic exposure to reduce side effects. Such pharmacokinetic evaluation may be achieved by measuring the amount of drug in the tumor by methods involving drug administration to preclinical models (usually mice), blood sampling at different time points and terminal collection of tumor tissue. This approach requires a large number of animals to provide a complete concentration-time profile of drug distribution in the tumor (7). The simplicity of the analysis of tumor homogenates is an advantage of this method. However, this –the traditional– approach does not provide information regarding drug distribution in the solid tumor compartments (extracellular, intracellular and vascular). Such information is relevant to understand drug activity (or lack thereof) and pharmacokinetic interactions. For instance, if the amount of drug detected in the homogenate is predominantly accumulated in the extracellular fluid of tumor (tECF), suitable intracellular drug targets might not be reached (7).

The combination of two different sampling methods, microdialysis and tumor homogenates, under steady state drug pharmacokinetics helps to accurately determine drug distribution in solid tumors using a low number of experimental animals. Microdialysis is used to sample the tECF for the subsequent analysis of levels of free (protein unbound) compounds, in equilibrium with the free compound in plasma (8). Then, the ratio at the steady state between the total drug concentration in the tumor homogenate and the unbound drug concentration in the tECF (calculated by microdialysis) provides the unbound drug volume of distribution in tumor ($V_{u,tumor}$), measured in mL/g tumor (9), as calculated from Eq. 1

$$V_{u,tumor} = \frac{A_{tot,\ tumor} - V_{tot,\ blood} \times C_{tot,\ blood}}{C_{ss,tumor}} \quad (1)$$

where $A_{tot,tumor}$ is the total amount of drug per gram of tumor homogenate (including tumor blood), $V_{tot,blood}$ is the volume of blood per gram of tumor, $C_{tot,blood}$ is the total concentration of drug in blood, and $C_{ss,tumor}$ is the concentration of unbound drug in the tECF at the steady state. High values of the $V_{u,tumor}$ parameter indicate high distribution of the drug in the intracellular compartment of the tumor or nonspecifically bound to tumor tissue components, whereas low values suggest that the drug is predominantly distributed in the extracellular space.

The steady state approach in animals with microdialysis probes allows the determination of real-time effects of concomitant treatments on the compartmental distribution of the assayed chemotherapeutic drug. Steady state intratumor microdialysis in combination with terminal tumor sampling (homogenates) was utilized for the first time to study the shift in the distribution toward the cellular compartment of the water-soluble drug topotecan in brain tumors upon the effect of efflux pump inhibition at the tumor cell level (10). However, the application of the microdialysis technique to highly hydrophobic anticancer drugs has remained elusive, due to the lack of reproducibility of the conventional microdialysis principle in compounds that bind nonspecifically to parts of the microdialysis device (internal surface of tubing and probe membrane) and other plastic or glass surfaces used during the posterior analysis (11–13). For instance, previous studies on the microdialysis of the anticancer drugs docetaxel and doxorubicin have resulted in low or erratic probe recovery due to nonspecific binding (11, 12). To overcome such problem some authors propose the addition of solubilizers to the perfusate, such as 2-hydroxypropyl-beta-cyclodextrin (HPBCD) (14, 15), proteins to block the nonspecific binding sites in the circuit (16), or chemical agents with affinity to the collected molecule (17), while others have applied mathematical approaches to eliminate the binding component from the microdialysis recovery value (13, 18).

The objective of this study was to develop a reproducible method for the assessment of the tumor pharmacokinetics of the highly hydrophobic anticancer drug SN-38 (7-ethyl-10-hydroxycamptothecin) in mice bearing patient-derived xenografts (PDX) of the pediatric solid tumor neuroblastoma. SN-38 is a potent topoisomerase I inhibitor that results from the hydrolysis of irinotecan, its soluble prodrug. Two forms of SN-38 are in equilibrium in water, the active lactone (SN-38 L) and the non-active hydrophilic carboxylate (SN-38 C). SN-38 L predominates under acidic pH conditions, whereas SN-38 C at neutral and basic pH. Here, we propose a steady state microdialysis-homogenate method to study the intratumor distribution of SN-38 L without the interference of SN-38 C.

MATERIALS AND METHODS

Reagents

SN-38 was obtained from Seqchem (Pangbourne, UK). Irinotecan for *in vivo* studies was purchased from Hospira

(Lake City, IL). Phosphate buffered saline (PBS) tablets, HPBCD (molecular weight of 1400 g/mol), collagenase IV, fluorescein isothiocyanate (FITC), *N*,*N*-dimethylformamide (DMF) and dimethyl sulfoxide (DMSO) were purchased from Sigma-Aldrich (St. Louis, MO). Triethylamine (TEA), glacial acetic acid, sodium phosphate monobasic monohydrate and di-sodium tetra-borate 10-hydrate were from Panreac (Barcelona, Spain), and acetonitrile and methanol from Merck (Darmstad, Germany).

Tumor Models

Two patient-derived neuroblastoma animal models were used: HSJD-NB-003 and HSDJ-NB-004. Both models have been produced from patient biopsies obtained at Hospital Sant Joan de Déu (HSJD) (Barcelona, Spain) from patients at diagnosis as part of an IRB-approved protocol. Additional information of both models is available in Suppl. Material. Fresh tumor fragments were transplanted to the flank of athymic nude mice (Harlan, Indianapolis, IN) to establish xenografts models. The research performed with mice adhered to the Principles of Laboratory Animal Care (NIH publication #85-23, revised in 1985).

SN-38 Analysis by High Performance Liquid Chromatography (HPLC)

The analytical technique was slightly modified from the one described by Warner and Burke (19). A stock solution of SN-38 (1 mg/mL in DMSO, stored at −80°C) was used to prepare standards (STDs) and quality controls (QCs) for analysis of SN-38 in dialysates, mouse plasma, mouse blood and tumor homogenates, prepared as previously described (10). The stock solution was first diluted in methanol to obtain an intermediate concentration of 0.02 mg/mL of SN-38. This solution was further diluted either in methanol (working solutions for SN-38 L) or di-sodium tetra-borate 10-hydrate 0.04 N in water (working solutions for SN-38 C) to achieve concentrations of 50, 100, 200, 500, 1000 and 2000 ng/mL (to prepare STDs) and 150 and 1500 ng/mL (to prepare QCs). Working solutions for SN-38 C were kept at room temperature for 45 min protected from light to achieve total conversion from lactone to carboxylate. Then, each working solution (5 μL) of each SN-38 concentration was added to PBS, 10% HPBCD in PBS (*w*/*v*), mouse plasma (Janvier, Saint Berthevin Cedex, France), mouse blood or tumor homogenate (490 μL) to build the STDs (final concentrations of 0.5, 1, 2, 5, 10, 20 ng/mL) and QCs (final concentrations of 1.5 and 15 ng/mL). The solution was then vortexed and quickly added (200 μL) to cold methanol (800 μL) to avoid the pH-dependent interconversion between SN-38 C and SN-38 L. Mouse plasma required centrifugation (2 min, 10,000 rpm) to separate methanol-precipitated plasma proteins before injection of the supernatant to the HPLC system (10 μL). Tumor homogenates and mouse blood required centrifugation (2 min, 10, 000 rpm) and filtration of the supernatant through 0.45 μm pore membrane CA Spin-X centrifuge tube filters (Costar, Cambridge, MA) before injection in the HPLC.

The HPLC system (Shimadzu, Kyoto, Japan) consisted of a pump model LC-20 AD, an autosampler module SIL-20 AC XR and a fluorescence detector RF-20A XS set at 379 nm and 560 nm for excitation and emission wavelengths. The mobile phase consisted of a pH 5.5 TE-acetate buffer (3% TE in water, *v*/*v*) and acetonitrile (74:26) and the column was a Tracer Excel 120 ODSA C18 (150 mm×4.6 mm, 5 μm) (Teknokroma, Barcelona, Spain).

Binding to Tubing

We studied whether increasing amounts of HPBCD in the perfusate would prevent nonspecific adsorption of SN-38 (L and C) to the plastic tubing of the microdialysis circuit. In a preliminary experiment, we determined the time to achieve the equilibrium between SN-38 L and SN-38 C (defined as less than 1% of SN-38 L-to-SN-38 C conversion in a period of 1 h) at pH 7.4 at room temperature by sequential sampling and HPLC analysis of a 20 ng/mL SN-38 L solution prepared in PBS. Then, 20 ng/mL SN-38 L solutions were prepared in PBS and allowed to reach the lactone-carboxylate equilibrium for the time determined. HPBCD in different proportions (0, 2, 4, 6, 8 and 10%*w*/*v*) was added to the equilibrated SN-38 solution. The solutions were then loaded into syringes and perfused with a pump (Kd Scientific KDS-101-CE, Holliston, MA) at a flow rate of 0.5 μL/min through polyurethane (0.35 mm internal diameter, donated by Raumedic, Voiron, France) and fluorinated ethylene propylene tubes (FEP, 0.13 mm internal diameter, Idex Health and Science, Oak Harbor, WA). The length of the tubes was selected to provide a total internal surface of 100 mm^2. Then, samples were collected every 20 min in glass sealed vials containing 40 μL methanol (methanol stops the interconversion of both SN-38 forms upon storage) placed in a CMA 470 refrigerated fraction collector (CMA, Kista, Sweden), at 6°C. Samples were stored at −80°C until HPLC analysis. Tube binding was defined as the absolute change in the concentration of the perfused solution during perfusion through the tube and calculated according to Eq. 2

$$\text{Binding}\ (\%) = \left|1 - \frac{C_{rec}}{C_{per}}\right| \times 100 \qquad (2)$$

where C_{rec} is the concentration of SN-38 recovered after perfusion through the tube and C_{per} is the concentration of SN-38 in the perfused solution.

We applied the one-sample *t*-test to compare mean tube binding values to a hypothetical zero value using Graphpad Prism 5 software (La Jolla, CA).

SN-38 Microdialysis: Enhanced Relative Recovery and Repeatability

Since the addition of HPBCD to the perfusate has been shown to enhance the relative recovery of hydrophobic drugs by microdialysis (14, 20, 21), we expected a similar result for SN-38, and more specifically for its hydrophobic and active form SN-38 L. Thus, we performed an experiment to address such enhancing effect. We used the CMA 20 microdialysis probe with a membrane length of 4 mm and 20 kDa molecular weight cutoff (CMA, Kista, Sweden), in a microdialysis circuit composed of a pump, a swivel (Instech 375/D/22QM; Plymouth Meeting, PA), a 25 cm length FEP tube and a CMA 470 refrigerated sample collector.

For enhanced relative recovery experiments, a clinically relevant 20 ng/mL SN-38 solution was prepared in PBS pH 7.4 and placed in a glass light-protected beaker, and stirred at room temperature overnight for equilibration between SN-38 L and SN-38 C. The next day, 10% HPBCD in PBS was perfused through the probe at 0.5 μL/min. An identical experiment was run in parallel using PBS alone (no HPBCD) as perfusate. Dialysate samples were collected over 20 min intervals for a total of 7 sampling periods and the relative recovery (RR) assessed according to Eq. 3

$$\mathrm{RR}\ (\%) = \frac{C_{dial}}{C_0} \times\ 100 \tag{3}$$

where C_{dial} is the concentration of SN-38 in the dialysates and C_0 is the concentration of SN-38 in the dialysed solution.

To address the repeatability of the enhanced recovery, following the relative recovery experiment the probe was transferred to SN-38-free PBS for 7 sampling periods and finally returneto the original 20 ng/mL SN-38 to collect 6 more sampling periods. Sealed glass vials with 40 μL of cold methanol were used to collect the samples.

To further study the enhancing effect of the cyclodextrin additive on the microdialysis relative recovery, a third experiment was performed under the same conditions; the SN-38 20 ng/mL solution was prepared in 10% HPBCD in PBS and dialyzed with a 10% HPBCD solution perfused at 0.5 μL/min.

Probe Calibration by the Zero Flow Rate Method (ZFR)

The predicted enhancing effect of HPBCD on the relative recovery of SN-38 is likely due to the formation of the inclusion complex between the drug and HPBCD in the probe lumen that drives additional mass transport of the drug towards the dialysate (21). Thus, the retrodialysis method or the use of internal standard in the perfusate were excluded to calculate the probe recovery *in vivo*. Alternatively, the most suitable method to calibrate the probe *in vivo* was the ZFR, which takes advantage of (i) the constant tECF concentration of the analyte at steady state plasma drug levels and (ii) the exponential relationship between relative recovery and flow rate through the probe (22). A set of experiments was performed *in vitro* to calculate the relative recovery by the ZFR method, in which SN-38 (20 ng/mL concentrations prepared in PBS and kept overnight to equilibrate SN-38 L and SN-38 C) was dialyzed with a CMA 20 probe perfused with 10% HPBCD in PBS at 0.5, 1, 1.5 and 2 μL/min flow rates. Dialysates were allowed to stabilize for at least twice the time required to wash the dead volume of the circuit after changing flow rates (80, 40, 30 and 20 min for 0.5, 1, 1.5 and 2 μL/min respectively). The exponential ZFR curve was extrapolated by nonlinear regression to fit the data using the following Eq. 4

$$C_{dial} = C_{ZFR} \times e^{(-KF)} \tag{4}$$

where C_{dial} is the concentration of SN-38 in dialysate samples at flow rate F, C_{ZFR} is the concentration of SN-38 calculated by nonlinear regression at the zero flow rate value, and K is a constant defined by the product of the mass transport coefficient and the surface area of the probe membrane, as previously described (23). Under enhancement conditions (*i.e.*, presence of 10% HPBCD as enhancer in the dialysate), the value calculated for C_{ZFR} is higher than C_0 and their relationship is defined by the enhancement factor (*f*) of the recovery, according to Eq. 5

$$f = \frac{C_{ZFR}}{C_0} \tag{5}$$

where C_0 and C_{ZFR} have been defined in Eqs. 3 and 4, respectively. Thus, the enhanced recovery (ER) at a given flow rate, when C_0 is unknown (*e.g.*, upon *in vivo* conditions), is the dialysate concentration at such flow rate divided by C_{ZFR} and multiplied by *f*, as expressed in Eq. 6

$$\mathrm{ER}\ (\%) = \frac{C_{dial}}{C_{ZFR}} \times f \times 100 \tag{6}$$

As an intermediate step between *in vitro* and *in vivo* assays, SN-38 microdialyses were performed using a suspension of digested tumor tissue as dialysis solution, stirred and maintained at 37°C during the experiments. Briefly, 1 g of tumor freshly excised from a mouse was digested with collagenase IV

(Sigma) for 1 h in a Thermomixer® shaking incubator (Eppendorf, Hamburg, Germany) set at 37°C and 1300 rpm. The digested tissue was filtered through a 40 μm pore cell strainer, centrifuged at 400 g and the pellet was resuspended with PBS (1 g tumor/1 mL PBS). A solution of SN-38 (10 μg/mL in methanol) was added to the suspension of digested tumor for a final concentration of 20 ng/mL SN-38. Once in equilibrium, a ZFR experiment was performed keeping the solution at 37°C and 300 rpm in the shaking incubator. Samples were collected and stored as detailed above.

Extravasation of HPBCD during Microdialysis

Because dialysates contain 10% HPBCD, we expected that a fraction of the enhancer would be transferred to the dialyzed sample or tissue during the microdialysis experiment. To study such effect *in vitro*, we labeled HPBCD with FITC by reacting 300 mg of cyclodextrin and 83 mg of the tracer in 5 mL of DMF at 32°C for 12 h protected from light. The product (HPBCD-FITC) was then dissolved 10%*w*/*v* in PBS and perfused at a flow rate of 0.5 μL/min through a CMA 20 probe immersed in a blank PBS solution. Perfusate, dialysate and blank solution were analyzed for HPBCD-FITC with a ND-1000 nanodrop spectrophotometer (Thermo Scientific, Waltham, MA) at 495 nm.

For *in vivo* studies, 10% HPBCD-FITC in PBS was perfused at 0.5 μL/min through CMA 20 microdialysis probes inserted in subcutaneous tumors (HSJD-NB-003) grown in the flank of athymic nude mice ($n=3$) in accordance with the institutional ethics committee for animal welfare. Perfusate and dialysate samples were analyzed after 2 h collection by spectrophotometry. At the end of the experiment, mice were anesthetized and perfused with PBS and formalin. Then the probe was removed, the tumor excised and cut frozen to study the distribution of HPBCD-FITC surrounding the probe by microscopy (Leica DM 5000 B, Wetzlar, Germany).

Blood Volume in Tumors

To calculate the fraction of blood volume in the tumor we counted the number of erythrocytes in blood and tumor (HSJD-NB-003 and HSJD-NB-004) in athymic nude mice ($n=4$ and $n=3$, respectively) using an Advia 2120 hematology analyzer (Siemens, Erlangen, Germany). Briefly, blood samples were obtained by retroorbital plexus and diluted with PBS prior to analysis. Then mice were euthanized and tumors (15 mm diameter) excised, weighed and digested with collagenase IV at a concentration of 100 mg tumor per mL of collagenase IV (1 h, 1300 rpm, 37°C). After digestion the cell suspension was filtered through a 40 μm pore nylon filter (Teknokroma), 5 mL PBS were added and the mixture centrifuged for 10 min at 400 g. The supernatant was removed and the pellet was resuspended in 5 mL PBS, filtered and centrifuged again. The pellet was finally resuspended in PBS for a final concentration of 100 mg tumor/mL and the number of erythrocytes quantified. From the erythrocyte counts in blood and tumor, we calculated the volume of blood (% *v*/*w*) in tumor tissue.

Plasma Protein Binding

To calculate the unbound fraction of SN-38 in plasma we used the ultrafiltration method (Centrifree Ultrafiltration Device with Ultracel YM-T membrane, Merk Millipore, Billerica, MA). Briefly, 150 μL samples of 200 ng/mL SN-38 in equilibrium in mouse plasma were ultrafiltrated in triplicate. The difference of concentration between the initial sample (bound and unbound SN-38, C_0) and the filtrated sample (free drug, C_f) was equivalent to the SN-38 protein binding (PB), as detailed in Eq. 7

$$\text{PB}\ (\%) = \frac{C_0 - C_f}{C_0} \times 100 \tag{7}$$

SN-38 Steady State Pharmacokinetics after Irinotecan Infusion

To achieve steady state concentrations of unbound SN-38 L in plasma ($C_{ss,plasma}$) and tECF ($C_{ss,tumor}$) we loaded the prodrug irinotecan in osmotic pumps (model 2001D, Alzet, Cupertino, CA) and implanted them subcutaneously in athymic nude mice. We performed a preliminary pharmacokinetic study to characterize the steady state concentrations of unbound SN-38 L achieved for 24 h, in which 19 mice received a dose of 130 μg/h irinotecan and were bled (50 μL) by the retroorbital plexus at times 1, 2, 3, 6, 16 and 24 h (maximum of 3 blood samples per mouse) after pump implantation. Samples were processed for HPLC analysis and data were fitted with ADAPT 5 software (BMSR, Los Angeles, CA) (24).

Combined Microdialysis-Tumor Homogenate Method

To produce subcutaneous solid tumors in nude mice (4 week old females), one fragment of viable tumor tissue (5–10 mm^3 of HSJD-NB-003 and HSJD-NB-004 models) was implanted in one flank under isoflurane anesthesia. When the tumor reached 15 mm diameter (7–8 weeks after insertion) a microdialysis experiment was performed in $n=3$ and $n=4$ mice, respectively. First, a CMA 20 probe was inserted in the tumor under isoflurane anesthesia. After probe equilibration (90 min at 0.5 μL/min; 10% HPBCD in PBS), an irinotecan-loaded osmotic pump (130 μg/h) was inserted subcutaneously in the

opposite flank under isoflurane anesthesia. Dialysates were collected overnight every 90 min, into glass sealed vials prefilled with 180 µL methanol in the refrigerated automatic fraction collector at 6°C. Mice remained awake and freely moving during sample collection. The next day (16–19 h after pump insertion), a blood sample was collected to determine the steady state concentration of SN-38 L in plasma ($C_{ss,plasma}$) and blood ($C_{tot,blood}$). Then, taking advantage of the steady state concentrations of SN-38 L in tECF, the ZFR method was performed during the last 3 h of the *in vivo* experiment, to calculate the recovery (ER) of the probe as detailed in Eq. 6. Thus, the real steady-state concentration of SN-38 L in tECF ($C_{ss,tumor}$) was calculated according to Eq. 8

$$C_{ss,tumor} = \frac{C_{dial}}{ER(\%)} \times 100 \quad (8)$$

where C_{dial} is the concentration in tumor dialysates (mean of 3 samples in steady state equilibrium). The steady state drug penetration of tECF (P_{tumor}) by unbound SN-38 L was calculated according to Eq. 9

$$P_{tumor} = \frac{C_{ss,tumor}}{C_{ss,plasma}} \quad (9)$$

After the microdialysis experiment mice were euthanized and the tumor terminally collected to process as homogenate. To calculate the $V_{u,tumor}$ parameter as defined in Eq. 1, homogenates and blood samples were terminally obtained from additional $n=8$ (HSJD-NB-003) and $n=8$ (HSJD-NB-004) mice at 16–19 h after the implantation of the pump. The tumor was weighed, mechanically minced and 10 µL of distilled water was added per mg of tumor. The mixture was sonicated with a Vibracell VCX 750 (Sonics, Newtown, CT) and processed for HPLC analysis.

RESULTS

HPLC Technique

Retention times of SN-38 C and SN-38 L were 7 and 10 min, respectively, and they were not altered by the presence of HPBCD in the samples. The lowest limit of quantification was 0.5 ng/mL for SN-38 L and SN-38 C in PBS, PBS with 10% HPBCD, plasma and blood and 5 ng/g for SN-38 L and SN-38 C in tumor homogenates. No carryover was detected upon the injection of analytical blanks. STDs and QCs were stable at −80°C for at least 2 months.

Binding to Tubing

Because SN-38 L undergoes conversion predominantly to SN-38 C in PBS at pH 7.4, we studied the time required to achieve the equilibrium between both forms in this medium at room temperature (Fig. 1). The conversion rate followed first-order kinetics. After 11 h, SN-38 C and SN-38 L were in equilibrium, with a final molar ratio of 7:93 (SN-38 L:SN-38 C) with a standard deviation of ±0.4%. Such equilibrated solution was used to study the binding of each SN-38 form to both tubing types. Results are shown in Fig. 2. The first observation was that in the absence of HPBCD SN-38 binds tightly and erratically to tubing (28–72%), regardless of its kind. The addition of increasing amounts of HPBCD reduced the binding until the values were not distinguishable from the 0% value observed with 10% HPBCD (one-sample *t*-test; $P=0.960$).

SN-38 Microdialysis

In vitro microdialysis experiments mimicked materials and dead volumes of the tubing and connections (*i.e.* swivel, CMA 20 probe, FEP tube and cannula for septa of the fraction collector) employed further for *in vivo* experiments. As shown in Fig. 3a, the recovery of SN-38 L and SN-38 C was neither enhanced nor repeatable when the perfusate solution was plain PBS. Carryover of SN-38 L persisted during several sampling periods after the probe was transferred to SN-38-free PBS. In contrast, the addition of 10% HPBCD to the perfusate enhanced RR up to 129.6±8.1% for SN-38 L and 71.9±8.9% for SN-38 C (Fig. 3b). There was no quantifiable SN-38 after 3 washing periods (60 min total) in SN-38-free PBS, corresponding to 1.8 times the dead volume (17 µL) of the system.

The enhancing effect of HPBCD was abolished, as expected, by the addition of the same compound (10% HPBCD) to the perfused SN-38 solution. Under this condition, RR for SN-38 L and SN-38 C were 23.9±1.2 and 18.2±0.7%, respectively, and remained constant during the experiment.

Probe Calibration by the ZFR Method

The ZFR method was performed at the end of each *in vitro* experiment to determine RR of SN-38 C and SN-38 L. Data from the ZFR experiments could be fitted to exponential curves by nonlinear regression. For experiments in PBS, R^2 values were 0.969±0.02 and 0.974±0.025 for SN-38 C and SN-38 L, respectively ($n=8$) (Fig. 4a). For experiments with tumor disaggregate suspensions, R^2 was 0.979±0.027 and 0.986±0.003 for SN-38 C and SN-38 L respectively ($n=3$) (Fig. 4b).

At 0.5 µL/min flow rate, the calculated recovery by the ZFR method was 70.8±4.9 and 70.3±7.8% for SN-38 L and

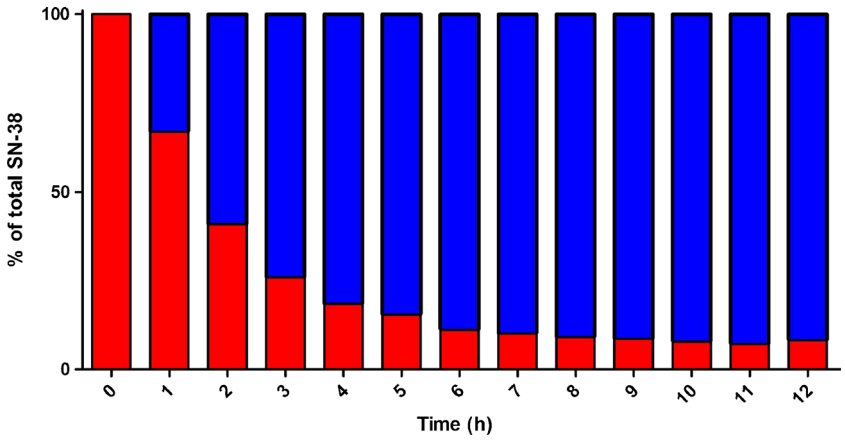

Fig. 1 Kinetics of the conversion of SN-38 L (*red bar*) to SN-38 C (*blue bar*) in PBS pH 7.4 at 20°C. At t = 0 h SN-38 L was 100%; equilibrium was achieved after 11 h of conversion with a final proportion of 7:93 (SN-38 L:SN-38 C).

SN-38 C in PBS solution, respectively. Slightly lower values of 56.6 ± 6.7 and 64.3 ± 3.8% were obtained for the lactone and the carboxylate in disaggregated tumor suspension. The *f* of SN-38 L in PBS was 1.94 ± 0.18. As expected, the RR of the hydrophilic SN-38 C was not significantly enhanced by HPBCD (*f* = 1.07 ± 0.20). When using disaggregated tumor as dialysis solution, *f* was 1.86 ± 0.26 and 1.13 ± 0.24 for SN-38 L and SN-38 C, respectively. Thus, *f* values in PBS solutions and stirred tumor suspensions matched well. The mean *f* value for SN-38 L obtained from experiments with SN-38 in digested tumor was consequently used to calculate the ER *in vivo* by the ZFR method.

Extravasation of HPBCD during Microdialysis

In vitro, 99.2% of the perfused HPBCD-FITC was recovered in the dialysate and 0.8% was delivered to the perfusate. *In vivo*, the recovered fraction of HPBCD-FITC was 100.2 ± 2.8%. The tumor in contact with the probe track in the HPBCD-FITC perfused tumors presented a microscopic histology similar to the tumor distant to the probe (Fig. 5a and b). The extravasation of the fluorescent HPBCD could be detected by microscopy at a distance of 1.6 mm surrounding the probe track (Fig. 5c).

Plasma Protein Binding and Blood Volume in Tumors

The ultrafiltrated fraction of SN-38 L was 18.6 ± 2.1%. Thus, 81.4% of SN-38 L was bound to plasma proteins. Blood volume in tumors determined by the hematology analyzer was 26.5 ± 5.4 µL/g tumor and 15.4 ± 4.5 µL/g tumor for HSJD-NB-003 and HSJD-NB-004, respectively ($n = 3$).

Pharmacokinetics of SN-38 Infusions

We evaluated the steady state concentration of SN-38 L in plasma samples obtained from 19 mice infused with irinotecan-loaded pumps at a rate of 130 µg irinotecan/h. The mean plasma concentration of unbound SN-38 L achieved after 16–24 h of infusion was 6.6 ± 1.9 ng/mL (Fig. 6).

Combined Microdialysis-Tumor Homogenate Method

The microdialysis-tumor homogenate experiment focused on the determination of SN-38 L in tumor dialysates, blood and tumor homogenates upon the administration of irinotecan by infusion. The enhancement factor (*f* = 1.86) determined in disaggregated tumors *in vitro* was used to calculate the enhanced

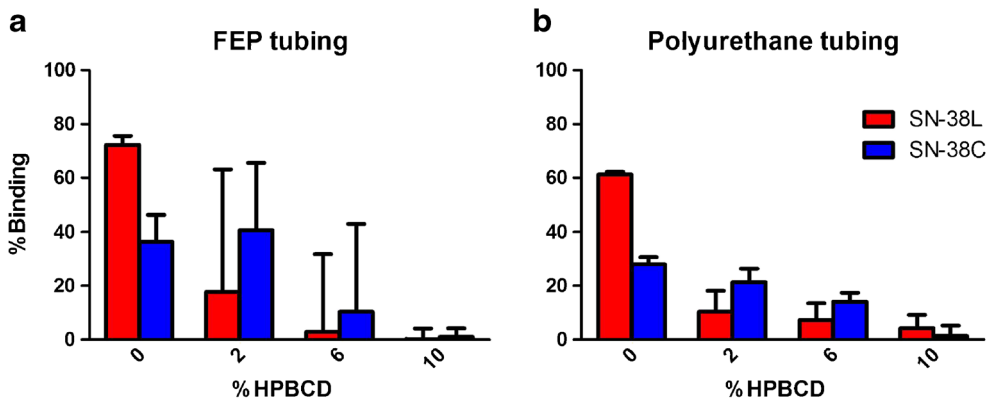

Fig. 2 Binding of SN-38 C and SN-38 L to FEP (**a**) and polyurethane (**b**) tubing perfused with and equilibrated SN-38 solution (20 ng/mL) in 0, 2, 6 and 10% HPBCD in PBS.

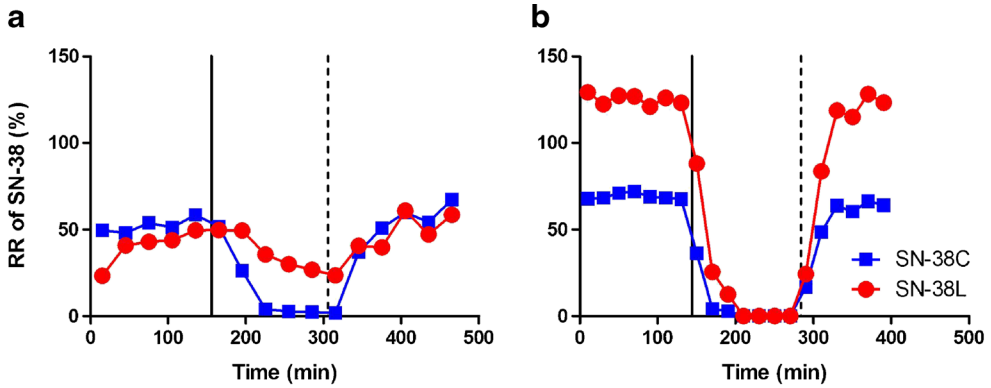

Fig. 3 Relative recoveries of SN-38 C and SN-38 L using plain PBS (HPBCD-free) (**a**) and PBS 10% HPBCD (*w/v*) (**b**) perfusates. *Solid lines* indicate the time when the microdialysis probe was transferred from the dialysis solution containing SN-38 to a plain PBS solution. *Dashed lines* indicate the time when the microdialysis probe was transferred from the plain PBS solution to the dialysis solution containing SN-38.

recoveries of the microdialysis experiments. After *in vivo* microdialysis experiments, ER values for SN-38 L were 132.2±23.7% and 130.4±25.9% for HSJD-NB-003 ($n=3$) and HSJD-NB-004 ($n=4$), respectively. These data were used to estimate the real concentration in tECF according to Eq. 8 (Fig. 7). Additionally, terminal homogenates and blood samples collected from additional mice infused with irinotecan were analyzed. Results of the whole set of experiments are shown in Table I.

DISCUSSION

Preclinical intratumor distribution of anticancer drugs is accurately addressed by specific sampling and analysis methods combining microdialysis and tumor homogenates (10). However, the application of microdialysis to lipophilic agents in a reproducible and controlled (calibrated) way *in vivo* has remained an unmet challenge (11, 25). Here, we describe a new method for the accurate determination of the distribution parameter $V_{u,tumor}$ of the highly hydrophobic agent SN-38 in patient derived solid tumor xenografts, using HPBCD-enhanced microdialysis under steady-state pharmacokinetics. We provide a way to calibrate the probe *in vivo*, based on the application of an enhancement factor-corrected ZFR method.

The microdialysis method proposed here is based on the addition of HPBCD as enhancer to the perfusate, as previously described for other drugs (21, 26). HPBCD was more effective than lipids (27) and polymeric surfactant (own experiments; data not shown). Cyclodextrins are cyclic oligosaccharides used in the pharmaceutical field to increment the apparent solubility and stability of compounds (28, 29). We demonstrated that without the addition of at least 10% HPBCD to the dialysate, drug recovery was erratic and low, as reported for doxorubicin and docetaxel elsewhere (11, 12). Our experimental design proved that, in the presence of 10% HPBCD in the perfusate, changes in concentration of the dialysate were not due to tubing uptake and washout. As expected, we found that the recovery of the hydrophilic SN-38 C compound in equilibrium with the hydrophobic SN-38 L was not enhanced by HPBCD, which is a direct evidence that HPBCD enhances only the recovery of hydrophobic compounds due to the formation of inclusion complexes (30). Our experimental observations contrast with previous reports using enhancer-free microdialysis for *in vivo* sampling of SN-38 (31, 32). However, such reports did not provide experimental

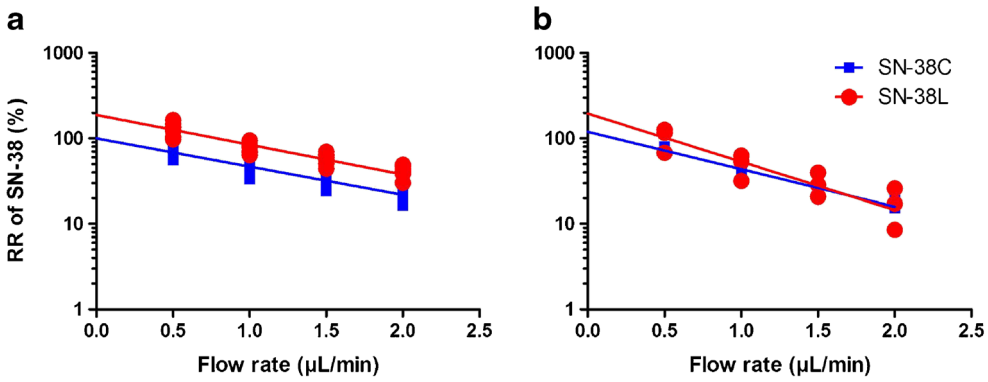

Fig. 4 Nonlinear regression analysis of data obtained from ZFR experiments using a dialysis solution consisting of SN-38 in (**a**) equilibrium in PBS solution ($n=8$ experiments) and (**b**) tumor disaggregate (**b**) ($n=3$ experiments). The value extrapolated in the curve at the theoretical zero flow rate gives C_{ZFR}.

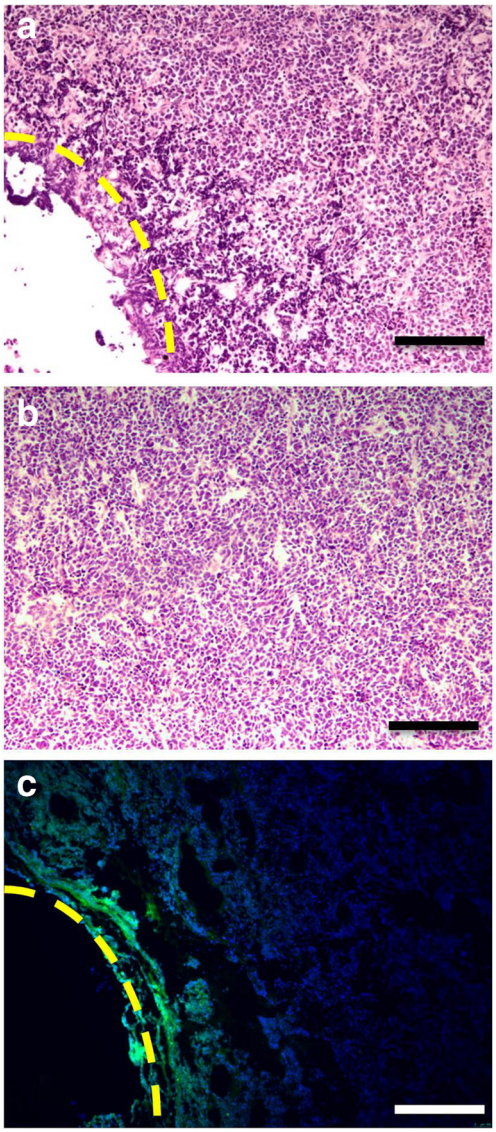

Fig. 5 Histological study of the microdialysis probe track after *in vivo* perfusion of 10% HPBCD-FITC. (**a**) HE-stained section of the probe track. (**b**) HE-stained section of tumor tissue distant from the probe. (**c**) Extravasation of fluorescent HPBCD-FITC from the probe. Cell nuclei were stained with DAPI. *Dashed yellow lines* mark the probe track. Scale bar: 500 μm.

evidences addressing the specific challenges associated with the technique, and they could not distinguish between SN-38 L and SN-38 C forms.

The use of HPBCD as enhancer raises concerns about its interference with the HPLC analytical technique (26). In fact, drug/cyclodextrin complexes are new entities and some of them, especially the complexes with hydrophobic cyclodextrins, display different retention time in HPLC than the free counterparts. This phenomenon takes place when the drug is forming a complex during the chromatographic analysis. Our data showed that the retention times of both SN-38 L and SN-38 C fitted those of cyclodextrin-free SN-38 and suggested that HPBCD complexes underwent decomplexation upon

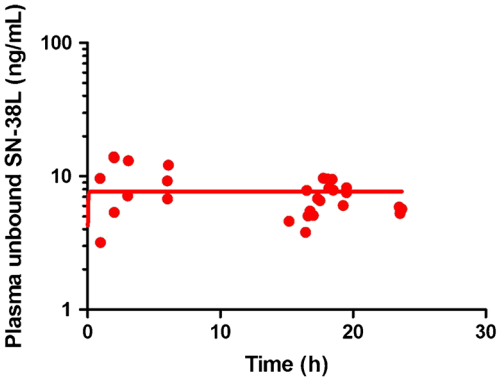

Fig. 6 Plasma concentration of unbound SN-38 L upon infusion with irinotecan-loaded osmotic pumps. Individual data collected during 24 h of study is represented. The *line* represents the best-fitting model obtained after analysis with ADAPT 5 software. Model-fitted $c_{ss,plasma}$ was 7.7 ng/mL.

the addition of methanol and mobile phase for HPLC analysis. At the same time, care should be taken in new applications with other drugs because specific cyclodextrins interfere with columns during drug analysis (33).

The question whether HPBCD interferes with drug distribution within the tumor tissue immediately surrounding the probe is not fully answered by our work. However, our data show limited extravasation of the fluorescent HPBCD derivative from the microdialysis probe, thus it is unlikely that HPBCD modifies drug distribution significantly in the dialyzed tissue. Also, we do not expect that the cyclodextrin will have enough affinity for the drug to alter the distribution in the tumor, because previous work shows that drug delivery from hydrophilic HPBCD-based systems is immediate *in vivo* (34). In a recent microdialysis study in patients using 10% HPBCD in perfusate, tissue metabolite concentrations were within the expected physiological range and tissue blood flow in the probe area was unaltered (26).

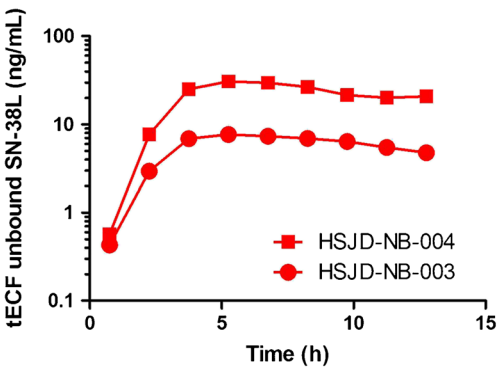

Fig. 7 Representative concentration-time data of unbound SN-38 L in tECF. Data represented come from the analysis of tumor dialysates upon the application of the *f* factor-corrected ZFR method in two animals, bearing the HSJD-NB-003 and HSJD-NB-004 subcutaneous tumor models. Plasma steady state unbound SN-38 L levels achieved for both experiments were 4.2 and 7.0 ng/mL, respectively.

Table I Results of the Combined Microdialysis-Tumor Homogenate Method Experiments for HSJD-NB-003 and HSJD-NB-004 Tumor Models. Data is Represented as mean ± SD (Value in Parenthesis is the Number of Experiments)

Tumor model	$C_{ss,tumor}$ (ng/mL)	$C_{ss,plasma}$ (ng/mL)	$A_{tot,tumor}$ (ng/g tumor)	$V_{tot,blood}$ (μL/g tumor)	$C_{tot,blood}$ (ng/mL)	P_{tumor} [a]	$V_{u,tumor}$ [b] (mL/g tumor)
HSJD-NB-003	7.7 ± 4.6 (3)	4.4 ± 1.9 (11)	25.4 ± 8.5 (10)	26.5 ± 6.6 (4)	21.3 ± 7.4 (4)	2.3 ± 1.4 (3)	3.2 ± 1.1
HSJD-NB-004	10.4 ± 7.6 (4)	6.2 ± 2.2 (12)	76.4 ± 58.7 (12)	15.4 ± 4.5 (3)	19.7 ± 13.7 (2)	1.9 ± 1.2 (4)	7.7 ± 6.0

[a] Calculated from Eq. 9

[b] Calculated from Eq. 1

To calibrate the probe *in vivo* we introduced for the first time the parameter *f* (Eq. 5) to correct for the extra convection of drug due to the presence of HPBCD in the perfusate. Thus, we preliminarily calculated *f* in tumor disaggregates *ex vivo*. We acknowledge the difficulty of reproducing intratumor microdialysis conditions *ex vivo*. This issue was addressed by the addition of extracellular volume to the tumor cell suspension and the careful reproduction of the experimental setup (probe, tubing connections, dead volume, flow rate, temperature, tumor cells) used *in vivo*. The validity of the method is strongly supported by the good reproducibility of the parameter *f* across several independent *in vitro* experiments. Moreover, *f* values were similar to those obtained in experiments performed under classical *in vitro* conditions (sample in PBS dialysate, unstirred, room temperature). We cannot exclude that our *ex vivo* estimation of *f* might change upon *in vivo* application. However, previous publications have shown similar *in vitro* and *in vivo* microdialysis recoveries (35, 36).

The hypothesis that suggests that only the free drug (plasma protein unbound) is able to distribute within tissues requires careful consideration in solid tumors. From microdialysis studies in our neuroblastoma models, P_{tumor} values higher than 1 at steady state suggest enhanced drug permeability and retention (EPR effect (37)) in tECF. Such effect was expected from previous microdialysis-based studies detecting enhanced unbound drug distribution in solid tumors (10, 38). Ours is the first report to assess it in neuroblastoma PDX.

From the combination of microdialysis and homogenate data, a $V_{u,tumor}$ value greater than 3 mL/g tumor for both neuroblastoma models suggested that SN-38 L efficiently penetrates tumor cells; compounds that do not enter tumor cells show $V_{u,tumor}$ smaller than 1. The relative contribution of the drug in the tumor vascular compartment ($V_{tot,blood} \times C_{tot,blood}$) to $V_{u,tumor}$ was almost negligible in our models. In fact, the elimination of the drug in the vascular compartment (Eq. 1) diminished this parameter in 0.07 and 0.03 mL/g tumor for HSJD-NB-003 and HSJD-NB-004, respectively, which is less than 3% of the $V_{u,tumor}$ value.

The *in vivo* microdialysis technique is challenging and thus, only few studies combined microdialysis and homogenate data to characterize drug distribution in tissues. Two of the most comprehensive works in the field showed the heterogeneity in the colchicine distribution in intra- and extracellular spaces of the hippocampus and other regions of the brain (39) and introduced the parameter of unbound volume of distribution in the brain upon the analysis of gabapentin in brain dialysates and homogenates (9). Such approaches have been further refined to describe the rate and extent of drug delivery to the brain compartments, including the intracellular one (40).

In summary, our detailed *in vitro* and *in vivo* study of the effect of the microdialysis enhancer HPBCD substantiates the reproducible sampling of a very potent and hydrophobic anticancer drug in tECF. We propose the calculation *ex vivo* of an enhancement factor to apply for *in vivo* probe calibration with the ZFR method. Upon the combination of the microdialysis-tumor homogenate method described here, we provide a powerful tool for further distribution studies of lipophilic drugs within solid tumors. In this context, this novel method is being used in our laboratory not only to characterize resistance mechanisms to anticancer agents related to drug distribution parameters in neuroblastoma, Ewing sarcoma and rhabdomyosarcoma PDX models but also to study the effect of novel delivery methods on drug distribution within tumor compartments. These investigations will further contribute to support the relevance of the developed analytical approach and refine it.

ACKNOWLEDGMENTS

AMC acknowledges funding from the AECC Scientific Foundation, MINECO (SAF2011-22660), Fundacion BBVA, European Union Seventh Framework Programme (FP7/2007-2013) under Marie Curie International Reintegration Grant (PIRG-08-GA-2010-276998) and ISCIII-FEDER (CP13/00189). AS thanks the European Union's - Seventh Framework Programme under grant agreement #612675-MC-NANOTAR. Work supported by the Xarxa de Bancs de Tumors de Catalunya (XBTC) sponsored by Pla Director d'Oncologia de Catalunya. We thank Dr. Mireia Camos for performing erythrocyte counts.

REFERENCES

1. Patel KJ, Tredan O, Tannock IF. Distribution of the anticancer drugs doxorubicin, mitoxantrone and topotecan in tumors and normal tissues. Cancer Chemother Pharmacol. 2013;72(1):127–38.
2. Minchinton AI, Tannock IF. Drug penetration in solid tumours. Nat Rev Cancer. 2006;6(8):583–92.
3. Kratz F, Warnecke A. Finding the optimal balance: challenges of improving conventional cancer chemotherapy using suitable combinations with nano-sized drug delivery systems. J Control Release. 2012;164(2):221–35.
4. Provenzano PP, Cuevas C, Chang AE, Goel VK, Von Hoff DD, Hingorani SR. Enzymatic targeting of the stroma ablates physical barriers to treatment of pancreatic ductal adenocarcinoma. Cancer Cell. 2012;21(3):418–29.
5. Fletcher JI, Haber M, Henderson MJ, Norris MD. ABC transporters in cancer: more than just drug efflux pumps. Nat Rev Cancer. 2010;10(2):147–56.
6. Holback H, Yeo Y. Intratumoral drug delivery with nanoparticulate carriers. Pharm Res. 2011;28(8):1819–30.
7. Tuntland T, Ethell B, Kosaka T, Blasco F, Zang RX, Jain M, *et al.* Implementation of pharmacokinetic and pharmacodynamic strategies in early research phases of drug discovery and development at Novartis Institute of Biomedical Research. Front Pharmacol. 2014;5:174.
8. Muller M. Microdialysis in clinical drug delivery studies. Adv Drug Deliv Rev. 2000;45(2–3):255–69.
9. Wang Y, Welty DF. The simultaneous estimation of the influx and efflux blood–brain barrier permeabilities of gabapentin using a microdialysis-pharmacokinetic approach. Pharm Res. 1996;13(3):398–403.
10. Carcaboso AM, Elmeliegy MA, Shen J, Juel SJ, Zhang ZM, Calabrese C, *et al.* Tyrosine kinase inhibitor gefitinib enhances topotecan penetration of gliomas. Cancer Res. 2010;70(11):4499–508.
11. Loos WJ, Zamboni WC, Engels FK, de Bruijn P, Lam MH, de Wit R, *et al.* Pitfalls of the application of microdialysis in clinical oncology: controversial findings with docetaxel. J Pharm Biomed Anal. 2007;45(2):288–94.
12. Whitaker G, Lunte CE. Investigation of microdialysis sampling calibration approaches for lipophilic analytes: doxorubicin. J Pharm Biomed Anal. 2010;53(3):490–6.
13. Lindberger M, Tomson T, Lars S. Microdialysis sampling of carbamazepine, phenytoin and phenobarbital in subcutaneous extracellular fluid and subdural cerebrospinal fluid in humans: an in vitro and in vivo study of adsorption to the sampling device. Pharmacol Toxicol. 2002;91(4):158–65.
14. Khramov AN, Stenken JA. Enhanced microdialysis recovery of some tricyclic antidepressants and structurally related drugs by cyclodextrin-mediated transport. Analyst. 1999;124(7):1027–33.
15. Elmeliegy MA, Carcaboso AM, Tagen M, Bai F, Stewart CF. Role of ATP-binding cassette and solute carrier transporters in Erlotinib CNS penetration and intracellular accumulation. Clin Cancer Res. 2011;17(1):89–99.
16. Müller M, Schmid R, Wagner O, Osten B, Shayganfar H, Eichler HG. In vivo characterization of transdermal drug transport by microdialysis. J Control Release. 1995;37(1–2):49–57.
17. Duo J, Fletcher H, Stenken JA. Natural and synthetic affinity agents as microdialysis sampling mass transport enhancers: current progress and future perspectives. Biosens Bioelectron. 2006;22(3):449–57.
18. Araujo BV, Silva CF, Haas SE, Dalla CT. Microdialysis as a tool to determine free kidney levels of voriconazole in rodents: a model to study the technique feasibility for a moderately lipophilic drug. J Pharm Biomed Anal. 2008;47(4–5):876–81.
19. Warner DL, Burke TG. Simple and versatile high-performance liquid chromatographic method for the simultaneous quantitation of the lactone and carboxylate forms of camptothecin anticancer drugs. J Chromatogr B Biomed Sci Appl. 1997;691(1):161–71.
20. Khramov AN, Stenken JA. Enhanced microdialysis extraction efficiency of ibuprofen in vitro by facilitated transport with beta-cyclodextrin. Anal Chem. 1999;71(7):1257–64.
21. Ao X, Stenken JA. Water-soluble cyclodextrin polymers for enhanced relative recovery of hydrophobic analytes during microdialysis sampling. Analyst. 2003;128(9):1143–9.
22. Menacherry S, Hubert W, Justice Jr JB. In vivo calibration of microdialysis probes for exogenous compounds. Anal Chem. 1992;64(6):577–83.
23. Jacobson I, Sandberg M, Hamberger A. Mass transfer in brain dialysis devices–a new method for the estimation of extracellular amino acids concentration. J Neurosci Methods. 1985;15(3):263–8.
24. D'argenio DZ, Schumitzky A. ADAPT 5 User's guide: pharmacokinetic/ pharmacodynamic systems analysis software. Los Angeles: Biomedical Simulations Resource; 2009.
25. Schuck VJ, Rinas I, Derendorf H. In vitro microdialysis sampling of docetaxel. J Pharm Biomed Anal. 2004;36(4):807–13.
26. May M, Batkai S, Zoerner AA, Tsikas D, Jordan J, Engeli S. Enhanced human tissue microdialysis using hydroxypropyl-ss-cyclodextrin as molecular carrier. PLoS One. 2013;8(4):e60628.
27. Ward KW, Medina SJ, Portelli ST, Mahar Doan KM, Spengler MD, Ben MM, *et al.* Enhancement of in vitro and in vivo microdialysis recovery of SB-265123 using Intralipid and Encapsin as perfusates. Biopharm Drug Dispos. 2003;24(1):17–25.
28. Irie T, Uekama K. Pharmaceutical applications of cyclodextrins. III. Toxicological issues and safety evaluation. J Pharm Sci. 1997;86(2):147–62.
29. Cwiertnia B, Hladon T, Stobiecki M. Stability of diclofenac sodium in the inclusion complex with beta-cyclodextrin in the solid state. J Pharm pharmacol. 1999;51(11):1213–8.
30. Vangara KK, Ali HI, Lu D, Liu JL, Kolluru S, Palakurthi S. SN-38-cyclodextrin complexation and its influence on the solubility, stability, and in vitro anticancer activity against ovarian cancer. AAPS PharmSciTech. 2014;15(2):472–82.
31. Metz MZ, Gutova M, Lacey SF, Abramyants Y, Vo T, Gilchrist M, *et al.* Neural stem cell-mediated delivery of irinotecan-activating carboxylesterases to glioma: implications for clinical use. Stem Cells Transl Med. 2013;2(12):983–92.
32. Dodds HM, Tobin PJ, Stewart CF, Cheshire P, Hanna S, Houghton P, *et al.* The importance of tumor glucuronidase in the activation of irinotecan in a mouse xenograft model. J Pharmacol Exp Ther. 2002;303(2):649–55.
33. Ngim KK, Gu Z, Catalano T. Characterization and resolution of reversed phase HPLC chromatography failure attributed to sulfobutylether-beta-cyclodextrin in a pharmaceutical sample preparation. J Pharm Biomed Anal. 2009;49(3):660–9.
34. Hirayama F, Uekama K. Cyclodextrin-based controlled drug release system. Adv Drug Deliv Rev. 1999;36(1):125–41.
35. Zamboni WC, Houghton PJ, Hulstein JL, Kirstein M, Walsh J, Cheshire PJ, *et al.* Relationship between tumor extracellular fluid exposure to topotecan and tumor response in human neuroblastoma xenograft and cell lines. Cancer Chemother Pharmacol. 1999;43(4):269–76.
36. Dukic S, Kaltenbach ML, Gourdier B, Marty H, Vistelle R. Determination of free extracellular levels of methotrexate by microdialysis in muscle and solid tumor of the rabbit. Pharm Res. 1998;15(1):133–8.
37. Matsumura Y, Maeda H. A new concept for macromolecular therapeutics in cancer chemotherapy: mechanism of tumoritropic accumulation of proteins and the antitumor agent smancs. Cancer Res. 1986;46(12 Pt 1):6387–92.

38. Zhou Q, Lv H, Mazloom AR, Xu H, Ma'ayan A, Gallo JM. Activation of alternate prosurvival pathways accounts for acquired sunitinib resistance in U87MG glioma xenografts. J Pharmacol Exp Ther. 2012;343(2):509–19.
39. Evrard PA, Ragusi C, Boschi G, Verbeeck RK, Scherrmann JM. Simultaneous microdialysis in brain and blood of the mouse: extracellular and intracellular brain colchicine disposition. Brain Res. 1998;786(1–2):122–7.
40. Hammarlund-Udenaes M, Friden M, Syvanen S, Gupta A. On the rate and extent of drug delivery to the brain. Pharm Res. 2008;25(8):1737–50.

Supplemental table. Molecular characterization of solid tumor models

Tumor model	Clinical stage	MYCN	TP53	ALK	DNA ploidy	Chromosome alterations		
						1p	11q	17q
HSJD-NB-003	4	NA[a]	wild type	wild type	quasi-2n	LOH[c]	no evidence of alterations	gain
HSJD-NB-004	4	A[b]	p.V173L, GTG>TTG	wild type	quasi-2n	trisomy	LOH	monosomy; 17q21-qter cnLOH[d]

[a]No amplification

[b]Amplification

[c]Loss of heterozygosity

[d]Copy neutral LOH

Chapter 2:

Intratumor drug distribution is reduced in xenografts derived from paired pediatric solid tumor biopsies obtained at later stages during patient treatment

Microdialysis technique combined with tumor homogenates and blood samples were of great value for the study of tumor chemoresistance. Here we present a manuscript that is of high interest in pediatric oncology since few works about tumor evolution have been published before. Our study is the first one using paired pediatric patient-derived xenografts at different stages of treatment showing that penetration issues could be involved in chemoresistance upon treatment.

Intratumor drug distribution is reduced in xenografts derived from paired pediatric solid tumor biopsies obtained at later stages during patient treatment

Carles Monterrubio[1,2], Guillem Pascual-Pasto[1,2], Sonia Paco[1,2], Nagore G. Olaciregui[1,2], Monica Vila-Ubach[1,2], Daniel J. Garcia-Dominguez[3], Lourdes Hontecillas-Prieto[3], Enrique de Alava[3], Carmen de Torres[1,2], Cinzia Lavarino[1,2], Jaume Mora[1,2], Angel M. Carcaboso[1,2*]

[1]Developmental Tumor Biology Laboratory, Fundacio Sant Joan de Deu, Barcelona, Spain

[2]Department of Pediatric Hematology and Oncology, Hospital Sant Joan de Deu, Barcelona, Spain

[3]Laboratory of Molecular Pathology- Instituto de Biomedicina de Sevilla (IBiS), Hospital Universitario Virgen del Rocio/CSIC/Universidad de Sevilla, Spain

Running title: Pediatric tumors evolve towards a limited drug distribution phenotype

Key words: pediatric solid tumor, intratumor drug delivery, ABC transporters, SN-38, drug resistance, pediatric cancer, tumor microdialysis

This work was supported in part by grants from the AECC Scientific Foundation, MINECO (SAF2011-22660), Fundacion BBVA, European Union Seventh Framework Programme (FP7/2007-2013) under Marie Curie International Reintegration Grant (PIRG-08-GA-2010-276998) and ISCIII-FEDER (CP13/00189).

Address for correspondence: Angel M. Carcaboso, PhD, Preclinical Therapeutics and Drug Delivery Research Program, Fundacio Sant Joan de Deu, Santa Rosa 39-57, Esplugues de Llobregat, 08950 Barcelona, Spain. +34 936009751; amontero@fsjd.org (A.M. Carcaboso)

The authors declare no conflict of interest.

Wordcount (excluding references): 5405

Number of figures: 5

Number of tables: 2

Abstract

Most patients with extracranial pediatric solid tumors are sensitive to chemotherapy at diagnosis, but most of the ones who relapse after treatment become chemoresistant. The changes in intratumoral drug pharmacokinetics associated to tumor evolution during treatment remain unknown. We hypothesized that intracellular drug distribution in tumors at later stages during treatment may be reduced as compared to earlier tumor stages, explaining in part acquired drug resistance in the patients. To explore this, we established several pairs of xenograft models from tumor biopsies obtained from patients with pediatric solid tumors (neuroblastoma, Ewing sarcoma and alveolar rhabdomyosarcoma) at different stages of their disease. We performed a combined microdialysis-tumor homogenate technique to study the unbound volume of distribution ($V_{u,tumor}$) of SN-38 (as a model drug with wide activity against these diseases) in the tumors. We found that $V_{u,tumor}$ was significantly lower in late stage tumors, as compared to the paired early stage tumors derived from the same patient, meaning that the distribution of the anticancer drug was shifted towards the extracellular compartment during tumor evolution. This observation held true when the original patients were initially responsive to treatment, becoming resistant at later stages, but not when they were refractory to treatment since diagnosis. Our findings substantiate the need of improved drug delivery systems in refractory pediatric solid tumors.

Introduction

Around 80% of extracranial pediatric solid tumors are sensitive to chemotherapy at diagnosis (1,2). However, at relapse a significant proportion of them respond poorly to anticancer drugs (3,4). This functional evolution of tumors towards chemoresistance may be related to new genomic alterations arising due to the selective pressure of treatments (5-7). As a consequence of them, multidrug-resistance associated genes might be increased in tumors or in endothelial cells associated to tumors, impeding intratumor drug distribution (8,9).

The inadequate penetration of chemotherapy to the solid tumor cells may account for an important tumor property that leads to drug resistance (10-13). However, whether tumor evolution during treatment produces intratumoral drug pharmacokinetic changes remains not characterized. In fact, the *in vivo* evaluation of drug distribution in tumor compartments (intracellular, extracellular and vascular) has been rarely studied, due to the challeging techniques that are needed (14-16). We have recently developed a reproducible microdialysis-tumor homogenate method that overcomes the limitations of the microdialysis technique in the highly hydrophobic drug 7-ethyl-10-hydroxycamptothecin (SN-38) by adding the solubilizer agent 2-hydroxypropyl-beta-cyclodextrin (HPBCD) in the perfusate solution (17). This technique provides a powerful tool to characterize compartmental anticancer drug distribution in tumors (17).

In this work, we hypothesized that tumors under clinical treatments evolve towards a drug-impenetrable phenotype. We have focused on the study of the distribution of the active metabolite of irinotecan, SN-38, in patient-derived xenografts (PDX) of highly aggressive pediatric solid tumors generated from

paired biopsies of pediatric solid tumor patients obtained at different stages during treatment.

Materials and methods

Patient samples and establishment of xenografts. Pediatric tumor biopsies were obtained under an IRB-approved protocol and informed consent at Hospital Sant Joan de Deu (HSJD, Barcelona, Spain).

Research with mice adhered to European regulations and was approved by the Universidad de Barcelona Animal Care and Use Committee. PDX models were established subcutaneously in athymic nude or nod.scid mice (Envigo, Barcelona, Spain) as previously described (17,18). For further experiments involving animals, upon initial engraftment neuroblastomas and Ewing sarcomas were propagated subcutaneously in athymic nude mice, and rhabdomyosarcomas in nod.scid mice.

Characterization of paired xenografts through analysis of copy number alterations (CNA). CNA analysis was performed using the high-density genome-wide CytoScan® HD platform (Affymetrix, Thermo Fischer Scientific). DNA was extracted from fresh frozen tumour xenograft samples using standard procedures. Analysis of the CytoScan® HD Array data was performed using the Chromosome Analysis Suite (ChAS) software (Affymetrix Thermo Fischer Scientific).

Drugs and reagents. SN-38 was from Carbosynth (Compton, UK). Irinotecan was purchased from Hospira (Lake City, IL, USA). Reagents for HPLC were from Merck (Darmstad, Germany). Reagents for cultures were from Life Technologies (Grand Island, NY, USA).

SN-38 penetration of tumor extracellular fluid. Immunodeficient mice were subcutaneously inoculated in one flank with freshly excised tumors from the previous generation of xenografts. All the drug distribution experiments were performed after the tumors achieved 10 mm diameter.

To calculate the extent of penetration of tumor extracellular fluid (tECF) by unbound SN-38 lactone (P_{tumor}), we used a microdialysis method with continuous infusion of irinotecan to maintain steady state (constant) concentrations in plasma ($C_{ss,plasma}$) and tECF ($C_{ss,tumor}$) (17). Briefly, we inserted 4 mm-length CMA 20 microdialysis probes (CMA, Kista, Sweden) in the tumors of mice under brief isoflurane anesthesia. The probes were continuously perfused at 0.5 µL/min with pH 7.4 phosphate buffered saline containing 10% HPBCD. After 90 min, mice were anesthetized with isoflurane to insert subcutaneous Alzet 2001D pumps (Durect, Palo Alto, CA) that infused the prodrug irinotecan at a rate of 130 µg/h constantly for 24 h. With this method, reported $C_{ss,plasma}$ of unbound SN-38 is in the range 7 ± 2 ng/mL (17). We calculated unbound plasma SN-38 lactone concentrations using already published plasma binding data in athymic nude mice (unbound fraction 18.6%) (17).

Tumor dialysates (90 min fractions) were collected overnight in a refrigerated fraction collector and conserved at -80 ºC until HPLC analysis. The next day

one blood sample was collected from the retroorbital plexus to determine the steady state concentration of SN-38 in plasma ($C_{ss,plasma}$) and blood ($C_{tot,blood}$) by HPLC (17). Then the probes were individually calibrated with a previously described zero flow rate method (17). Upon HPLC analysis and recovery correction, $C_{ss,tumor}$ values were calculated as the mean of 3 consecutive dialysate samples at steady state. After the microdialysis experiment mice were euthanized and the tumor terminally collected to process as homogenate.

P_{tumor} was calculated as the tECF-to-plasma steady state concentration ratio, according to Equation 1:

$$P_{tumor} = \frac{C_{ss,tumor}}{C_{ss,plasma}} \quad (1).$$

Compartmental distribution of SN-38 in tumors. Tumor homogenates and blood samples collected at steady state from the microdialysis experiments and from additional mice with tumors receiving the same irinotecan dose through infusion (3-6 mice of each tumor model) were processed as previously described to quantify SN-38 (17). Then, to characterize the relative distribution of SN-38 in tumor compartments (i.e., tECF, vascular compartment and tumor cells) in each tumor model, we calculated the unbound drug volume of distribution in tumor ($V_{u,tumor}$; mL/g tumor) (15,17) as follows:

$$V_{u,tumor} = \frac{A_{tot,tumor} - V_{tot,blood} \times C_{tot,blood}}{C_{ss,tumor}} \quad (2)$$

where $A_{tot,tumor}$ is the total concentration of SN-38 in tumor homogenate (ng/g), $V_{tot,blood}$ is the volume of blood in tumor (mL/g; calculated by erythrocyte counts in blood and tumor for each xenograft model, as already described (17)),

$C_{tot,blood}$ is the total concentration of SN-38 in blood (ng/mL), and $C_{ss,tumor}$ is the mean $C_{ss,tumor}$ of SN-38 (ng/mL) determined in each xenograft model by microdialysis.

If $V_{u,tumor}$ is high it suggests a preferential distribution of the drug in the tumor cells (intracellular compartment). If $V_{u,tumor}$ is low then the drug is predominantly distributed in the extracellular compartment of the tumor. The subtraction of $V_{tot,blood}$ x $C_{tot,blood}$ corrects the tumor homogenate data for the drug contained in blood (vascular compartment).

Drug activity assays. To study whether changes in intratumor drug distribution correlated with changes in drug activity, we performed *in vitro* and *in vivo* activity assays. Primary cultures of xenograft models were established and antiproliferative activity of SN-38 was evaluated with the MTS Cell Proliferation Colorimetric assay (Promega, Madison, WI, USA) as previously described (18).

For the in vivo activity studies, athymic nude mice (n=6-11 per tumor model; paired models from each patient) bearing 100-500 mm^3 subcutaneous tumors were randomized to control or treatment groups. Treatment groups received one cycle of intraperitoneal irinotecan 10 mg/kg/day doses in a 5 consecutive days a week for two consecutive weeks regimen , following published methods (19). Control groups did not receive treatment. Tumor volume was measured three times a week with an electronic caliper, until day 14, in which response to treatment was evaluated. We defined complete response (CR) as tumor mass <50 mm^3 and >50% reduction at the end of treatment (day 14); partial response (PR) was tumor volume regression ≥50% at day 14 but tumor ≥50 mm^3; stable disease (SD) was <50% regression and ≤25% increase in initial volume at day

14; and progressive disease (PD) was <50% regression from initial volume and >25% increase in initial volume at day 14.

Xenograft models showing 100% CR at day 14 were enrolled in a long term survival study and followed up weekly until tumor regrowth to endpoint (1500 mm^3) or day 100.

mRNA expression analysis of ATP-binding cassete (ABC) transporters. Total RNA from freshly excised engrafted tumors was isolated using TRIzol (Life Technologies). Quantity and quality of the total RNA was determined with a Nanodrop ND-2000 Spectrophotometer (Thermo Scientific). Previously, we treated all RNA samples with Turbo DNA-free kit (Applied Biosystems) to remove genomic DNA. For gene expression analysis we used 1 µg of total RNA for the reverse transcription using the High Capacity reverse transcription kit (Applied Biosystems) according to the manufacturer's protocol. The real-time quantitative RT-PCR (qRT-PCR) were performed with gene-specific fluorescent Taqman probes (Taqman Gene Expression Assays, Applied Biosystems) including probes for: ABCG2/BCRP (Hs01053790_m1), P-gp/MDR1 (Hs00184500_m1) and MRP1 (Hs01561502_m1). TPT1 (Hs02621289-g1) was used as endogenous control to normalize variations in the quantities of input cDNA. Applied Biosystems 7900HT Fast Real Time PCR System was used with the following PCR conditions: 50℃ 2 min; 94.5℃ 10 min; 40 cycles of melting 97℃ 30 sec and annealing 59.7℃ 1 min. All qRT-PCR measurements were analysed with the ExpressionSuite Software v1.0 (Applied Biosystems).

Statistics. Replicate data are presented as mean ± SD. Student's t test was used for comparisons of two groups with similar variances. Mann Whitney test was used to compare two groups when the variances where different.

Results

Paired xenograft models of pediatric solid tumor patients.

We established 4 pairs of xenograft models from biopsies of 4 different patients. Each pair of biopsies was obtained from the same patient at different stages of treatment, namely "early" and "late" biopsies, to establish "early" and "late" xenografts. All patients died due to disease progression. Clinical data of each patient was as follows.

Patient 1 was a 2 year old (y.o.) male diagnosed of stage 4 neuroblastoma and treated in an external institution with chemotherapy and incomplete surgery. Upon progression he was treated at HSJD. First, his suprarrenal tumor was biopsed (to establish early xenograft HSJD-NB-001; TP53-mutated and MYCN-amplified) and treated with chemotherapy and surgery according to a published protocol (1), achieving partial response. Upon further progression he was treated with irinotecan and CTX. Late xenograft HSJD-NB-002 was established from a bone marrow biopsy refractory to treatment at this late stage (during progression in treatment).

Patient 2 (2 y.o. female) was biopsied at diagnosis (early xenograft HSJD-NB-004; from lymph node). Her primary tumor (from suprarrenal origin) was a TP53-mutated and MYCN-amplified stage 4 neuroblastoma, and it progressed

during intensive chemotherapy treatment (1). A bone marrow biopsy was obtained 5 months after diagnosis (late xenograft HSJD-NB-005), during progression in treatment. The tumor did not respond to additional rescue treatments that included irinotecan.

Patient 3 (12 y.o. male) was diagnosed of non metastatic Ewing sarcoma with EWS-FLI1 type 1 fusion gene (early xenograft HSJD-ES-002; obtained from the fibula at diagnosis). He was treated with 5 cycles of chemotherapy, surgery and radiation therapy (RT), according to a published protocol (2). He was in remission until tumor relapsed in the lung 1.5 years after diagnosis (late xenograft HSJD-ES-006). The relapsed tumor was refractory to further chemotherapy treatments.

Patient 4 (10 y.o. male) was diagnosed of alveolar rhabdomyosarcoma (PAX3-FKHR fusion-positive) and achieved complete response after intensive treatment of chemotherapy (several agents including irinotecan), surgery and RT, following a published protocol (20). Three months after completing the treatment he relapsed with massive pleural effusion (early xenograft HSJD-ARMS-001) that was treated with chemotherapy (including topotecan) and RT achieving complete response by PET evaluation. Second relapse appeared shortly with massive pleural effusion, unresponsive to further chemotherapy treatment. The late xenograft HSJD-ARMS-002 was established from such pleural relapse 1.2 years after first relapse.

Comparison of overall copy number alterations between xenografts derived from early and late tumor biopsies.

We characterized and compared genomic copy number (CN) profiles of xenograft samples derived from paired biopsies of patients 1, 2 and 3.

Neuroblastoma xenografts from patients 1 and 2 showed highly unstable genomes with several CN alterations (CNAs) in the early xenograft and additional aberrations in the late xenograft. For patient 1, genomic profiles of the early xenograft HSJD-NB-001 showed, among others, chromosome 1p, 1q, 3q and 17q gain, and chromosome 3p and 7p loss. In the late xenograft (HSJD-NB-002), we observed additional CNAs including segmental and numerical gains and losses affecting a large proportion of chromosomes (Fig. 1A and 1B). For patient 2, the early xenograft (HSJD-NB-004) showed both segmental and numerical CNAs affecting numerous chromosomes, including chromosome 1, 2, 11 and 17, whereas the late xenograft HSJD-NB-005 showed exclusively segmental CNAs, part of which were similar to the paired xenograft, chromosome 11q, 16q and 17p (Fig. 1C and 1D).

For patient 3 (Ewing sarcoma) both early and late xenografts showed similar profiles with a CN gain of chromosome 8 (gain of 1-2 copies of the entire chromosome) and a focal deletion of the CDKN2A locus (9p21.3) (Fig. 1E and 1F). Both alterations have been reported previously as highly recurrent in Ewing sarcoma (7). The presence of no additional CN alteration at relapse, underscores that pediatric tumors driven by recurrent translocations, such as Ewing sarcoma, have relatively stable genomes.

Xenografts from patient 4 (alveolar rhabdomyosarcoma) showed aberrant ploidy (data not shown).

SN-38 penetration of tECF was similar in patient-matched xenografts. We performed microdialysis experiments in each of the xenograft models (3-7 mice per model). Representative microdialysis experiments in single mice are shown in Figure 2. Upon individual calibration of the probes and analysis of the dialysate and plasma samples, we compared mean P_{tumor} values between patient-matched paired models (Table 1). P_{tumor} values were in the range 1.0-3.5 and were not significantly different among the patient-matched models.

Drug distribution is reduced in the intracellular compartment of patient-matched xenografts obtained at later stages of treatment.

To test our hypothesis that during the evolution of tumors anticancer drugs would be displaced from the intracellular compartment, we compiled the data from microdialysis samples, blood samples and tumor homogenates at the steady state in each tumor model (Table 2), and calculated the unbound volume of distribution in tumors ($V_{u,tumor}$). As shown in Figure 3, we observed that paired tumors from patients 1, 2 and 4 (patients that became refractory to treatments after being responders at earlier stages) presented significantly lower $V_{u,tumor}$ values in late xenografts, as compared to early ones. Thus, at earlier stages during treatment a greater proportion of SN-38 was intracellular rather than as unbound drug in the tECF. For patient 3, whose tumor was refractory to treatment since diagnosis, we did not observe the same shift in the compartmental distribution of the drug, and her $V_{u,tumor}$ was higher in the later xenograft.

Antiproliferative activity of irinotecan was diminished in patient-matched preclinical models obtained at later stages of treatment.

To evaluate whether the shift in drug distribution towards the extracellular compartment correlated with decreased efficacy of SN-38 (a drug targeting an intracellular protein), we studied the antitumor activity of SN-38 *in vitro* against cell lines derived from the biopsies of patient 1, and against primary cultures from freshly excised xenograft tissues for patients 2, 3 and 4, as previously described (18) (Fig. 4A). Resistance to SN-38 was increased in late-stage tumors as compared to their early counterparts in patients 1 (HSJD-NB-001 and -002 models) and 3 (HSJD-ES-002 and -006 models). For patient 1, IC50 increased from 2.15 (1.27-3.64) nM to 37.4 (17.1-81.7) nM; for patient 3, from 276 (167-454) nM to 2,024 (1,309-3,130) nM (means and 95% confidence intervals). In patient 2, IC50 values were 2.39 (1.92-2.98) nM for HSJD-NB-004 and 1.06 (0.946-1.18) nM for HSJD-NB-005. Primary cultures from xenograft models from patient 4 (alveolar rhabdomyosarcoma) were highly resistant to SN-38 and IC50 values could not be calculated.

The activity of a single cycle of irinotecan was evaluated in paired models from patients 2 and 3 (Fig. 4B). At day 14, response of neuroblastoma xenografts from patient 2 was predominantly SD (10/11) in the early xenograft and PR (5/11) in the late xenograft. In both Ewing sarcoma xenografts derived from patient 3, 100% tumors achieved complete response. These tumors were followed until day 100 or endpoint. Mice bearing the late model HSJD-ES-006 relapsed in 100% of cases (6/6) achieving endpoint before day 100, whereas 83% (5/6) tumors from the early model HSJD-ES-002 maintained the complete response by day 100.

Expression of BCRP was increased in late xenograft models showing increased resistance to SN-38.

We expected that the expression of genes (ABC transporters) involved in SN-38 efflux would be increased in the cases in which SN-38 was reduced in the intracellular compartment upon tumor evolution (i.e., patients 1, 3 and 4). We found BCRP upregulated in the late model of patient 1, as compared to the early model ($P < 0.05$). Expression of MDR1 and MRP1 was not significantly increased in the late tumors derived from these patients (Figure 5).

Discussion

Our results show for the first time in patient-matched xenografts obtained at different stages of treatment that drug penetration issues might be involved in chemoresistance of pediatric solid tumors acquired upon treatment. Such "pharmacokinetic evolution" of tumors had not been shown to date using *in vivo* models.

Previous studies on the evolution of tumors have been focused in finding genomic alterations, but have not addressed functional changes. Tumors acquire new mutations during treatment that confer a more aggressive phenotype (5,6). A mutational analysis conducted by Johnson *et al.* demonstrated such evolution as a result of treatment pressure in patients with brain tumors. They showed high grade glioma recurrences contained increased number of somatic mutations restricted to the relapsed tumor as compared with the initial one (5). In children with neuroblastoma, several mutations have been identified at relapse, some of them related with signaling pathways involved in

messenchymal transition and tumor suppressor genes such as CHD5 (6). In Ewing sarcoma, treatment pressure also results in an increased number of mutations (which are very few in the original tumors), including TP53 and STAG2 (7). The mentioned changes during treatment are involved in worse prognosis and drug resistance (7,21). The genomic landscape of rhabdomyosarcoma has been studied in samples at diagnosis, showing a low number of mutations, but not in relapsed samples (22).

In neuroblastoma, clonal evolution and chromosomic changes have been identified during the course of therapy and clinical progression, including chromosome 9p losses and changes in ploidy (6,23). Our analysis of copy number alterations in paired early and late xenografts revealed similar changes in neuroblastomas, in contrast with stable chromosomic profile in Ewing sarcoma.

To address our experimental approach there were two main limiting steps to establish the PDX models: (i) the collection of more than one sample from the same patient at different treatment stages, and (ii) the engraftment of the patient sample in immunodeficient mice. We observed that relapse samples are more likely to engraft, as compared to biopsies at diagnosis (data not shown). Overall, our success rate of engraftment (around 30%; not shown) was in line with published records from St. Jude Children's Research Hospital (24).

Once we established the models, our experimental results suggested that pediatric solid tumors acquiring resistance during treatment (patients 1, 3 and 4) evolve towards a "drug-impenetrable" phenotype. In contrast, treatment-refractory tumors at diagnosis (patient 2) did not show such evolution. These functional observations are limited to these specific cases, although they might

explain that drug delivery systems increasing drug distribution in these or similar tumor models are able to improve antitumor efficacy, as we have previously observed with our model drug SN-38 (18), and other authors have shown with the same drug (25).

Using the combined microdialysis-homogenate method we have previously observed changes in the compartmental distribution of topotecan in brain tumors upon the administration of drug transporter inhibitors (14), suggesting that drug transport might be involved in intra-tumor cell drug delivery *in vivo*. Because SN-38 is a substrate of the ABC transporters BCRP, MDR1 and MRP1 (26-28), in the present study we evaluated the gene expression of such transporters in the xenograft pairs. Our finding of BCRP gene overexpressed in the late model of patient 1 (a model with a highly significant shift in the drug distribution phenotype) is consistent with previous findings by Citti *et al.* demonstrating by immunohistochemistry (IHC) increased expression of MDR1 and MRP1 proteins after chemotherapy of pediatric soft tissue sarcomas (29). Another IHC study in patient-matched samples has shown that the transporter lung resistance-related protein (LRP-1) is upregulated in rhabdomyosarcomas after treatment (30). Our attempts to stain and quantify BCRP, MDR1 and MRP1 by IHC did not produce interpretable data (not shown).

Our findings of changes in drug delivery during tumor evolution might be clinically relevant because genes related with drug delivery, such as MRP1 and MRP4, are prognostic indicators of poor outcome in neuroblastoma (31-33). MRP4 also confers resistance to irinotecan in neuroblastoma (33). Henderson *et al.* demonstrated that neuroblastoma tumors can be sensitized to drugs known as MRP1 substrates by pharmacological or genetic inhibition of MRP1

(34). Surprisingly, Henderson *et al.* also determined MRP1 as a contributor in the development of neuroblastoma tumors probably independent of the drug efflux function (34).

In summary, we have identified that drug distribution in tumor cells becomes restricted during tumor evolution under treatment pressure. Our results might be relevant to justify novel treatments that enhance drug delivery in the tumors at relapse.

Acknowledgements

We thank the patient families for supporting our research.

References

1. Mora J, Cruz O, Lavarino C, Rios J, Vancells M, Parareda A, et al. Results of induction chemotherapy in children older than 18 months with stage-4 neuroblastoma treated with an adaptive-to-response modified N7 protocol (mN7). Clin Transl Oncol 2015;17(7):521-9.
2. Mora J, de Torres C, Parareda A, Torner F, Galvan P, Rodriguez E, et al. Treatment of Ewing sarcoma family of tumors with a modified P6 protocol in children and adolescents. Pediatr Blood Cancer 2011;57(1):69-75.
3. Rodriguez-Galindo C, Billups CA, Kun LE, Rao BN, Pratt CB, Merchant TE, et al. Survival after recurrence of Ewing Tumors. Cancer 2002;94(2):561-69.
4. Mazzoleni S, Bisogno G, Garaventa A, Cecchetto G, Ferrari A, Sotti G, et al. Outcomes and prognostic factors after recurrence in children and adolescents with nonmetastatic rhabdomyosarcoma. Cancer 2005;104(1):183-90.
5. Johnson BE, Mazor T, Hong C, Barnes M, Aihara K, McLean CY, et al. Mutational analysis reveals the origin and therapy-driven evolution of recurrent glioma. Science 2014;343(6167):189-93.
6. Schramm A, Koster J, Assenov Y, Althoff K, Peifer M, Mahlow E, et al. Mutational dynamics between primary and relapse neuroblastomas. Nat Genet 2015;47(8):872-77.
7. Crompton BD, Stewart C, Taylor-Weiner A, Alexe G, Kurek KC, Calicchio ML, et al. The genomic landscape of pediatric Ewing sarcoma. Cancer discovery 2014;4(11):1326-41.
8. Hida K, Akiyama K, Ohga N, Maishi N, Hida Y. Tumour endothelial cells acquire drug resistance in a tumour microenvironment. Journal of Biochemistry 2013;153(3):243-49.
9. Oue T, Yoneda A, Uehara S, Yamanaka H, Fukuzawa M. Increased expression of multidrug resistance-associated genes after chemotherapy in pediatric solid malignancies. J Pediatr Surg 2009;44(2):377-80.
10. Zamboni WC, Houghton PJ, Hulstein JL, Kirstein M, Walsh J, Cheshire PJ, et al. Relationship between tumor extracellular fluid exposure to topotecan and tumor response in human neuroblastoma xenograft and cell lines. Cancer Chemother Pharmacol 1999;43(4):269-76.
11. Zamboni WC, Stewart CF, Thompson J, Santana VM, Cheshire PJ, Richmond LB, et al. Relationship between topotecan systemic exposure and tumor response in human neuroblastoma xenografts. J Natl Cancer Inst 1998;90(7):505-11.
12. Patel KJ, Tredan O, Tannock IF. Distribution of the anticancer drugs doxorubicin, mitoxantrone and topotecan in tumors and normal tissues. Cancer Chemother Pharmacol 2013;72(1):127-38.
13. Tredan O, Galmarini CM, Patel K, Tannock IF. Drug resistance and the solid tumor microenvironment. J Natl Cancer Inst 2007;99(19):1441-54.

14. Carcaboso AM, Elmeliegy MA, Shen J, Juel SJ, Zhang ZM, Calabrese C, et al. Tyrosine kinase inhibitor gefitinib enhances topotecan penetration of gliomas. Cancer Res 2010;70(11):4499-508.
15. Wang Y, Welty DF. The simultaneous estimation of the influx and efflux blood-brain barrier permeabilities of gabapentin using a microdialysis-pharmacokinetic approach. Pharm Res 1996;13(3):398-403.
16. Langer O, Karch R, Muller U, Dobrozemsky G, Abrahim A, Zeitlinger M, et al. Combined PET and microdialysis for in vivo assessment of intracellular drug pharmacokinetics in humans. J Nucl Med 2005;46(11):1835-41.
17. Monterrubio C, Paco S, Vila-Ubach M, Rodriguez E, Glisoni R, Lavarino C, et al. Combined Microdialysis-Tumor Homogenate Method for the Study of the Steady State Compartmental Distribution of a Hydrophobic Anticancer Drug in Patient-Derived Xenografts. Pharm Res 2015;32(9):2889-900.
18. Monterrubio C, Pascual-Pasto G, Cano F, Vila-Ubach M, Manzanares A, Schaiquevich P, et al. SN-38-loaded nanofiber matrices for local control of pediatric solid tumors after subtotal resection surgery. Biomaterials 2016;79:69-78.
19. Thompson J, Zamboni WC, Cheshire PJ, Lutz L, Luo X, Li Y, et al. Efficacy of systemic administration of irinotecan against neuroblastoma xenografts. Clin Cancer Res 1997;3(3):423-31.
20. Dharmarajan KV, Wexler LH, Wolden SL. Concurrent radiation with irinotecan and carboplatin in intermediate- and high-risk rhabdomyosarcoma: a report on toxicity and efficacy from a prospective pilot phase II study. Pediatr Blood Cancer 2013;60(2):242-7.
21. Garcia I, Mayol G, Rios J, Domenech G, Cheung NK, Oberthuer A, et al. A three-gene expression signature model for risk stratification of patients with neuroblastoma. Clin Cancer Res 2012;18(7):2012-23.
22. Shern JF, Chen L, Chmielecki J, Wei JS, Patidar R, Rosenberg M, et al. Comprehensive genomic analysis of rhabdomyosarcoma reveals a landscape of alterations affecting a common genetic axis in fusion-positive and fusion-negative tumors. Cancer discovery 2014;4(2):216-31.
23. Mora J, Cheung NK, Gerald WL. Genetic heterogeneity and clonal evolution in neuroblastoma. Br J Cancer 2001;85(2):182-9.
24. Morton CL, Houghton PJ. Establishment of human tumor xenografts in immunodeficient mice. Nat Protoc 2007;2(2):247-50.
25. Sumitomo M, Koizumi F, Asano T, Horiguchi A, Ito K, Kakizoe T, et al. Novel SN-38-incorporated polymeric micelle, NK012, strongly suppresses renal cancer progression. Cancer Res 2008;68(6):1631-5.
26. Houghton PJ, Germain GS, Harwood FC, Schuetz JD, Stewart CF, Buchdunger E, et al. Imatinib mesylate is a potent inhibitor of the ABCG2 (BCRP) transporter and reverses resistance to topotecan and SN-38 in vitro. Cancer Res 2004;64(7):2333-37.

27. Luo FR, Paranjpe PV, Guo A, Rubin E, Sinko P. Intestinal transport of irinotecan in Caco-2 cells and MDCK II cells overexpressing efflux transporters Pgp, cMOAT, and MRP1. Drug Metab Dispos 2002;30(7):763-70.
28. Abdallah EA, Fanelli MF, Souza ESV, Machado Netto MC, Gasparini Junior JL, Araujo DV, et al. MRP1 expression in CTCs confers resistance to irinotecan-based chemotherapy in metastatic colorectal cancer. Int J Cancer 2016;139(4):890-8.
29. Citti A, Boldrini R, Inserra A, Alisi A, Pessolano R, Mastronuzzi A, et al. Expression of multidrug resistance-associated proteins in paediatric soft tissue sarcomas before and after chemotherapy. International journal of oncology 2012;41(1):117-24.
30. Klunder JW, Komdeur R, Van Der Graaf WT, De Bont EJ, Hoekstra HJ, Van Den Berg E, et al. Expression of multidrug resistance-associated proteins in rhabdomyosarcomas before and after chemotherapy: the relationship between lung resistance-related protein (LRP) and differentiation. Human pathology 2003;34(2):150-5.
31. Haber M, Smith J, Bordow SB, Flemming C, Cohn SL, London WB, et al. Association of high-level MRP1 expression with poor clinical outcome in a large prospective study of primary neuroblastoma. J Clin Oncol 2006;24(10):1546-53.
32. Norris MD, Bordow SB, Marshall GM, Haber PS, Cohn SL, Haber M. Expression of the gene for multidrug-resistance-associated protein and outcome in patients with neuroblastoma. N Engl J Med 1996;334(4):231-8.
33. Norris MD, Smith J, Tanabe K, Tobin P, Flemming C, Scheffer GL, et al. Expression of multidrug transporter MRP4/ABCC4 is a marker of poor prognosis in neuroblastoma and confers resistance to irinotecan in vitro. Mol Cancer Ther 2005;4(4):547-53.
34. Henderson MJ, Haber M, Porro A, Munoz MA, Iraci N, Xue C, et al. ABCC multidrug transporters in childhood neuroblastoma: clinical and biological effects independent of cytotoxic drug efflux. J Natl Cancer Inst 2011;103(16):1236-51.

Figures

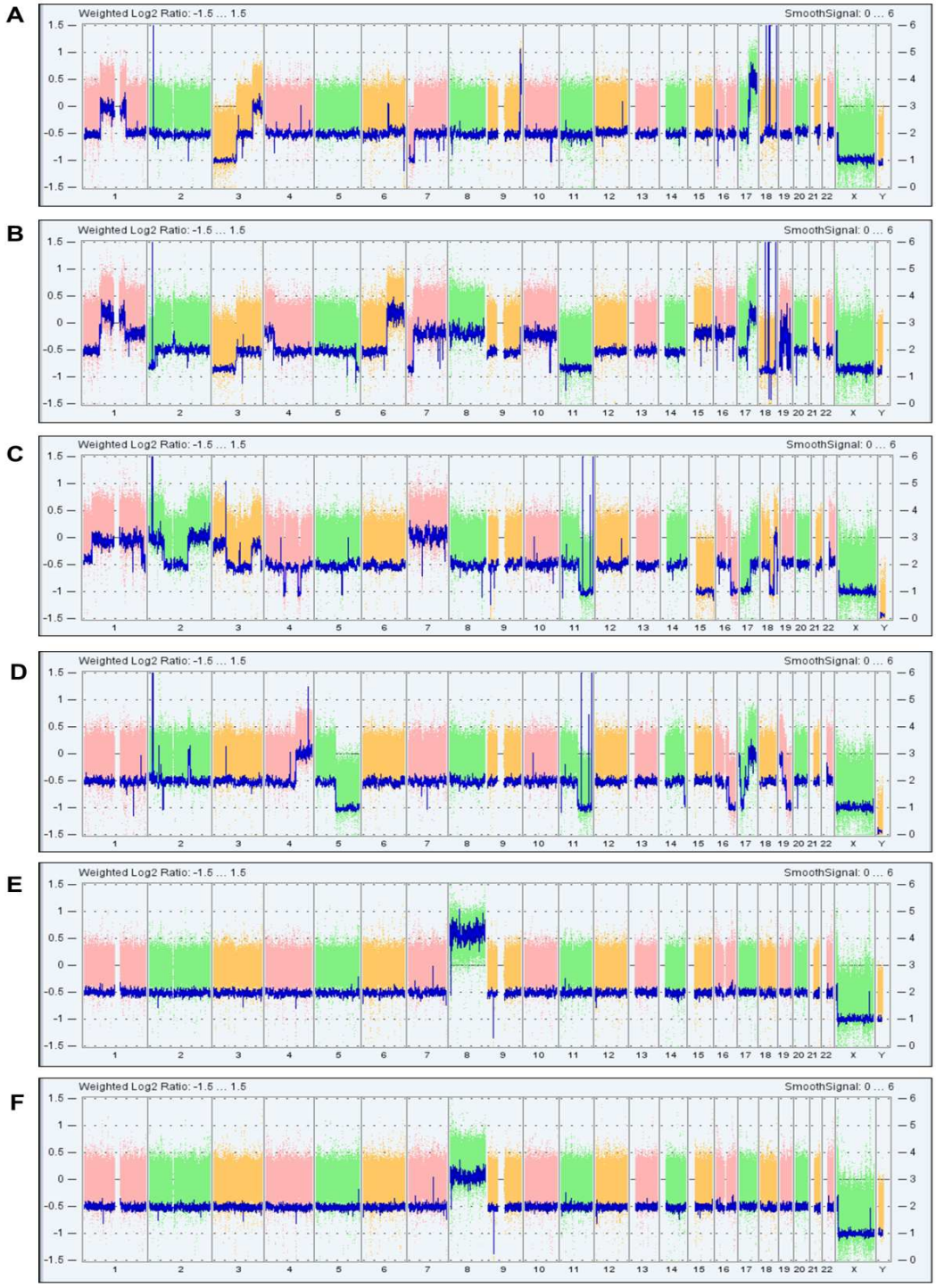

Figure 1. Comparison of whole-genome copy number profiles of paired xenografts derived of tumor biopsies obtained at early and late stages during treatment of patient 1 (A: HSJD-NB-001, early; B: HSJD-NB-002, late), patient 2 (C: HSJD-NB-004, early; D: HSJD-NB-005, late) and patient 3 (E: HSJD-ES-002, early; F: HSJD-ES-006, late). The log2 copy number track and the smooth signal represent the segmental and high copy number (amplification) aberrations observed in the samples. Each column represents a different chromosome.

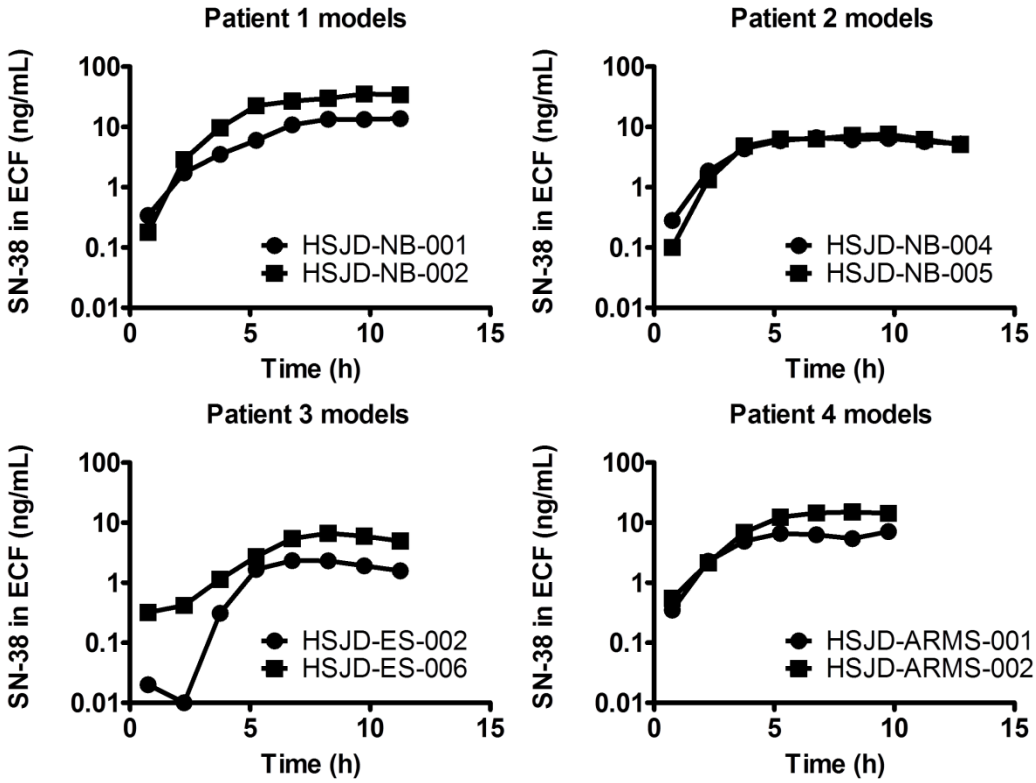

Figure 2. Representative concentration-time data of unbound SN-38 in tECF, obtained from individual microdialysis experiments in paired xenograft models obtained from each patient. Data represented in each curve come from the analysis of tumor dialysates, recovery-corrected, from one single mouse.

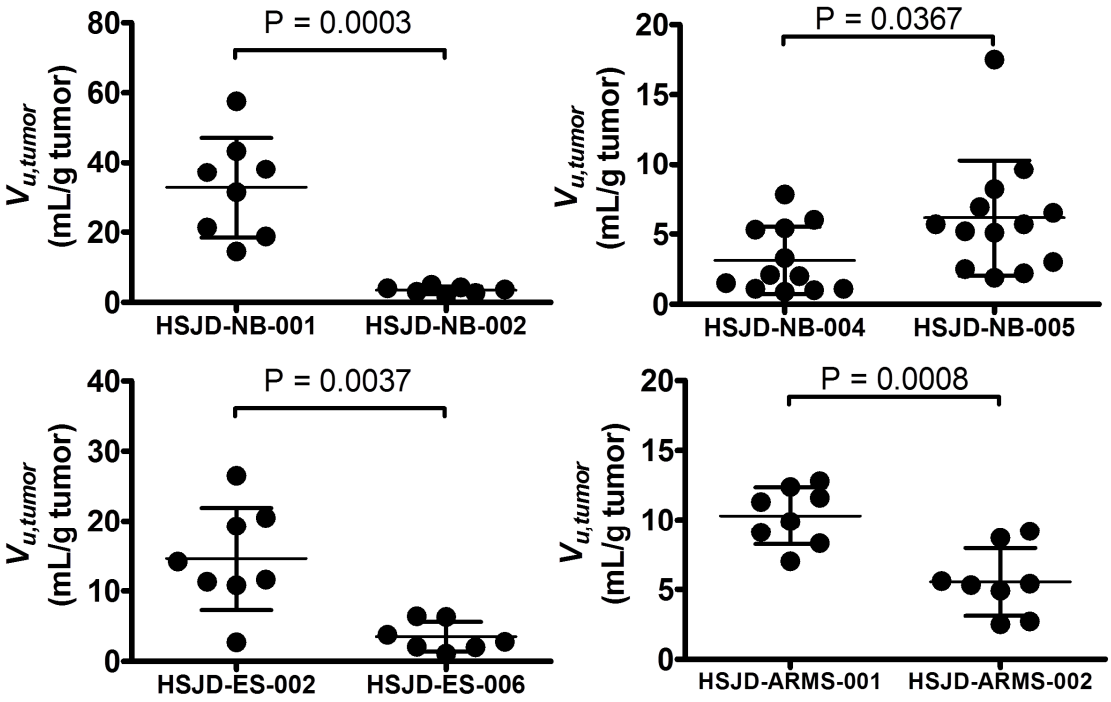

Figure 3. Vu,tumor values (data from individual mice) calculated at steady state in paired tumor models. Points, mean; bars, SD. Values were calculated using the data shown in Table 2 and applying Equation 2.

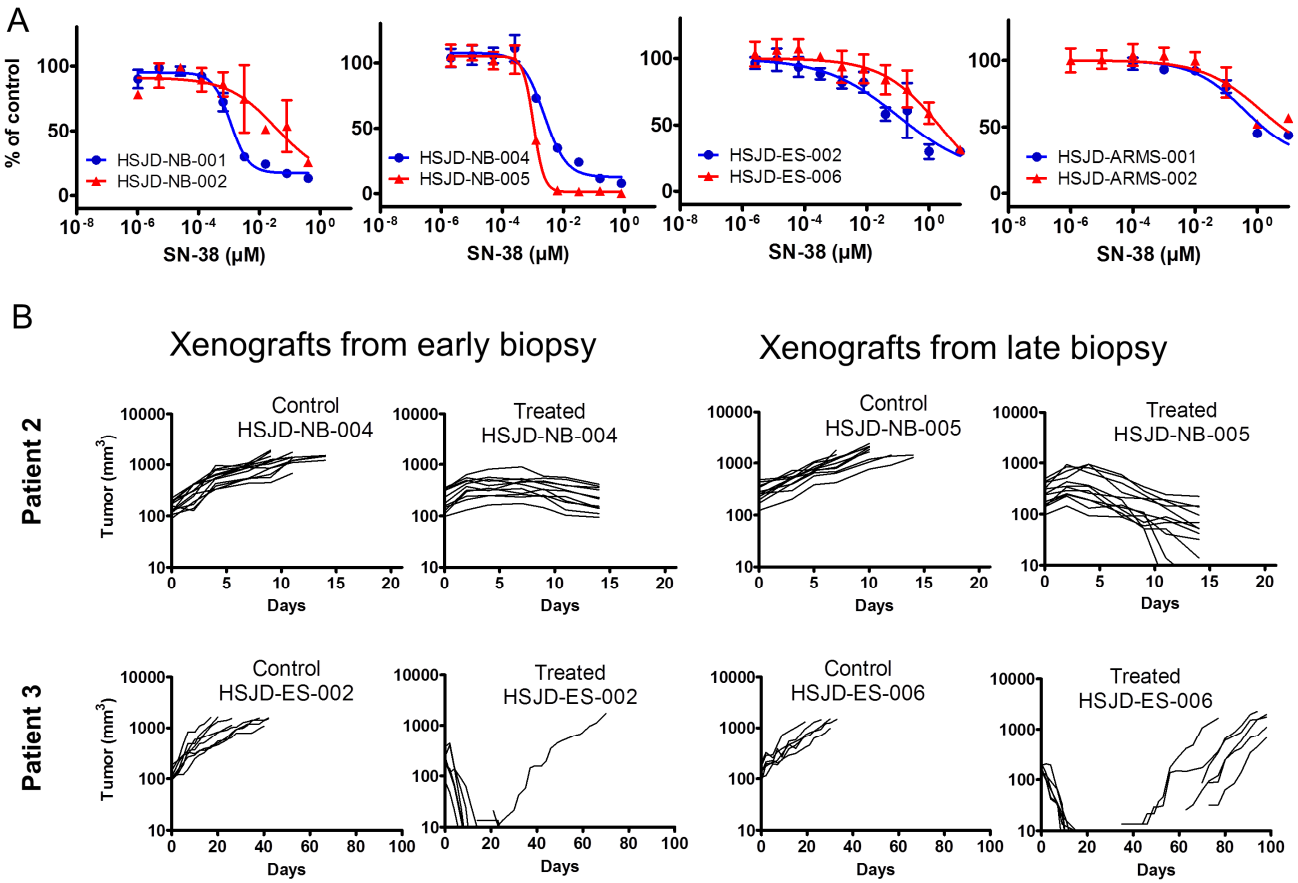

Figure 4. *In vitro* (A) and *in vivo* (B) activity of SN-38 and irinotecan. A) Efficacy of SN-38 against patient-matched tumor models. Dots, mean percentage of growth in treated cells (3-6 replicates), as referenced to untreated controls; bars, SD. Data from models obtained at earlier stages during patient disease are represented in blue. Data from models obtained at later stages are in red. B) Activity of a single cycle of irinotecan in PDX models from patients 2 (HSJD-NB-004 and -005) and 3 (HSJD-ES-002 and -006). Lines represent tumor volumes of individual mice.

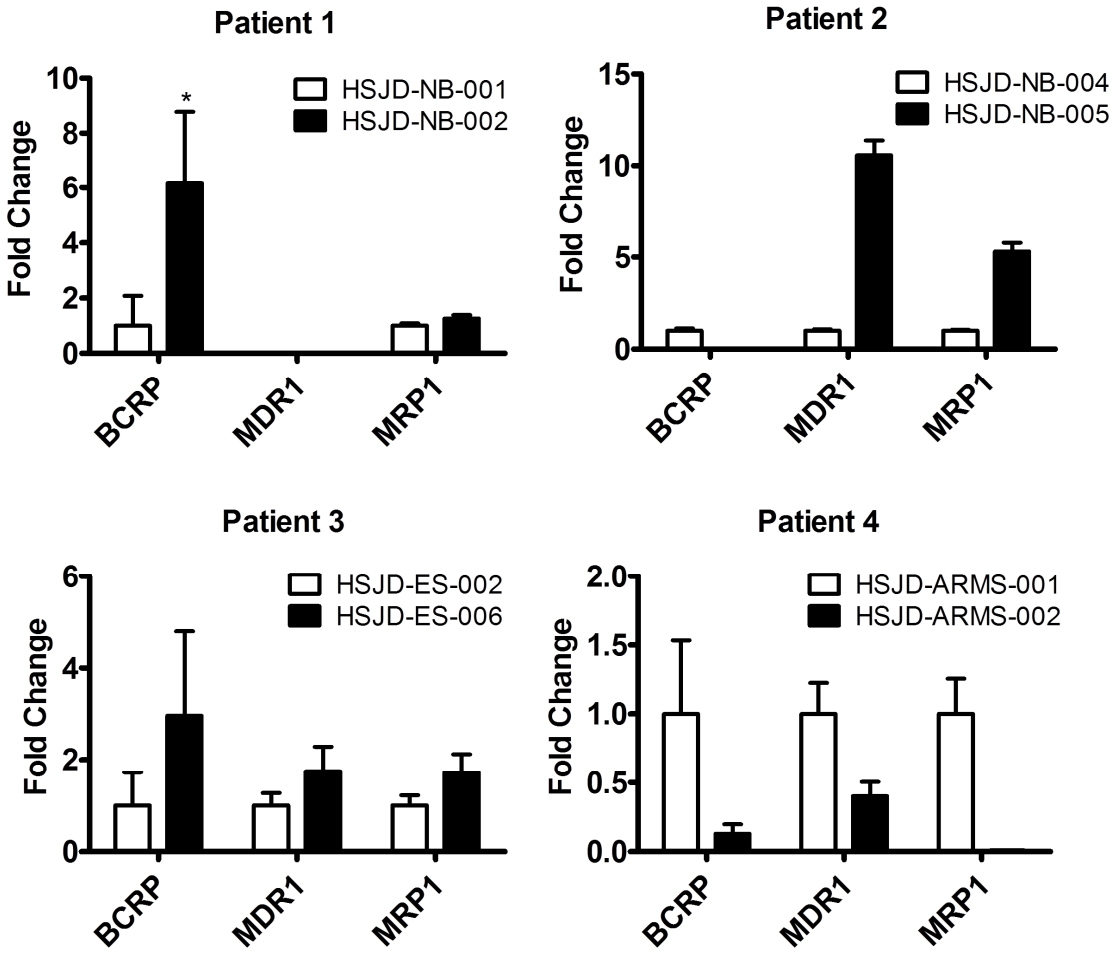

Figure 5. Expression of ABC-transporters BCRP, MDR1 and MRP1 in patient-matched xenografts. Transcript levels in xenografts obtained at later stages during patient treatment (black columns) were quantified relative to those detected in the paired xenografts obtained at earlier stage (white columns); mean and standard deviation. *P = 0.034 as compared to the reference.

Tables

Table 1. Results of the microdialysis experiments in tumor pairs. Data is represented as mean ± SD. Value in parenthesis is the number of mice.

Patient	Tumor model	Disease stage	$C_{ss,tumor}$ (ng/mL)	$C_{ss,plasma}$ (ng/mL)	P_{tumor}[a]
1	HSJD-NB-001	Early	8.4 ± 4.5 (6)	5.2 ± 4.7 (6)	2.6 ± 2.0 (6)
	HSJD-NB-002	Late	16.2 ± 10.0 (5)	5.1 ± 2.5 (5)	3.2 ± 0.8[b] (5)
2	HSJD-NB-004	Early	24.6 ± 26.1 (6)	6.7 ± 2.2 (6)	3.5 ± 3.6 (6)
	HSJD-NB-005	Late	9.5 ± 5.6 (7)	7.6 ± 1.3 (7)	1.2 ± 0.7[c] (7)
3	HSJD-ES-002	Early	3.2 ± 1.8 (3)	4.1 ± 1.3 (3)	1.0 ± 0.9 (3)
	HSJD-ES-006	Late	5.0 ± 2.5 (3)	2.1 ± 0.3 (3)	2.5 ± 1.3[d] (3)
4	HSJD-ARMS-001	Early	4.2 ± 2.4 (3)	3.6 ± 0.9 (3)	1.1 ± 0.4 (3)
	HSJD-ARMS-002	Late	8.8 ± 5.4 (3)	6.3 ± 2.5 (3)	1.4 ± 0.5[e] (3)

[a]Calculated from Equation 1.
[b]P = 0.6055, as compared to paired model.
[c]P = 0.1199, as compared to paired model.
[d]P = 0.1718, as compared to paired model.
[e]P = 0.5023, as compared to paired model.

Table 2. Results of the combined microdialysis-tumor homogenate experiments for tumor pairs. Data is represented as mean ± SD. Value in parenthesis is the number of mice with tumors homogenized.

Patient	Tumor model	$A_{tot,tumor}$ (ng/g tumor)	Mean $V_{tot,blood}$ (mL/g tumor)	$C_{tot,blood}$ (ng/mL)	Mean $C_{ss,tumor}$ (ng/mL)
1	HSJD-NB-001	273.8 ± 119.7 (8)	0.05	6.1 ± 5.1 (8)	8.4
	HSJD-NB-002	57.4 ± 17.0 (7)	0.07	4.7 ± 2.0 (7)	16.2
2	HSJD-NB-004	76.4 ± 58.7 (12)	0.02	6.2 ± 2.3 (12)	24.6
	HSJD-NB-005	58.7 ± 39.3 (13)	0.03	6.9 ± 1.7 (13)	9.5
3	HSJD-ES-002	28.3 ± 14.1 (8)	0.03	3.5 ± 1.0 (8)	3.2
	HSJD-ES-006	17.6 ± 10.5 (7)	0.02	4.0 ± 3.2 (7)	5.0
4	HSJD-ARMS-001	43.7 ± 8.7 (8)	0.03	4.2 ± 1.0 (8)	4.2
	HSJD-ARMS-002	48.9 ± 21.4 (8)	0.02	5.1 ± 2.0 (8)	8.8

Chapter 3:

SN-38-loaded nanofiber matrices for local control of pediatric solid tumors after subtotal resection surgery

In this published work we explain with detail the procedures of generating electrospun polymeric nanofiber matrices for local administration of SN-38 at the tumor site and the preclinical *in vitro* and *in vivo* evaluation. The previously developed microdialysis technique was useful to determine the local PK of SN-38 at the virtual surgical bed when released from this new local DDS as well as to evaluate the extent of diffusion of the SN-38 through the tumor tissue *in vivo*, which was limited to the first millimeters of tissue in contact with the loaded nanofibers.

Biomaterials 79 (2016) 69–78

Contents lists available at ScienceDirect

Biomaterials

journal homepage: www.elsevier.com/locate/biomaterials

SN-38-loaded nanofiber matrices for local control of pediatric solid tumors after subtotal resection surgery

Carles Monterrubio [a, b], Guillem Pascual-Pasto [a, b], Francisco Cano [c], Monica Vila-Ubach [a, b], Alejandro Manzanares [a, d], Paula Schaiquevich [e], Jose A. Tornero [c, f], Alejandro Sosnik [g, h], Jaume Mora [a, b], Angel M. Carcaboso [a, b, *]

[a] Preclinical Therapeutics and Drug Delivery Research Program, Developmental Tumor Biology Laboratory, Fundació Sant Joan de Déu, Santa Rosa 39-57, Esplugues de Llobregat, 08950, Barcelona, Spain
[b] Department of Pediatric Hematology and Oncology, Hospital Sant Joan de Déu Barcelona, Passeig Sant Joan de Déu 2, Esplugues de Llobregat, 08950, Barcelona, Spain
[c] Institut de Investigació Tèxtil i Cooperació Industrial de Terrassa (INTEXTER), Universitat Politecnica de Catalunya, Colom 15, Terrassa, 08222, Barcelona, Spain
[d] Department of Pediatric Surgery, Hospital Sant Joan de Déu Barcelona, Passeig Sant Joan de Déu 2, Esplugues de Llobregat, 08950, Barcelona, Spain
[e] CONICET-Clinical Pharmacokinetics Unit, Hospital de Pediatría JP Garrahan, Combate de los Pozos 1881, 1245, Buenos Aires, Argentina
[f] Cebiotex Biomedical Nanofibers, Parc Cientific de Barcelona, Baldiri i Reixac 4, 08028, Barcelona, Spain
[g] Department of Materials Science and Engineering, Technion-Israel Institute of Technology, Technion City, Haifa, Israel
[h] Russell Berrie Nanotechnology Institute (RBNI), Technion-Israel Institute of Technology, Technion City, Haifa, Israel

ARTICLE INFO

Article history:
Received 1 September 2015
Received in revised form
10 November 2015
Accepted 29 November 2015
Available online 2 December 2015

Keywords:
Local chemotherapy delivery
SN-38
Poly(lactic acid) electrospun nanofibers
Pediatric solid tumor
Pharmacokinetics
Microdialysis

ABSTRACT

In addition to surgery, local tumor control in pediatric oncology requires new treatments as an alternative to radiotherapy. SN-38 is an anticancer drug with proved activity against several pediatric solid tumors including neuroblastoma, rhabdomyosarcoma and Ewing sarcoma. Taking advantage of the extremely low aqueous solubility of SN-38, we have developed a novel drug delivery system (DDS) consisting of matrices made of poly(lactic acid) electrospun polymer nanofibers loaded with SN-38 microcrystals for local release in difficult-to-treat pediatric solid tumors. To model the clinical scenario, we conducted extensive preclinical experiments to characterize the biodistribution of the released SN-38 using microdialysis sampling *in vivo*. We observed that the drug achieves high concentrations in the virtual space of the surgical bed and penetrates a maximum distance of 2 mm within the tumor bulk. Subsequently, we developed a model of subtotal tumor resection in clinically relevant pediatric patient-derived xenografts and used such models to provide evidence of the activity of the SN-38 DDS to inhibit tumor regrowth. We propose that this novel DDS could represent a potential future strategy to avoid harmful radiation therapy as a primary tumor control together with surgery.

1. Introduction

Treatment of most malignant solid tumors in children relies on a combination of local control (surgery and radiation therapy; RT) and systemic chemotherapy [1]. Local tumor recurrence after resection surgery and RT remains a challenge. Despite local control of high-risk neuroblastoma, local tumor recurrences are developed in 10% of newly diagnosed patients and 50% of patients with locally persistent re-resected disease [2,3]. Incidence of local recurrence after first complete remission in other pediatric malignancies such as Ewing sarcoma and primary localized rhabdomyosarcoma is 25% and 22%, respectively [4,5]. The relevance of an adequate local control is underscored by the worse outcome observed in patients that develop local failure after initial complete remission [6].

The intensification of RT to improve local control after resection surgery is limited by unacceptable toxicity, especially in young children [7], and the increased risk of second malignancies [8]. In this context, new technology platforms are urgently called for to overcome the drawbacks associated with RT after tumor resection in children [9].

* Corresponding author. Address: Fundació Sant Joan de Déu, Santa Rosa 39-57, Esplugues de Llobregat, 08950, Barcelona, Spain.
E-mail address: amontero@fsjd.org (A.M. Carcaboso).

http://dx.doi.org/10.1016/j.biomaterials.2015.11.055
0142-9612/

Polymeric drug delivery systems (DDSs) for the localized delivery of anticancer drugs emerged as one of the most promising approaches to treat resectable solid tumors [10]. Advantages of localized delivery comprise reduced systemic exposure to highly toxic agents and achievement of high local concentration of potent anticancer agents that are not suitable for systemic administration due to poor aqueous solubility [10,11]. However, the lack of comprehensive preclinical studies aiming to understand the pharmacokinetics of localized DDS in cancer still represents a significant hurdle towards a robust bench-to-bedside translation. One of the fundamental questions that remain unanswered is whether a substance locally released in the proximity of a solid tumor penetrates into the bulk of the malignant tissue or, conversely, the penetration is restricted to the tumor margins in direct contact with the DDS. To elucidate this, complex imaging techniques [12], radiation [13], or computer simulation [14] are usually required. In a previous study, we demonstrated the potential use of microdialysis to gain insight into these complex mechanisms *in vivo* [15].

SN-38 (10-hydroxy-campthothecin) in its lactone (active) form is a poorly soluble molecule that has shown potent preclinical activity against several pediatric solid tumors [16,17]. Irinotecan, the marketed soluble prodrug of SN-38, undergoes extensive conversion (>70%) to SN-38 in nude mice [18], though it has demonstrated low clinical efficacy, likely due to only partial conversion (less than 10%) into the active derivative upon systemic administration in patients [19]. In addition, SN-38 is rapidly hydrolyzed to an inactive carboxylate form in plasma. The encapsulation of SN-38 into polymeric nanocarriers protected it from biodegradation and prolonged the half-life of the active form [20]. In this framework, SN-38 emerges as an optimal model anticancer drug to investigate the development of a novel DDS for application in the localized chemotherapy of pediatric solid tumors.

Electrospun polymer nanofiber matrices appear as one of the most versatile, reproducible and scalable nano-DDS [21]. They allow to adjust their size and shape to fill the space left by tumor resection, and provide a large surface area and porosity that facilitate the efficient release of the active cargo from the DDS to the tumor tissue [21]. Moreover, their monolithic nature eases manipulation, implantation and retention in the action body site, and prevents the characteristic migration of nanoparticles and microparticles.

Following this rationale, the present work reports for the first time on the development of a novel nanofiber DDS loaded with SN-38 microcrystals for the localized chemotherapy of pediatric solid tumors and the comprehensive characterization of the release rate, the *in vivo* localized biodistribution, the systemic pharmacokinetics and the antitumor activity in pediatric solid tumor models. A unique feature of the study is the use of microdialysis probes inserted in the tissue targeted by the localized release of SN-38 to quantify local drug levels at different depths in the tumor bulk or in the virtual space of the resection bed [15]. To our knowledge, such sampling technique has not yet been employed to monitor localized drug delivery in tumors.

2. Materials and methods

2.1. Reagents

SN-38 was obtained from Seqchem (Pangbourne, UK). Poly(-lactic acid) (PLA) was from Velox, GmbH (Hamburg, Germany). Pluronic® F68 block polymer was a gift from BASF (Ludwigshafen, Germany). Irinotecan was purchased from Hospira (Lake City, IL, USA). 2-Hydroxypropyl-beta-cyclodextrin (HPBCD; molecular weight of 1400 g/mol) and dimethyl sulfoxide (DMSO) were from Sigma–Aldrich (St. Louis, MO, USA). Methanol was from Merck (Darmstad, Germany). RPMI high glucose medium and supplements (fetal bovine serum, glutamine, penicillin and streptomycin) were from Life Technologies (Grand Island, NY, USA).

2.2. Preparation of PLA nanofiber matrices loaded with SN-38 microcrystals

SN-38 microcrystal suspensions were prepared by pH-dependent crystallization the day before the preparation of the nanofiber matrices. The crystallization method takes advantage of the pH-dependent reversible equilibrium between SN-38 carboxylate (water soluble and predominant at basic or neutral pH) and SN-38 lactone (insoluble in water and predominant at acidic pH). To form the microcrystals, one volume (100 μL) of SN-38 solubilized in basic pH (4 mg/mL in NaOH 0.1 N) was mixed with 9 volumes (900 μL) of pH 5.0 acetate buffer containing 2% Pluronic® F68. The mixture resulted in a final pH value of 5.5 and it was stored at 4 °C for 24 h with hourly agitation during the first 6 h to favor the slow precipitation of the SN-38 lactone microcrystals. The size of the crystals at 24 h was measured by dynamic light scattering (DLS) with a ZetaSizer Nano ZS (Malvern Instruments, Malvern, UK).

SN-38 microcrystal-loaded nanofiber matrices were prepared by electrospinning. PLA (10% in dichloromethane) was loaded in a 2 mL syringe and pumped at a constant rate of 0.5 mL/h at a 10 kV voltage. The PLA solution was spun for 20 min on a rotating rod wrapped with vegetal paper, to build a first layer of SN-38-free nanofibers that would prevent the direct release of the intact drug microcrystals to the physiologic medium. During the following 45 min, the SN-38 microcrystal suspension (loaded in a syringe) was pumped (90 μL/min) simultaneously from the opposite part of the rotating rod, and sprayed with a pneumatic nozzle. The theoretical load of SN-38 in the matrix was 18 $\mu g/cm^2$. Finally, after loading the complete suspension of the drug microcrystals, the PLA solution was spun for extra 20 min to generate another free-drug layer that isolates the cargo. Finally, the matrix was dried under vacuum for 24 h, at room temperature. The products (SN-38-loaded nanofiber matrices cut into 0.25, 0.5 or 1 cm^2 sheets) were characterized by scanning electron microscopy (SEM; Phenom G1, Eindhoven, The Netherlands), fluorescence microscopy (Leica DM 5000 B, Wetzlar, Germany), and differential scanning calorimetry (DSC 2 STAR^e system simultaneous thermal analyzer with STAR^e Software V13, Mettler-Toledo, Schwerzenbach, Switzerland) equipped with intra-cooler Huber TC100 under dry N_2 atmosphere and In as standard. The amount of SN-38 loaded in the matrices was analyzed by extraction of the drug with methanol and injection of the extract in a high-performance liquid chromatography (HPLC) system with fluorescence detector, as previously described [15].

2.3. SN-38 release

Several *in vitro* and *in vivo* experiments characterized the release profile of SN-38 from the matrices upon dissolution of internal SN-38 microcrystals in physiologic conditions.

In vitro, SN-38 matrices containing 5 μg SN-38 in 0.25 cm^2 (n = 24) were placed in glass vials with 5 mL of pre-warmed PBS (pH 7.4) and incubated at 37 °C away from light. At time points 0.25, 2, 4, 8, 24, 48, 72 and 96 h, three matrices were removed from the vials for drug analysis by HPLC. The removed matrices were vigorously vortexed in 5 mL methanol to extract the unreleased SN-38 for analysis. To favor sink conditions, the release medium of the remaining matrices was completely replaced with fresh pre-warmed PBS at all sampling times.

We repeated the *in vitro* release experiment described above though in the presence of the solubilizer HPBCD (10% w/v in PBS). The sampling times in these experiments were 0.25, 0.5, 0.75, 1, 2,

4, 8 and 24 h.

In a third experiment, 0.25 cm^2 matrices containing 5 μg SN-38 crystals were introduced in 24 well plates containing 400 μL of cell culture medium (RPMI supplemented with 10% FBS, 2 mM L-glutamine, penicillin 100 U/mL and streptomycin 100 μg/mL) at 37 °C. We used culture medium to simulate the conditions of the *in vitro* cytotoxicity studies. The complete volume was removed for HPLC analysis at 8 h and renewed with fresh medium. At 24 h, SN-38 release was analyzed again.

Finally, SN-38 release *in vivo* was evaluated using 0.5 cm^2 matrices containing 9 μg of SN-38 and subcutaneously (s.c.) implanted in 12 mice. Mice were sacrificed and matrices were removed at different time points (1, 4, 24 and 48 h). The amount of SN-38 remaining in the matrices was extracted with methanol and analyzed as already described.

2.4. Tumor models

Pediatric solid tumor models (neuroblastoma cell lines LAN-1 and SK-N-AS, Ewing sarcoma cell line SK-ES-1 and rhabdomyosarcoma cell line Rh30) were obtained from the repository maintained at Hospital Sant Joan de Déu (HSJD, Barcelona, Spain). Two patient-derived xenografts (PDX), HSJD-NB-005 (neuroblastoma) and HSJD-ES-001 (Ewing sarcoma) were established and maintained in athymic nude mice (Harlan, Barcelona, Spain) as previously described [15,22]. Primary cultures were established by disaggregation of the PDX models with collagenase-DNase enzymes (Sigma–Aldrich). Additional information of the PDX models is available in Table 1 and published elsewhere [23]. The research performed with mice was approved by the institutional ethics committee.

2.5. In vitro activity

The MTS assay (Promega, Fitchburg, WI, USA) was used for determination of cell viability after *in vitro* cytotoxicity experiments. Each treatment condition was assayed at least in triplicate.

To determine the activity of SN-38 against the pediatric solid tumor cell models (LAN-1, SK-N-AS, SK-ES-1 and Rh30 cell lines; HSJD-NB-005 and HSJD-ES-001 primary cultures), we performed assays in 96 well-plates with 3000 cells per well and 3–4 days of incubation with the drug (stock solubilized in DMSO), as previously described [24].

The activity of the SN-38 matrices (0.25 cm^2; 5 μg SN-38) was studied in 24-well plates. For this, 12,000 cells were plated in each well and cultured until they formed monolayers of tumor cells covering the growth area of 1.9 cm^2 provided by the well. In a first experiment, SN-38 matrices were added to the culture monolayers and removed after 8, 24, 48 and 96 h, renewing the culture medium at each time point. After 96 h, cell viability was determined as described before. Blank matrices (no SN-38 content) were used as a control.

In a second experiment, SN-38 matrices were preconditioned in cell culture medium without cells (400 μL) at 37 °C for 24 or 48 h. After the preconditioning stage, the matrices were transferred to the wells with cell monolayers in culture. Thus, a significant fraction of the drug would have been released before cell treatments. After 72 h of incubation, the matrices were removed and the viability of the cells was determined.

In a third assay, blank matrices and SN-38-loaded matrices were co-incubated for 24 h in 24-well plates containing 400 μL cell-free culture medium. Thus, SN-38 from drug-loaded matrices that underwent solubilization in the medium could be absorbed by blank matrices during the co-incubation time. Then, all the matrices were washed by fast immersion in cold PBS, and transferred to 24 well-plates containing tumor cells monolayers in culture. Cell viability was determined after 72 h.

2.6. Systemic pharmacokinetics

One cm^2 SN-38-loaded matrix containing 18 μg SN-38 was implanted s.c. in 6-weeks old athymic nude mice (n = 13). Such administration provides a 1 mg/kg SN-38 dose (the average weight of the mice was 18 g). At 0.25, 0.5, 1, 3, 6, 12, 24 and 48 h after matrix implantation, mice were bled (50 μL) by the retroorbital plexus.

A second group of mice received an intravenous injection of irinotecan at an equimolar dose (44 μg irinotecan trihydrate in 100 μL vehicle) and they were bled at 0.25, 1, 4 and 10 h after injection. To calculate the equimolar dose of irinotecan and SN-38, we considered published work in which 70% of systemic irinotecan is converted to SN-38 in nude mice [18].

A maximum of 3 blood samples were obtained from each mouse. SN-38 in plasma was analyzed as previously described [15]. We used the trapezoid method to calculate the area under the concentration-time curve (AUC) of SN-38 lactone in plasma.

2.7. Local pharmacokinetics of SN-38 matrices in the surgical bed

To study the release of soluble SN-38 in the virtual space of the subcutaneous surgical bed upon administration of SN-38 matrices or soluble prodrug irinotecan, we performed a series of *in vivo* microdialysis experiments in 9 nude mice, as previously described [15]. First, we inserted a CMA 20 microdialysis probe (CMA, Kista, Sweden) s.c. in the flank of the mouse, under isoflurane anesthesia. The probe was infused continuously with perfusate (PBS containing 10% HPBCD) using an infusion pump at 0.5 μL/min. The microdialysis probe was stabilized for 1 h before the administration of the dose. A first group of mice (n = 3) was anesthetized with isoflurane, a small incision was made in the skin 1 cm away from the probe, and a 1 cm^2 SN-38 matrix (18 μg SN-38; 1 mg/kg) was inserted between the probe and the mouse skin. The wound was sutured with clips. A second group (n = 3) was slightly anesthetized with isoflurane to receive a local injection of irinotecan s.c. in the

Table 1
Clinical details of the PDX models.

Model code	Source of biopsy[a]	Age at biopsy	Primary tumor	Age at diagnosis	Metastasis at diagnosis	Demography	Tumor properties	Patient status
HSJD-NB-005	Tumor refractory to treatment (metastasis in bone marrow)	2.5 y	Mass arising from kidney	2.0 y	Yes (ganglia, bone marrow, lungs)	Female, white	Stage 4 neuroblastoma, MYCN amplified, P53 mutation	Died of disease
HSJD-ES-001	Local relapse in scapula[b]	21.7 y	Scapula	17 y	Yes (lungs, bone, bone marrow)	Male, white	EWS-FLI1 fusion gene, STAG2 mutation, P53 mutation	Died of disease

[a] Tumor tissue was collected with informed consent under an Institutional Review Board-approved protocol.
[b] Further details on this tumor are published in Refs. [23], named after the code SJDES023.

probe area, at a dose (44 μg irinotecan in 100 μL) that was equimolar to the one used for SN-38. A third group (n = 3) received 44 μg irinotecan intravenously. Dialyzate samples were collected in an autosampler and analyzed by HPLC [15]. Probes were calibrated using the mean recovery value (70%) previously determined *in vivo* at steady state SN-38 plasma levels [15]. Blood samples (30 μL) were obtained at 0.25, 1, 4 and 24 h after dose administration and every 24 h until the end of the experiment with SN-38 matrices; and at 0.25, 1, 4 and 10 h after irinotecan injections. After HPLC analysis, we calculated the AUC of SN-38 lactone in the surgical bed and plasma from each individual microdialysis experiment.

2.8. Diffusion of locally released SN-38 through the solid tumor tissue

To investigate the depth of local SN-38 diffusion into the extracellular fluid (ECF) of tumor tissue upon localized release in the tumor periphery by SN-38 matrices, we implanted (s.c.) the HSJD-NB-005 PDX model in one flank of 16 mice. When the tumor reached a diameter of at least 10 mm, we anesthetized the mice with isoflurane and inserted a microdialysis probe into the tumor. The 4 mm length probe was introduced so that it was aligned in parallel to the tumor surface, at a determined distance from the tumor surface (range 0–8 mm, depending on each individual experiment).

After probe equilibration, a small incision was made in the skin 1 cm away from the probe, and a 1 cm^2 SN-38-loaded matrix (18 μg SN-38; 1 mg/kg) was inserted in 14 mice between the probe and the mouse skin. In a subgroup of 2 mice, the SN-38 matrix was implanted in the contralateral flank. The wound was sutured with clips. Dialyzate samples were taken overnight. At the endpoint of the experiment the probe was perfused with methylene blue to stain the probe track, the tumor was sectioned transversally to the probe track and the distance between the blue track and the SN-38 matrix was measured with a caliper. After HPLC analysis, we calculated the AUC (0–9 h) of SN-38 lactone in tumor ECF from each individual microdialysis experiment.

2.9. In vivo antitumor activity

We evaluated the local activity of the SN-38 matrices in the PDX models HSJD-NB-005 and HSJD-ES-001. In a first set of experiments, both tumor models were implanted s.c. in both flanks of n = 8 and n = 7 mice, respectively. When the tumors reached 1000–2000 mm^3, we performed a subtotal resection surgery under ketamine-xylazine anesthesia. At that point, tumors were infiltrating the surrounding tissues (muscle and skin). Most of the tumor volume was macroscopically removed from both flanks with the exception of a well-vascularized and viable tumor fragment of approximately 2 × 1 mm (length x width). We covered such tumor rest with one SN-38 matrix in one flank, and a blank matrix in the opposite. Wounds were closed with clips and the animals recovered. The size of tumor recurrences in both flanks was measured with a caliper at different time points during the following 3 weeks.

Finally, we performed a survival experiment in the HSJD-NB-005 PDX model. For the survival studies, 31 nude mice bearing s.c. tumors of 0.1–0.5 cm^3 in one flank were randomized in 4 groups of 7–8 mice for subtotal tumor resection surgery. One group received local SN-38 matrix (18 μg SN-38); a second group was treated with equimolar local s.c. irinotecan; a third group received equimolar systemic irinotecan (via intraperitoneal injection); and a fourth group received a blank matrix on the tumor bed. Tumor recurrences were measured 3 times a week and mice were sacrificed when the tumor diameter reached 2 cm^3. The study finalized at day 100 after resection surgery. Animal survival was defined as the time interval between the initial date of treatment and the date in which 2 cm^3 tumor volume was reached.

2.10. Statistics

Statistical analysis was performed with Graphpad Prism 5 software (La Jolla, CA). Aggregate data are presented as mean ± SD. Pharmacokinetic data was log-transformed before analysis and the one-way ANOVA test with Bonferroni's multiple comparison was used to compare parameters between groups. Paired t test was used to compare tumor size in treated animals with tumors in both flanks (treated *versus* control). Median survivals were calculated using Kaplan–Meier curves and the log-rank test with Bonferroni-corrected threshold was applied for comparison of multiple survival curves.

3. Results

3.1. Characterization of SN-38-loaded matrices

The size of the SN-38 microcrystals before spraying in the nanofiber matrices was 1.7 ± 0.34 μm (mean ± SD z-average; polydispersion index 0.201). SEM analysis of dry matrices showed the presence of SN-38 microcrystals on the surface of PLA nanofibers, covered by a thin layer of surfactant (Fig. 1A). The presence of SN-38 microcrystals in the internal layer of the matrix (Fig. 1B) but not in the external layer (Fig. 1C) was also detected by fluorescence

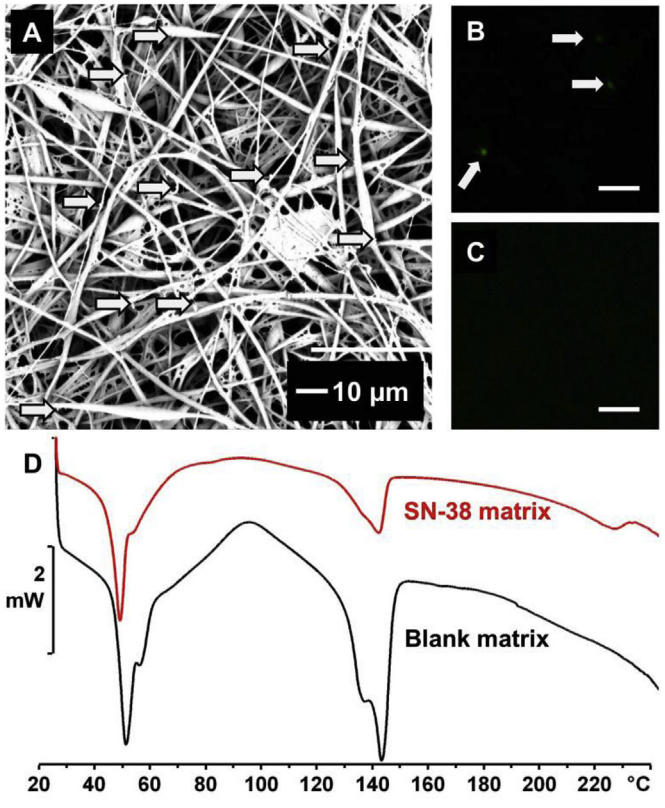

Fig. 1. Physical characterization of the SN-38-loaded matrices. A. SEM micrograph of the internal layer of the nanofiber matrix. Note the fibers are covered by a layer of surfactant (Pluronic F68). SN-38 microcrystals are labeled with arrows. B. Fluorescent image of SN-38 microcrystals in the internal layer of the matrix. Bar = 10 μm. C. Absence of fluorescent SN-38 microcrystals in the external layer of the matrix. Bar = 10 μm. D. DSC thermograms of SN-38-loaded and SN-38 free (blank) matrices. The endothermal peak at 232 °C in the SN-38-loaded matrices corresponds to crystalline SN38.

microscopy.

DSC analysis provided comparable thermograms of blank matrices and SN-38-loaded matrices that included characteristic thermal transitions of semi-crystalline PLA, with the exception of an endothermal peak at 232 °C in the latter that was consistent with the presence of crystalline SN-38 (Fig. 1D). Drug load was analyzed in 1 cm^2 SN-38 matrices containing a theoretical load of 18 μg SN-38/cm^2. Loading efficiency was 97.7 ± 9.2% (mean ± SD; n = 9).

3.2. SN-38 release from matrices

Fig. 2A shows the *in vitro* release profile from SN-38-loaded matrices incubated in the absence of HPBCD solubilizer. Release was sustained in time and achieved 72.1 ± 10.6% of the payload after 96 h of incubation. Unreleased SN-38 remained mainly in the lactone form (98.5 ± 0.2%) and not in the carboxylate one (1.5 ± 0.2%). Drug analysis was not performed in the release medium because, in the absence of HPBCD, SN-38 extensively binds to glassware and plasticware, leading to irreproducible results [15]. As expected, the addition of HPBCD permitted reproducible drug analysis in the release medium in a cumulative release experiment (Fig. 2B). Due to the presence of HPBCD in the release medium, the released SN-38 was water-solubilized and the matrices were completely deprived of the cargo within 24 h; drug load in the matrices was 0.49 ± 0.77% at the end of the study. *In vivo* release data from individual SN-38 matrices overlapped the *in vitro* release curve (Fig. 2A). SN-38 remaining in the matrices of the *in vivo* assay was mainly lactone (93.1 ± 3.2%) over carboxylate SN-38 (6.9 ± 3.2%) at all the time points. In culture medium, SN-38 matrices achieved concentrations above 1 μM (range 0.88–6.07; n = 6) after 8 h of incubation, and above 0.1 μM at 24 h (range 0.14–3.54; n = 6) (Fig. 2C).

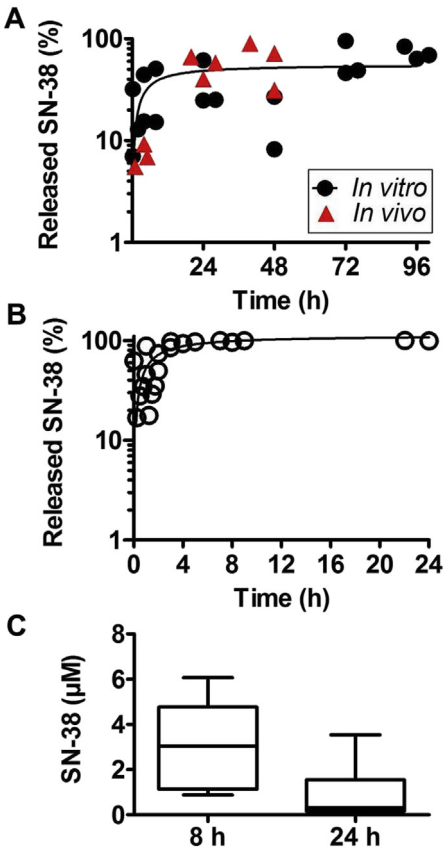

Fig. 2. Release from the SN-38 matrices. A. *In vitro* release profile without solubilizer. The remaining amount of SN-38 was analyzed in individual matrices (n = 24; black dots) and the released drug was calculated as the difference between the theoretical payload (100%) and the remaining drug. *In vivo* release data (red triangles) are superposed in the *in vitro* curve. Each dot represents one individual matrix removed from one mouse (n = 12). B. Cumulative *in vitro* release profile from SN-38 matrices in the presence of HPBCD in the release medium (n = 3). Because SN-38 is unstable upon solubilization in the release medium, release values were corrected to 100% of the amount analyzed by HPLC (i.e., 100% was the sum of the released amounts of drug and the remaining amount analyzed at the end of the experiment). C. Concentrations achieved in cell culture medium (400 μL) upon incubation of SN-38 matrices containing 5 μg SN-38 during 8 or 24 h (n = 6). (For interpretation of the references to colour in this figure legend, the reader is referred to the web version of this article.)

3.3. In vitro activity

As shown in Table 2, all the pediatric solid tumor cell models employed in the study were sensitive to SN-38, and the concentrations causing 50% decrease in cell proliferation (IC50) were in the nM range. The proliferation of culture monolayers exposed to SN-38 matrices was significantly reduced even at short exposures (8 h), as compared to blank matrices that did not induce changes in cell proliferation (Fig. 3A). SN-38-loaded matrices preconditioned in cell culture medium during 24 or 48 h conserved their anti-proliferative activity when transferred to cell monolayers in culture (Fig. 3B). Blank matrices co-cultured with SN-38 matrices and transferred subsequently to cell cultures did not acquire anti-proliferative activity (Fig. 3C).

3.4. Plasma pharmacokinetics

SN-38 lactone levels in mouse plasma are shown in Fig. 4. Mice receiving SN-38 matrices achieved median lactone SN-38 peak plasma level (C_{max}) of 1.05 ng/mL (range 0.53–1.27) at 1 h after s.c. insertion. SN-38 plasma concentrations were below the limit of quantification (0.25 ng/mL) at 12 h. The calculated AUC (0–6 h) was 3.78 ng*h/mL. After intravenous injections, SN-38 plasma levels were fitted to a two compartment model and the extrapolated C_{max} was 122 ng/mL and the calculated AUC (0–7 h) was 104 ng*h/mL.

3.5. SN-38 pharmacokinetics in the surgical bed

Lactone SN-38 concentrations were quantified in the s.c. space and plasma from mice with microdialysis probes placed in the s.c. surgical bed (Fig. 5). SN-38-loaded matrices induced high drug concentrations in the surgical bed (408 ± 284 ng/mL; mean concentration during the first 12 h of three experiments). Such levels were sustained and above 10 ng/mL (i.e. 25 nM; above the IC50 in 4 out of 6 cell models shown in Table 2) until the end of the 4-day microdialysis experiments. A representative experiment in which the probe was in close proximity to the SN-38 matrix is shown in Fig. 5A. In comparison, local s.c. injection of equimolar irinotecan achieved peak levels in the surgical bed of 41.6 ± 3.4 ng/mL (mean C_{max} from 3 experiments), which dropped to less than 10 ng/mL after 7 h (Fig. 5B). Maximum SN-38 levels in the surgical bed of mice injected i.v. were 3.55 ± 1.16 ng/mL and they were below 0.25 ng/mL, the limit of quantification (L.O.Q.), after 6 h (Fig. 5C).

SN-38 plasma levels were slightly above the L.O.Q. only until 6 h in mice receiving SN-38 matrices, as compared to higher plasma levels in mice receiving irinotecan s.c. or i.v. (Fig. 5A–C). SN-38 exposure (AUC) in the surgical bed surrounding the SN-38-loaded matrices, and surgical bed-to-plasma AUC ratio, were at least 2 logs higher as compared to the exposures of animals receiving s.c. or i.v. irinotecan (Fig. 5D and E). Concomitantly, plasma AUC in animals receiving SN-38-loaded matrices was lower than in counterparts receiving irinotecan s.c. or i.v (Fig. 5D).

Table 2
Antiproliferative activity of SN-38 (stock solution in DMSO) against pediatric solid tumor models.

Model	Properties	IC50 (nM)	95% Confidence interval (nM)
LAN-1	NB cell line	60.8	33.1–111
SK-N-AS	NB cell line	215	162–284
HSJD-NB-005	NB PDX primary culture	25.2	17.1–37.1
SK-ES-1	ES cell line	0.927	0.747–1.15
HSJD-ES-001	ES PDX primary culture	1.48	1.06–2.06
Rh30	aRMS cell line	7.57	4.62–12.4

NB: neuroblastoma; ES: Ewing sarcoma; aRMS: alveolar rhabdomyosarcoma.

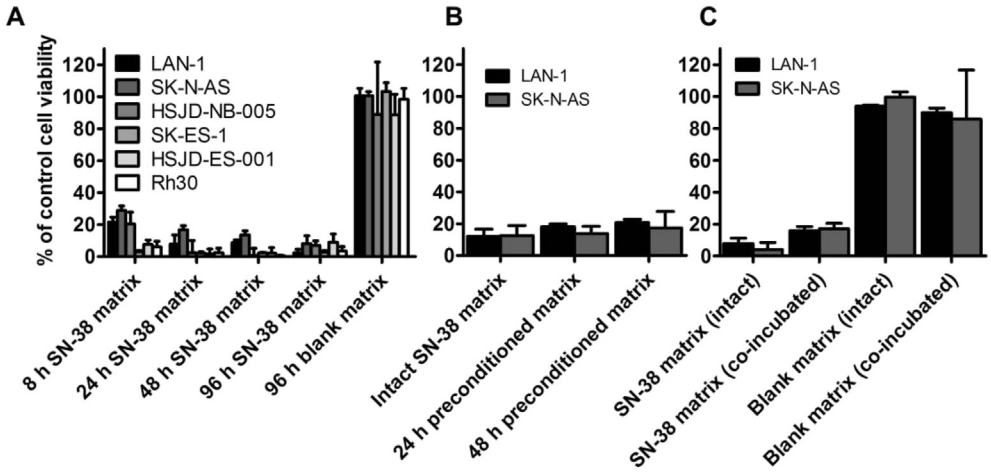

Fig. 3. Antiproliferative activity of the SN-38 matrices. A) Activity of the SN-38 matrices against pediatric cell culture monolayers upon exposures ranging 8–96 h. Blank matrices did not exhibit antiproliferative activity. B) SN-38 matrices preconditioned in cell culture medium during 24 or 48 h conserved their activity, as compared to the activity of the not preconditioned (intact) formulation. C) Blank matrices co-incubated with SN-38 matrices during 24 h did not acquire antiproliferative activity, whereas co-cultured SN-38 matrices conserved their activity as compared to the activity of the intact SN-38 matrices. All the experiments were performed in triplicate.

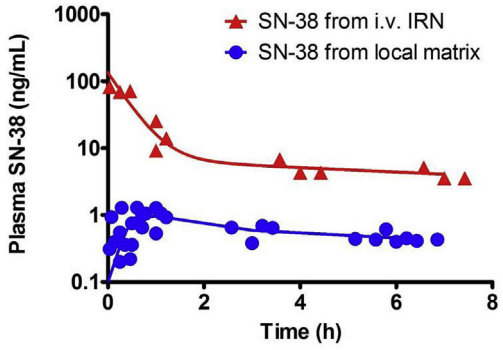

Fig. 4. Plasma concentration-time data of SN-38 lactone upon administration of equimolar dosages of SN-38 matrices (1 mg/kg; s.c.; local matrix) and systemic irinotecan (i.v. IRN) in nude mice (n = 13 and n = 4, respectively).

3.6. Diffusion of locally released SN-38 through the solid tumor tissue

Upon measuring the distance between the peritumoral SN-38-loaded matrix and the intratumoral microdialysis probe track at the experimental endpoint, we grouped the experiments in distance ranges of 0–1 mm (n = 4), 1–2 mm (n = 3), 2–5 mm (n = 4), and 5–10 mm (n = 3). Release from SN-38-loaded matrices resulted in significantly higher SN-38 concentrations in tumor ECF when the probe was placed up to 2 mm distance from the matrix, as compared to when such distance was >2–5 mm ($P < 0.05$; Fig. 6A). Mean SN-38 concentration achieved in the 2–5 mm distance range experiments was 2.0 ± 1.1 ng/mL (i.e., 5.1 ± 2.8 nM) and thus it was below the IC50 of 4 out of 6 cell models studied in this work (Table 2). SN-38 in tumor ECF was undetectable at distances greater than 5 mm or when it was released in the flank contralateral to the tumor. Tumor SN-38 exposures (AUC 0–9 h) were significantly higher in the <1 mm and 1–2 mm distance groups, as compared to the 2–5 mm group ($P < 0.01$ and $P < 0.05$; Fig. 6B). Exposures were below the detection limit when the distance between tumor and probe was greater than 5 mm. Two representative microdialysis experiments are shown from mice with s.c. probes located either in close contact with the matrix (Fig. 6C; < 1 mm) or distant from the matrix (Fig. 6D; 4 mm).

3.7. In vivo antitumor activity

SN-38 matrices delayed tumor growth in the surgical bed after subtotal resection of PDX models HSJD-NB-005 and HSJD-ES-001. Contralateral tumors receiving blank matrices were significantly larger than the treated ones at the studied time points ($P < 0.05$; paired t test; Fig. 7).

3.8. Survival

Median survival of the animals receiving SN-38-loaded matrices (n = 8), blank matrices (n = 8), s.c. irinotecan (n = 7) and systemic irinotecan (n = 8) after subtotal tumor resection was 76, 37, 46 and 40 days, respectively (Fig. 8). Mice treated with SN-38-loaded matrices after surgery survived significantly longer than mice treated with blank matrices ($P = 0.0068$). In contrast, localized s.c. or systemic irinotecan did not provide a significant benefit in

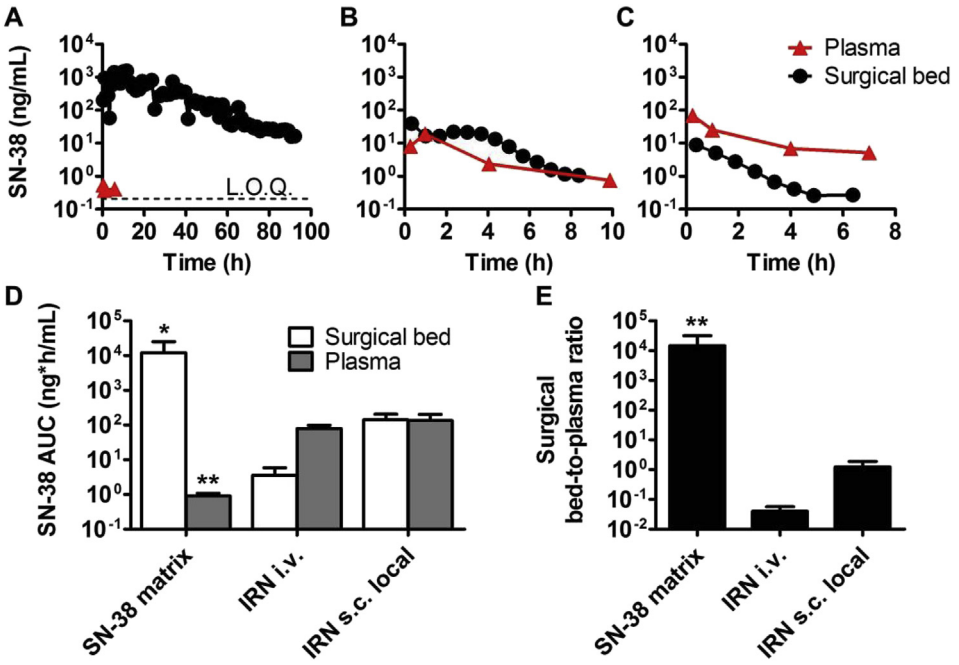

Fig. 5. SN-38 pharmacokinetics in the s.c. surgical bed and in plasma upon administration of equimolar doses from s.c. SN-38 matrices (1 mg/kg) or irinotecan (IRN), either s.c. or i.v. Representative individual experiments are shown in A (SN-38 matrix, s.c.), B (IRN s.c. local), and C (IRN i.v.). Black dots represent SN-38 levels (dialyzable fraction, recovery-corrected) in the virtual space of the s.c. surgical bed. Red triangles are plasma data. L.O.Q: Limit of quantification (0.25 ng/mL). D. SN-38 AUCs in surgical bed and plasma. E. Surgical bed-to-plasma SN-38 AUC ratios. Data are mean ± SD from triplicate experiments. *P < 0.01 and **P < 0.001 as compared to IRN i.v. and IRN s.c. local groups (one-way ANOVA test with Bonferroni's multiple comparison). (For interpretation of the references to colour in this figure legend, the reader is referred to the web version of this article.)

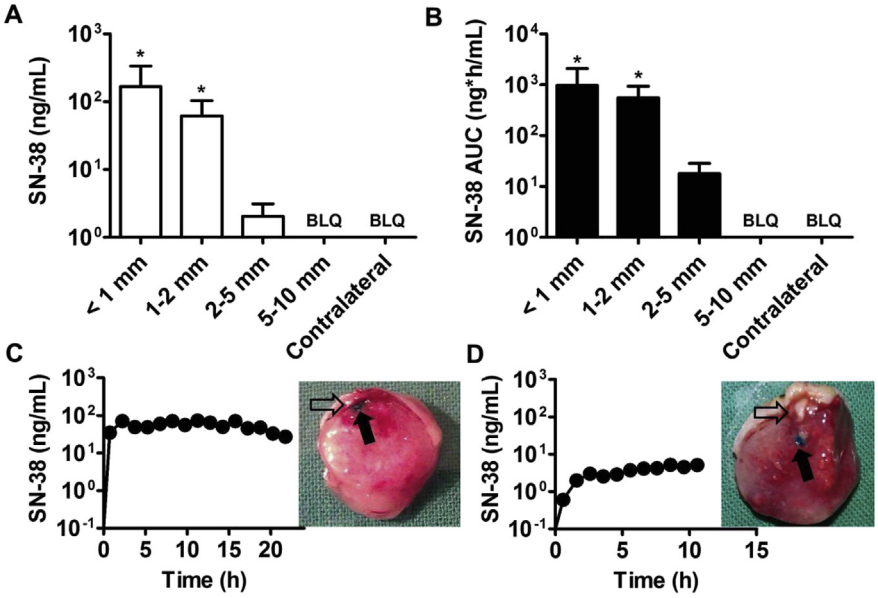

Fig. 6. Intratumoral penetration of SN-38 upon administration of SN-38 matrices. A. SN-38 concentrations in tumor ECF sampled by an intratumoral microdialysis probe positioned at different depths (<1 mm, 1–2 mm, 2–5 mm, 5–10 mm) relative to the position of the SN-38 matrix covering the tumor periphery. Mean ± SD concentrations during the first 9 h of 3–4 experiments are shown. "Contralateral" refers to experiments in which the SN-38 matrix was located s.c. in the flank contralateral to the intratumoral probe (n = 2 experiments). B. AUC data obtained in each relative position (mean ± SD). C, D. Individual microdialysis experiments showing plots of SN-38 levels in tumor ECF. Side pictures in C and D are corresponding tumor sections displaying the relative position between the probe track (black arrow) and the SN-38 matrix (empty arrow). The distance track-matrix was <1 mm in C and 4.3 mm in D. BLQ: Below limit of quantification. *P < 0.05 as compared to the 2–5 mm group (one-way ANOVA test with Bonferroni's multiple comparison).

animal survival (P = 0.3292 and P = 0.5944, respectively) as compared to blank matrices. Treatment with SN-38 matrices performed better than s.c. irinotecan (P = 0.0080). Difference in survival between the SN-38-loaded matrix group and the systemic irinotecan group was not statistically significant (P = 0.120).

4. Discussion

Local tumor control in pediatric oncology requires new treatments in addition to surgery, to delay or replace radiotherapy. However, such innovative treatments are currently unavailable in

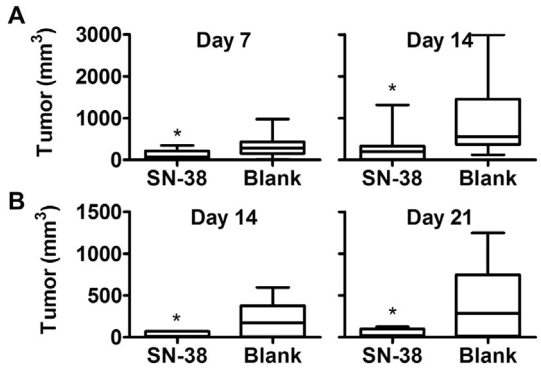

Fig. 7. *In vivo* activity of the SN-38 matrices in HSJD-NB-005 (A) and HSJD-ES-001 (B) PDX models after subtotal bilateral tumor resection. Time from surgery until recurrence in the tumor side treated with SN-38 matrices (SN-38) was significantly delayed as compared to recurrence in the opposite flank treated with blank matrix (Blank). Mean and SD data from 8 to 11 mice with bilateral tumors are represented. *P < 0.05 (Paired t test). Sampling times are different between both models because of different tumor growth kinetics.

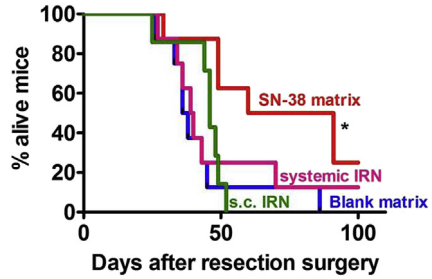

Fig. 8. Survival of mice bearing HSJD-NB-005 tumors, upon subtotal resection and treatment with local SN-38 matrices (SN-38 matrix) or control treatments (Blank matrix, systemic IRN, s.c. IRN). Median survival of each group was determined and the Bonferroni-corrected threshold was applied for comparison of multiple survival curves (i.e. for 4 groups, there are 6 pairwise comparisons). With the Bonferroni correction, P < 0.0083 was considered significant. *P = 0.0080 as compared to control group (Blank matrix).

the clinic. Motivated by this unmet need, we have developed a clinically translatable nano-DDS for the local release of SN-38, a poorly-water soluble camptothecin with proved antitumor activity against several pediatric solid tumors. To select the surgical scenarios in which the new system would be suitable, we first conducted preclinical experiments to characterize the distribution of the released drug in the surgical bed and in the tumor bulk, using microdialysis sampling *in vivo*. We observed that the released drug achieves high concentrations in the virtual space of the surgical bed and it penetrates a maximum distance of 2 mm within the bulk of the tumor. Therefore, we propose that surgeries achieving macroscopically complete resection or minimal tumor residues surrounding vital structures could be optimal candidates for the new treatment strategy. Subsequently, we developed a model of subtotal tumor resection in clinically relevant pediatric PDX models and we used such model to provide evidence of the activity of the SN-38 DDS to inhibit tumor growth after surgical resection.

Irinotecan is potently active as single agent in preclinical models of neuroblastoma [17], rhabdomyosarcoma [25] and Ewing sarcoma (own results in PDX models, unpublished). In our present study, we confirmed the potency of its active metabolite SN-38 against pediatric cancer cell lines and against primary cultures derived from PDX models established at our institution (Tables 1 and 2 and Fig. 3). However, irinotecan in pediatric cancer clinical trials has not replicated the reported preclinical activity, either as single agent [26,27] or combined with other drugs [28]. The reasons for this lack of correlation between preclinical and clinical efficacies are not totally understood, but they could be related to suboptimal SN-38 distribution in human tumors. Greater activity of murine carboxylesterases (the enzymes required to metabolize systemic irinotecan into SN-38) as compared to the human counterparts leads to 70% irinotecan conversion into SN-38 in mice as opposed to less than 10% in humans [18,19,29,30]. As a consequence of this, higher tumor exposure to SN-38 might be achieved in the murine model. Further evidence supports that increased SN-38 exposure in tumors leads to improved survival of mice with aggressive neuroblastoma [31].

The identification of the pharmacokinetic limitations of irinotecan warranted the development of several DDS carrying SN-38 for systemic and local administration [32,33]. In our study, an electrospun nanofiber matrix made of an approved biodegradable biocompatible polyester, PLA, was chosen as drug carrier because the shape and malleability of the matrix is adaptable to the surgical bed that may vary between patients. The manufacturing process (simultaneous microcrystal spraying during polymer electrospinning) was selected after a series of preliminary feasibility studies where the drug was blended with the polymer solution and electrospun, an approach that resulted in extremely slow delivery rates controlled mainly by the polymer degradation (data not shown and [33]). The final configuration took advantage of the poor solubility and dissolution rate of SN-38 in the physiologic medium that was slow enough to produce a bimodal release kinetics (initial fast release and terminal slow release), as demonstrated both *in vitro* and *in vivo* (Fig. 2A,B). This type of release is likely clinically relevant because initially faster release would achieve high local drug concentration (as we demonstrate by the microdialysis sampling approach), whereas long-lasting release at a slower rate could be important for recruiting more tumor cells at the S-phase of the cycle. Because the microcrystals are incrusted in the internal layers of the nanofiber matrix, the drug cannot be released from the DDS unless the fluids permeating through the highly porous nanofiber mesh solubilize it.

To demonstrate that the drug crystals loaded in the polymeric matrix provide a sustained localized release and confer long-term antitumor activity, we performed two specifically designed *in vitro* experiments (preconditioning in culture medium and co-incubation with blank matrices). In fact, preservation of long term activity might be related to the chemical stabilization of the SN-38 lactone in the hydrophobic PLA matrix, in line with previous studies reporting that campthothecins loaded in polymers or gels were stabilized in the active lactone form [34–37]. Drugs blended in polymers are usually in molecular dispersion (amorphous) and not crystalline [38]. Our work shows for the first time that microcrystals of a poorly water-soluble hydrolyzable drug such as SN-38 could be stabilized by incorporation into the nanofiber mesh.

One fundamental contribution of our research in pediatric cancer is the application of the microdialysis method to study local drug delivery to the tumor bulk *in vivo*. In this work, we showed that the local penetration was restricted to 2 mm depth into the solid tumor tissue. These findings are consistent with the report of Arifin et al. using computer simulation that showed penetration of less than 2 mm after local (intracerebral) release of BCNU from Gliadel implants [14]. Interestingly, the Arifin study defined the term “therapeutic penetration” as “the length from the remnant tumor interface for which the drug concentration is above the therapeutic concentration” [14]. Other authors have used terminal sampling methods to propose that localized drug delivery might achieve such therapeutic penetration to ratios greater than 2 mm [38]. However, we suggest that the terminal sampling methods (after animal death) might have overestimated the drug

penetration distance due to maintained drug release from the DDS into the tissue until sample collection. For instance, in a previous study, we demonstrated that upon local administration in the periocular space of topotecan, another camptothecin used in the treatment of pediatric solid tumors like retinoblastoma, postmortem sampling dramatically increased topotecan levels in the posterior segment of the eye (an organ with positive pressure, like most solid tumors). The reason for this observation would be the termination of the active drug elimination process upon the animal death [39]. In another study of local drug release in ocular cancer, we increased intraocular drug distribution by the administration of concomitant local adrenaline to inhibit local blood flow [40]. We thus speculate that the inclusion of vasoconstrictors in the local DDS might help achieve deeper therapeutic drug penetration in solid tumors and further studies will be focused on this topic.

Previous preclinical models of local DDS activity against extracranial tumors have been based on the insertion of the local DDS next to intact solid tumors established in mice, either in s.c. or orthotopic location. In such scenario, local DDS releasing paclitaxel and cisplatin have performed poorly to control s.c. glioma xenografts [41] and mouse uterine tumors [42], respectively. Such results could be explained by our studies of therapeutic penetration into the solid tumor bulk. In contrast, other preclinical models reproduced the context of "microscopic tumor rests", either by the injection of cancer cells on top of a previously implanted local DDS [37] or by the total macroscopic resection of established xenografts previous to the insertion of the local DDS [43–45]. Such strategies have been used in the work of Grinstaff and Colson to study the activity of hydroxycampthothecin-loaded DDS polymer films against lung carcinoma cells [37] and paclitaxel-loaded films against non-small-cell lung cancer cell line xenografts [44] and sarcoma xenografts [43], achieving prolonged control of local tumor recurrences.

The results of our local pharmacokinetic studies led us to design preclinical *in vivo* models resembling subtotal tumor resection surgery. Such surgical model is likely the most realistic approach to study the activity of local DDSs in pediatric oncology because in most patients, especially the ones with stage 4 neuroblastoma, tumors infiltrate or invade tissues surrounding vital vascular structures, a phenomenon that precludes complete tumor resection. Importantly, a recent study has reported on the activity of a doxorubicin-loaded local DDS to control neuroblastoma local recurrences after subtotal resection of orthotopic xenografts of neuroblastoma cell lines [46]. Because SN-38 is not in the standard of care regimen of the pediatric oncologic disease (as opposed to doxorubicin), our candidate DDS would provide an additional alternative in patients previously exposed to doxorubicin and showing resistance or tumor relapse. In addition, we performed all the *in vivo* activity studies in PDX models because they are likely more predictive of drug activity than cell lines and represent a first step towards a personalized therapy [47]. The Ewing sarcoma model HSJD-ES-001 is a subset of aggressive tumor with STAG2 and p53 mutation [48], whereas the neuroblastoma HSJD-NB-005 was derived from a stage 4 neuroblastoma tumor with amplification of MYCN and mutation of p53.

Our first set of *in vivo* studies in mice with bilateral tumors confirmed local activity of the DDS, because control tumors contralateral to the local DDS did not respond to local treatment upon subtotal bilateral resection (Fig. 7). Such selective local activity is further supported by the finding of almost undetectable plasma SN-38 levels upon administration of the matrices, so that contralateral tumors are not exposed to SN-38 (Figs. 4–6). The survival experiment on the neuroblastoma PDX model confirmed that the local DDS provided significant control of tumor recurrence, whilst equimolar injections of irinotecan (either local or systemic) did not perform better than the control treatment with blank matrices. Because a few tumors responded in the group receiving systemic irinotecan upon resection, we did not find a significant difference in survival between the group receiving SN-38 matrices and the one receiving systemic irinotecan. Nevertheless, systemic treatment immediately after resection is not a clinically acceptable practice because systemic drug exposure may lead to hematological (including thrombocytopenia), gastrointestinal and renal adverse effects, among others, that interfere with the surgical recovery. Although it was out of the scope of this work, we did not observe bleeding or alterations in wound healing upon the administration of the local DDS. However, whether the exposure to the local DDS may lead to adverse events in the surgery niche or not should be addressed carefully in future work.

In summary, we have addressed an unmet medical need in pediatric oncology by developing an advanced DDS that localizes the release of an anticancer drug with broad activity spectrum in pediatric cancers. We have also characterized local drug distribution, a procedure that we believe is critical to select the patients that would likely benefit of this novel therapeutic approach. Moreover, due to the potency of the model drug employed for the development, the system could be applicable to other oncologic diseases in which local control is crucial for the improvement of the therapeutic index. Ongoing work in the laboratory is focused on the activity of the new DDS on orthotopic pediatric tumor PDX models, and in the study of the systemic and local toxicology of the DDS upon administration next to vital organs like vessels, nerves and viscera.

Acknowledgments

AMC acknowledges funding from the AECC Scientific Foundation, MINECO (SAF2011-22660), Fundacion BBVA, European Union Seventh Framework Programme (FP7/2007–2013) under Marie Curie International Reintegration Grant (PIRG-08-GA-2010-276998) and ISCIII-FEDER (CP13/00189). AS thanks the Technion (grant # 76535316). Work supported by the Xarxa de Bancs de Tumors de Catalunya (XBTC) sponsored by Pla Director d'Oncologia de Catalunya.

References

[1] A.M. Davidoff, I. Fernandez-Pineda, V.M. Santana, S.J. Shochat, The role of neoadjuvant chemotherapy in children with malignant solid tumors, Sem. Pediatr. Surg. 21 (2012) 88–99.
[2] B.H. Kushner, S. Wolden, M.P. LaQuaglia, K. Kramer, D. Verbel, G. Heller, et al., Hyperfractionated low-dose radiotherapy for high-risk neuroblastoma after intensive chemotherapy and surgery, J. Clin. Oncol. 19 (2001) 2821–2828.
[3] B.S. Rich, M.P. McEvoy, M.P. LaQuaglia, S.L. Wolden, Local control, survival, and operative morbidity and mortality after re-resection, and intraoperative radiation therapy for recurrent or persistent primary high-risk neuroblastoma, J. Pediatr. Surg. 46 (2011) 97–102.
[4] C. Rodriguez-Galindo, F. Navid, T. Liu, C.A. Billups, B.N. Rao, M.J. Krasin, Prognostic factors for local and distant control in Ewing sarcoma family of tumors, Ann. Oncol. 19 (2008) 814–820.
[5] S. Mazzoleni, G. Bisogno, A. Garaventa, G. Cecchetto, A. Ferrari, G. Sotti, et al., Outcomes and prognostic factors after recurrence in children and adolescents with nonmetastatic rhabdomyosarcoma, Cancer 104 (2005) 183–190.
[6] C. Rodriguez-Galindo, C.A. Billups, L.E. Kun, B.N. Rao, C.B. Pratt, T.E. Merchant, et al., Survival after recurrence of Ewing tumors, Cancer 94 (2002) 561–569.
[7] C.H. Pui, A.J. Gajjar, J.R. Kane, I.A. Qaddoumi, A.S. Pappo, Challenging issues in pediatric oncology, Nat. Rev. Clin. Oncol. 8 (2011) 540–549.
[8] R.A. Kleinerman, M.A. Tucker, D.H. Abramson, J.M. Seddon, R.E. Tarone, J.F. Fraumeni Jr., Risk of soft tissue sarcomas by individual subtype in survivors of hereditary retinoblastoma, J. Natl. Cancer Inst. 99 (2007) 24–31.
[9] A. Sosnik, A.M. Carcaboso, Nanomedicines in the future of pediatric therapy, Adv. Drug Deliv. Rev. 73C (2014) 140–161.
[10] J.B. Wolinsky, Y.L. Colson, M.W. Grinstaff, Local drug delivery strategies for cancer treatment: gels, nanoparticles, polymeric films, rods, and wafers, J. Control Release 159 (2012) 14–26.
[11] M.A. Moses, H. Brem, R. Langer, Advancing the field of drug delivery: taking aim at cancer, Cancer Cell. 4 (2003) 337–341.

[12] J.R. Thiagarajah, J.K. Kim, M. Magzoub, A.S. Verkman, Slowed diffusion in tumors revealed by microfiberoptic epifluorescence photobleaching, Nat. Methods 3 (2006) 275–280.
[13] L.K. Fung, M.G. Ewend, A. Sills, E.P. Sipos, R. Thompson, M. Watts, et al., Pharmacokinetics of interstitial delivery of carmustine, 4-hydroperoxycyclophosphamide, and paclitaxel from a biodegradable polymer implant in the monkey brain, Cancer Res. 58 (1998) 672–684.
[14] D.Y. Arifin, K.Y. Lee, C.H. Wang, K.A. Smith, Role of convective flow in carmustine delivery to a brain tumor, Pharm. Res. 26 (2009) 2289–2302.
[15] C. Monterrubio, S. Paco, M. Vila-Ubach, E. Rodriguez, R. Glisoni, C. Lavarino, et al., Combined microdialysis-tumor homogenate method for the study of the steady state compartmental distribution of a hydrophobic anticancer drug in patient-derived xenografts, Pharm. Res. 32 (2015) 2889–2900.
[16] P.J. Grohar, L.E. Segars, C. Yeung, Y. Pommier, M. D'Incalci, A. Mendoza, et al., Dual targeting of EWS-FLI1 activity and the associated DNA damage response with trabectedin and SN38 synergistically inhibits Ewing sarcoma cell growth, Clin. Cancer Res. 20 (2014) 1190–1203.
[17] J. Thompson, W.C. Zamboni, P.J. Cheshire, L. Lutz, X. Luo, Y. Li, et al., Efficacy of systemic administration of irinotecan against neuroblastoma xenografts, Clin. Cancer Res. 3 (1997) 423–431.
[18] C.F. Stewart, W.C. Zamboni, W.R. Crom, P.J. Houghton, Disposition of irinotecan and SN-38 following oral and intravenous irinotecan dosing in mice, Cancer Chemother. Pharmacol. 40 (1997) 259–265.
[19] J.G. Slatter, L.J. Schaaf, J.P. Sams, K.L. Feenstra, M.G. Johnson, P.A. Bombardt, et al., Pharmacokinetics, metabolism, and excretion of irinotecan (CPT-11) following I.V. infusion of [(14)C]CPT-11 in cancer patients, Drug Metab. Dispos. 28 (2000) 423–433.
[20] F. Koizumi, M. Kitagawa, T. Negishi, T. Onda, S. Matsumoto, T. Hamaguchi, et al., Novel SN-38-incorporating polymeric micelles, NK012, eradicate vascular endothelial growth factor-secreting bulky tumors, Cancer Res. 66 (2006) 10048–10056.
[21] A.J. Meinel, O. Germershaus, T. Luhmann, H.P. Merkle, L. Meinel, Electrospun matrices for localized drug delivery: current technologies and selected biomedical applications, Eur. J. Pharm. Biopharm. Off. J. Arbeitsgemeinschaft fur Pharmazeutische Verfahrenstechnik eV 81 (2012) 1–13.
[22] J.L. Ordonez, A.T. Amaral, A.M. Carcaboso, D. Herrero-Martin, M. Del Carmen Garcia-Macias, V. Sevillano, et al., The PARP inhibitor olaparib enhances the sensitivity of ewing sarcoma to trabectedin, Oncotarget 6 (22) (2015) 18875–18890.
[23] B.D. Crompton, C. Stewart, A. Taylor-Weiner, G. Alexe, K.C. Kurek, M.L. Calicchio, et al., The genomic landscape of pediatric Ewing sarcoma, Cancer Discov. 4 (2014) 1326–1341.
[24] A.M. Carcaboso, M.A. Elmeliegy, J. Shen, S.J. Juel, Z.M. Zhang, C. Calabrese, et al., Tyrosine kinase inhibitor gefitinib enhances topotecan penetration of gliomas, Cancer Res. 70 (2010) 4499–4508.
[25] P.J. Houghton, P.J. Cheshire, J.C. Hallman, M.C. Bissery, A. Mathieu-Boue, J.A. Houghton, Therapeutic efficacy of the topoisomerase I inhibitor 7-ethyl-10-(4-[1-piperidino]-1-piperidino)-carbonyloxy-camptothecin against human tumor xenografts: lack of cross-resistance in vivo in tumors with acquired resistance to the topoisomerase I inhibitor 9-dimethylaminomethyl-10-hydroxycamptothecin, Cancer Res. 53 (1993) 2823–2829.
[26] A.S. Pappo, E. Lyden, P. Breitfeld, S.S. Donaldson, E. Wiener, D. Parham, et al., Two consecutive phase II window trials of irinotecan alone or in combination with vincristine for the treatment of metastatic rhabdomyosarcoma: the children's oncology group, J. Clin. Oncol. 25 (2007) 362–369.
[27] B. Morland, K. Platt, J.S. Whelan, A phase II window study of irinotecan (CPT-11) in high risk Ewing sarcoma: a Euro-E.W.I.N.G. study, Pediatr. Blood Cancer 61 (2014) 442–445.
[28] R. Bagatell, W.B. London, L.M. Wagner, S.D. Voss, C.F. Stewart, J.M. Maris, et al., Phase II study of irinotecan and temozolomide in children with relapsed or refractory neuroblastoma: a children's oncology group study, J. Clin. Oncol. 29 (2011) 208–213.
[29] M. Xie, D. Yang, M. Wu, B. Xue, B. Yan, Mouse liver and kidney carboxylesterase (M-LK) rapidly hydrolyzes antitumor prodrug irinotecan and the N-terminal three quarter sequence determines substrate selectivity, Drug Metab. Dispos. 31 (2003) 21–27.
[30] T. Satoh, M. Hosokawa, R. Atsumi, W. Suzuki, H. Hakusui, E. Nagai, Metabolic activation of CPT-11, 7-ethyl-10-[4-(1-piperidino)-1- piperidino]carbonyloxycamptothecin, a novel antitumor agent, by carboxylesterase, Biol. Pharm. Bull. 17 (1994) 662–664.
[31] M.K. Danks, K.J. Yoon, R.A. Bush, J.S. Remack, M. Wierdl, L. Tsurkan, et al., Tumor-targeted enzyme/prodrug therapy mediates long-term disease-free survival of mice bearing disseminated neuroblastoma, Cancer Res. 67 (2007) 22–25.
[32] V. Bala, S. Rao, B.J. Boyd, C.A. Prestidge, Prodrug and nanomedicine approaches for the delivery of the camptothecin analogue SN38, J. Control Release 172 (2013) 48–61.
[33] E.J. Falde, J.D. Freedman, V.L. Herrera, S.T. Yohe, Y.L. Colson, M.W. Grinstaff, Layered superhydrophobic meshes for controlled drug release, J. Control Release 214 (2015) 23–29.
[34] C. Xie, X. Li, X. Luo, Y. Yang, W. Cui, J. Zou, et al., Release modulation and cytotoxicity of hydroxycamptothecin-loaded electrospun fibers with 2-hydroxypropyl-beta-cyclodextrin inoculations, Int. J. Pharm. 391 (2010) 55–64.
[35] A. Shenderova, T.G. Burke, S.P. Schwendeman, The acidic microclimate in poly(lactide-co-glycolide) microspheres stabilizes camptothecins, Pharm. Res. 16 (1999) 241–248.
[36] G. Chang, T. Ci, L. Yu, J. Ding, Enhancement of the fraction of the active form of an antitumor drug topotecan via an injectable hydrogel, J. Control Release 156 (2011) 21–27.
[37] J.B. Wolinsky, R. Liu, J. Walpole, L.R. Chirieac, Y.L. Colson, M.W. Grinstaff, Prevention of in vivo lung tumor growth by prolonged local delivery of hydroxycamptothecin using poly(ester-carbonate)-collagen composites, J. Control Release 144 (2010) 280–287.
[38] S.H. Ranganath, Y. Fu, D.Y. Arifin, I. Kee, L. Zheng, H.S. Lee, et al., The use of submicron/nanoscale PLGA implants to deliver paclitaxel with enhanced pharmacokinetics and therapeutic efficacy in intracranial glioblastoma in mice, Biomaterials 31 (2010) 5199–5207.
[39] A.M. Carcaboso, G.F. Bramuglia, G.L. Chantada, A.C. Fandino, D.A. Chiappetta, M.T. de Davila, et al., Topotecan vitreous levels after periocular or intravenous delivery in rabbits: an alternative for retinoblastoma chemotherapy, Invest Ophthalmol. Vis. Sci. 48 (2007) 3761–3767.
[40] A.M. Carcaboso, D.A. Chiappetta, J.A. Opezzo, C. Hocht, A.C. Fandino, J.O. Croxatto, et al., Episcleral implants for topotecan delivery to the posterior segment of the eye, Invest Ophthalmol. Vis. Sci. 51 (2010) 2126–2134.
[41] S.H. Ranganath, C.H. Wang, Biodegradable microfiber implants delivering paclitaxel for post-surgical chemotherapy against malignant glioma, Biomaterials 29 (2008) 2996–3003.
[42] S. Zong, X. Wang, Y. Yang, W. Wu, H. Li, Y. Ma, et al., The use of cisplatin-loaded mucoadhesive nanofibers for local chemotherapy of cervical cancers in mice, Eur. J. Pharm. Biopharm. Off. J. Arbeitsgemeinschaft fur Pharmazeutische Verfahrenstechnik eV 93 (2015) 127–135.
[43] R. Liu, J.B. Wolinsky, P.J. Catalano, L.R. Chirieac, A.J. Wagner, M.W. Grinstaff, et al., Paclitaxel-eluting polymer film reduces locoregional recurrence and improves survival in a recurrent sarcoma model: a novel investigational therapy, Ann. Surg. Oncol. 19 (2012) 199–206.
[44] R. Liu, J.B. Wolinsky, J. Walpole, E. Southard, L.R. Chirieac, M.W. Grinstaff, et al., Prevention of local tumor recurrence following surgery using low-dose chemotherapeutic polymer films, Ann. Surg. Oncol. 17 (2010) 1203–1213.
[45] S. Liu, X. Wang, Z. Zhang, Y. Zhang, G. Zhou, Y. Huang, et al., Use of asymmetric multilayer polylactide nanofiber mats in controlled release of drugs and prevention of liver cancer recurrence after surgery in mice, Nanomedicine 11 (2015) 1047–1056.
[46] B. Chiu, J. Coburn, M. Pilichowska, C. Holcroft, F.P. Seib, A. Charest, et al., Surgery combined with controlled-release doxorubicin silk films as a treatment strategy in an orthotopic neuroblastoma mouse model, Br. J. Cancer 111 (2014) 708–715.
[47] M. Hidalgo, F. Amant, A.V. Biankin, E. Budinska, A.T. Byrne, C. Caldas, et al., Patient-derived xenograft models: an emerging platform for translational cancer research, Cancer Discov. 4 (2014) 998–1013.
[48] F. Tirode, D. Surdez, X. Ma, M. Parker, M.C. Le Deley, A. Bahrami, et al., Genomic landscape of Ewing sarcoma defines an aggressive subtype with co-association of STAG2 and TP53 mutations, Cancer Discov. 4 (2014) 1342–1353.

Chapter 4:

Targeted polymeric nanoparticles for long-term SN-38 biodistribution and efficacy in GD2-positive pediatric patient-derived xenografts

The development, characterization and efficacy of a new systemic DDS consisting on polymeric monolithic nanoparticles targeted to the ganglioside GD2, a protein highly expressed on the surface of neuroblastoma cells, is exposed in this manuscript. Microdialysis was used to determine SN-38 distribution at the tumor tissue when released from the nanoparticles compared with the commercially available prodrug IRN. *In vivo* studies evaluated the efficacy of this DDS over neuroblastoma PDX implanted in immunodeficient mice as well as drug exposure in plasma and the extracellular fluid of the tumor, showing promising long-term disposition of SN-38 at the tumor site while keeping low plasma concentration.

Submitted manuscript

Targeted polymeric nanoparticles for long-term SN-38 biodistribution and efficacy in GD2-positive pediatric patient-derived xenografts

Carles Monterrubio[1,2], Sonia Paco[1,2], Monica Vila-Ubach[1,2], Mar Ferrandiz-Lorenzo[1,2], Romina Glisoni[3], Nataliya Kuplennik[4], Jaume Mora[1,2], Alejandro Sosnik[4], Angel M. Carcaboso[1,2*]

[1]Developmental Tumor Biology Laboratory, Fundacio Sant Joan de Deu, Barcelona, Spain

[2]Department of Pediatric Hematology and Oncology, Hospital Sant Joan de Deu, Barcelona, Spain

[3]CONICET-Department of Pharmaceutical Technology, Faculty of Pharmacy and Biochemistry, Universidad de Buenos Aires, Argentina

[4]Department of Materials Science and Engineering, Technion-Israel Institute of Technology, Haifa, Israel

Grant information: AECC Scientific Foundation, MINECO (SAF2011-22660 and PRI-AIBAR-2011-0977), Fundacion BBVA, European Union Seventh Framework Programme (FP7/2007-2013) under Marie Curie International Reintegration Grant (PIRG-08-GA-2010-276998) and ISCIII-FEDER (CP13/00189).

*Corresponding author: Angel M. Carcaboso, PhD, Preclinical Therapeutics and Drug Delivery Research Program, Fundacio Sant Joan de Deu, Santa Rosa 39-57, Esplugues de Llobregat, 08950 Barcelona, Spain. +34 936009751; amontero@fsjd.org (A.M. Carcaboso)

Abstract:

Some pediatric solid tumors, such as neuroblastoma, express the tumor antigen ganglioside GD2. It remains not totally understood whether drugs can be targeted, while carried in nanoparticle (NP) formulations, to specific tumor antigens. In this work we have loaded the potent chemotherapy agent SN-38 in polymer nanoparticles conjugated to the anti-GD2 mouse monoclonal antibody 3F8. In animals bearing neuroblastoma patient-derived xenografts, we used a microdialysis technique to sample tumor extracellular fluid upon administration of the 3F8-conjugated (targeted) and nontargeted (conjugated to a similar mouse antibody) formulations. We observed that the extent of penetration of the tumor by unbound SN-38 was significantly higher in mice receiving the targeted formulation. In agreement with the pharmacokinetic result, the antitumor activity of the targeted formulation *in vivo* improved the one provided by the prodrug irinotecan administered at equimolar SN-38 dosages and schedules. Thus, our work shows for the first time that drug delivery can be targeted to antigens expressed by pediatric solid tumors, resulting in improved drug accumulation and efficacy.

Keywords

SN-38, delivery, polymeric nanoparticle, neuroblastoma, distribution, microdialysis, targeted therapy

Neuroblastoma is the most frequent extracranial solid tumor in children under 5 years of age and 50-60% of the patients present high-risk disease.[1,2] Although the standard of care (intensive chemotherapy and surgery) has improved the

outcome of these patients in the past decades, several patients develop chemoresistance.[3] Because inadequate drug distribution within the tumor tissue might play an important role in limiting drug efficacy,[4-8] several nanotechnology approaches are focused on improving drug delivery to tumors.[9]

Tumors may express surface proteins that can be used as potential targets for drug delivery. Active targeting with antibody-drug conjugates likely improves drug distribution in antigen-bearing tumors.[10] However, it remains not totally understood whether drugs can be targeted, while carried in nanoparticle (NP) formulations, to specific tumor antigens. In this context, GD2 ganglioside is a membrane protein highly expressed in the surface of neuroblastoma cells and other pediatric tumors as compared to its expression in healthy tissues.[11-20] Ch14.18 humanized anti-GD2 antibody, commercially known as dinutuximab (Unituxin®, United Therapeutics Corporation, Silver Spring, USA), has been approved for clinical use showing promising results in pediatric patients with high-risk neuroblastoma.[21] Novel paclitaxel-loaded gold nanocarriers target neuroblastoma cells throughout conjugation to the humanized anti-GD2 antibody (Hu14.18K322A), making cells more vulnerable to radiotherapy, thus enhancing neuroblastoma cell death.[22] Although different nanodrugs targeting GD2 have been evaluated,[23-29] whether drug distribution is improved by active targeting rather than by the enhanced permeability and retention effect (EPR)[30] leading to NP accumulation, has not been thoroughly demonstrated. Microdialysis is a sampling technique for the determination of drug concentration in the extracellular fluid (ECF) of tissues.[31-34] The potential of this technique to characterize drug delivery obtained by liposome formulations in tumor ECF (tECF) has been previously demonstrated.[35,36] We have recently

developed a microdialysis technique to assess the intratumor drug distribution of SN-38, a potent topoisomerase-I inhibitor.[34,37] In this study, we have developed SN-38-loaded polymeric NPs conjugated to a murine anti-GD2 monoclonal antibody, 3F8, to target GD2-expressing neuroblastoma cells. We have used the microdialysis technique to study drug distribution in tECF of patient-derived xenograft (PDX) models of neuroblastoma.

RESULTS AND DISCUSSION

Development of GD2-targeted, SN-38-loaded NPs. Our approach to target the potent chemotherapy agent SN-38 in neuroblastoma was substantiated by the low solubility of the drug, that allows encapsulation in hydrophobic biodegradable polymers,[34] the availability of clinical-grade antibodies targeting GD2,[38] and previous work showing the feasibility of clinical translation of similar approaches targeting other cancer antigens.[39] Our first goal was to develop drug-loaded NPs with an appropriate size and technical reproducibility. In preliminary tests we determined that 10% w/w was an appropriate load for SN-38 in PLGA-PEG and PLGA NPs by the single emulsion technique. Then, to provide a hydrophilic surface with chemically reactive groups to conjugate antibodies, we optimized the proportion of our synthetic PLA-PEG-COOH copolymer (Mw 15 kDa as determined by Gel Permeation Chromatography, GPC) in the PLGA polymer. We set such proportion at 5% for further formulations because 10 and 20% batches resulted in unstable emulsions and free SN-38 crystals (Table 1). Upon conjugation of antibodies through EDC/NHS chemistry, Table 1 summarizes the properties of reference NPs (R-

NPs), NPs conjugated to a nonspecific IgG3 (NPs-IgG3) and NPs conjugated to the anti-GD2 mouse monoclonal antibody 3F8 (NPs-3F8). As observed by dynamic light scattering (DLS) and scanning electron microscopy (SEM), mean NP size was below 300 nm and thus it was considered appropriate for the accumulation of NPs in tumors through extravasation[30,40,41] (Figure 1). SEM images showed smooth surface in R-NPs, while the conjugation of both antibodies produced dots smaller than 20 nm in the surface of NPs-3F8 and NPs-IgG3 (Figure 1), similar to the ones previously reported upon conjugation of proteins to monolithic NPs[42] and in line with the reported size of IgG antibodies.[43] Zeta potential and drug load efficiency were in a similar range for the developed formulations with 5% PLA-PEG-COOH (Table 1), including the fluorescent ones (conjugated to FITC).

Because SN-38 crystallizes and adheres to surfaces upon release from NPs in vitro,[34] we included a solubilizer (2-hydroxypropyl-β-cyclodextrin, HPBCD) in the pH 7.4 medium for the release assays. We observed identical release profiles in GD2-targeted and nontargeted NPs, with no relevant burst release and first order release kinetics that achieved the plateau at 48 h and released the complete load in 72 h (Figure 2). This release profile is likely relevant for *in vivo* studies because the drug is released fast enough once in the target tissue, but slow enough while in the systemic blood.

Expression of the tumor antigen GD2 in pediatric solid tumor models. LAN-1 (neuroblastoma cell line) and HeLa cells were selected *a priori* as GD2(+) and GD2(-) models, respectively, because of available data.[44,45] We

confirmed their expected expression of GD2 by immunofluorescence (IF) (Figure 3A). Through a real-time quantitative PCR (RT-qPCR) we quantified the expression of *GD2 synthase* in both models, and also in a battery of neuroblastoma cell lines and pediatric patient-derived xenograft (PDX) models established at our institution including 5 neuroblastomas, 6 Ewing sarcomas and 3 rhabdomyosarcomas (Figure 3B). Upon this analysis, we confirmed the high expression of *GD2 synthase* in most neuroblastomas, as compared to lower or absent expression in Ewing sarcomas and rhabdomyosarcomas. Because adherent cultures of primary PDX models are challenging to establish,[46] we selected the cell lines LAN-1 and HeLa for further *in vitro* assays in adherent conditions, and the high-GD2-expressing PDX HSJD-NB-007 for *in vivo* assays.

Functional stability of 3F8 conjugated in NPs. To evaluate whether the activity of 3F8 antibody was conserved upon chemical conjugation to NPs, we performed a competitive binding assay on plates covered by LAN-1 cells expressing GD2 antigens (Figure 4A). We observed that incremental concentrations of NPs-3F8 added to LAN-1 cells, from 1 µg/mL (Figure 4A) to 1000 µg/mL (Figure 4B), saturated GD2 binding sites for competing free 3F8, in a dose-response fashion (Figure 4C). As controls, NPs-IgG3 (10000 µg/mL) did not compete for GD2 sites on LAN-1 cells (Figure 4D). Thus, it was concluded that 3F8 antibody conserved its selectivity and affinity for GD2 upon chemical conjugation.

Antiproliferative activity of NPs in culture. We evaluated whether the encapsulation of SN-38 in polymer NPs conserved the potent antiproliferative effect of SN-38 *in vitro*. In LAN-1 cells we found that the activity of SN-38-loaded NPs (R-NPs, NPs-IgG3 and NPs-3F8) was in the low nanomolar concentration range, similar to the one of the free drug (SN-38 stock in DMSO) (Figure 5A). The half maximal inhibitory concentration (IC50; mean and 95% confidence intervals) were 5.8 (3.8-8.8) nM for free SN-38, 1.7 (0.65-4.2) nM for R-NPs, 0.54 (0.24-1.2) nM for NPs-IgG3 and 3.3 (1.8-6.4) nM for NPs-3F8. Thus, the conjugation of antibodies on the NPs surface did not decrease significantly the cytotoxicity of SN-38, as previously shown for other SN-38 nanoparticle formulations.[47] We also tested the antiproliferative activity of the antibody 3F8 alone, and found that it inhibited the proliferation of GD2-expressing cells LAN-1 (IC50 1.6 nM; range 0.96-2.5), but not the one of control GD2(-) cells (HeLa) (Figure 5B). This direct antiproliferative effect of 3F8 on the proliferation of LAN-1 cells is consistent with previously reported data.[48]

Distribution of SN-38 in plasma and tumor extracellular fluid (tECF). To answer the question whether GD2 targeting enhances drug delivery in the tECF of GD2(+) neuroblastoma, we obtained pharmacokinetic data from plasma and tumor dialysates of mice with tumors upon receiving either irinotecan or equimolar SN-38 dosages carried by NPs-IgG3 and NPs-3F8. Conjugation of IgG3 in non-targeted formulations allowed discriminating between the nonspecific targeting (produced by the EPR effect *in vivo* or by nonspecific protein-protein binding) and the putative GD2-targeting effect provided by 3F8.

Plasma SN-38 concentration-time curves are shown in Figure 6A. Because total amount of SN-38 in plasma of mice receiving NPs was a combination of SN-38 encapsulated in NPs and SN-38 released from NPs (either bound or unbound to proteins), we processed these samples as ultrafiltrates to determine unbound SN-38 in the released fraction. Then, unbound SN-38 plasma levels were fitted to a two compartment model and the extrapolated peak SN-38 levels (C_{max}) were 28.4, 53.3 and 30.0 ng/mL for irinotecan, NPs-IgG3 and NPs-3F8 groups, respectively. As expected, we observed that the half life of SN-38 in the terminal elimination phase was greater for the NP formulations (3.8 and 5.3 h for NPs-IgG3 and NPs-3F8), as compared to irinotecan (2.1 h), which could be due to sustained release of SN-38 from circulating NPs. Similar pharmacokinetics have been observed in other SN-38-releasing formulations.[49] The calculated areas under the concentration-time curves (AUC) defining plasma exposures to SN-38 are represented in Figure 6C. Lower plasma exposures to unbound SN-38 upon administration of NPs might have implications for safer treatments.[50]

Upon recovery-corrected analysis of tumor dialysates from microdialysis experiments (3-5 individual experiments per condition), we built unbound SN-38 concentration-time curves in the tECF of mice (Figure 6B). SN-38 levels were measurable during periods longer than 24 h after administration of GD2-targeting NPs-3F8 in 3 out of 3 experiments. Two of these experiments reached 48 h with detectable drug levels. In contrast, in 5 out of 5 experiments, SN-38 was below the limit of quantification in tECF after 15 h of a single injection of intravenous irinotecan. Also, mice receiving NPs-IgG3 showed longer SN-38 tECF exposure as compared with the irinotecan group, although SN-38 levels

dropped below the detectable level after 21 h. Mean AUCs of SN-38 in tECF are shown in Figure 6C.

The extent of penetration of the targeted tumor by unbound SN-38, calculated as the mean tECF-to-plasma AUC ratio, was significantly higher in mice receiving NPs-3F8 (Figure 6D). Together, these results suggest that GD2-targeted SN-38 was released slowly in the extracellular compartment of the tumor, due to accumulation of NPs. Whether the NPs remained in the tECF, or reached the intracellular compartment, could not be addressed with our experimental design. We did not analyze SN-38 from tumor homogenates in this study because such analysis would detect a combination of released and unreleased drug in different tumor compartments (intracellular, extracellular, and vascular).[31] In contrast, analysis of dialysates made possible to compare the distribution of free SN-38 in a single compartment (tECF) for the 3 groups. The microdialysis approach has been previously reported to characterize tECF distribution of drugs released from liposomal formulations.[35,36] To our knowledge, our study is the first using microdialysis to characterize tECF distribution of drug released from systemic monolithic polymer formulations, and the first to report enhanced drug distribution in tECF provided by targeting a specific tumor antigen. Because unbound drug concentrations in tECF correlated well with antitumor activity in previous microdialysis studies,[51-53] and protracted exposure to irinotecan and topotecan improve antitumor response,[54-57] our result suggest that GD2 targeted formulations carrying SN-38 might improve activity in neuroblastoma.

Targeted accumulation of NPs in tumor. We used fluorescent NPs to study the GD2-targeting effect of 3F8 conjugation in neuroblastoma, as compared to conjugation to the control murine antibody IgG3. Both fluorescent NPs-IgG3 and NPs-3F8 were detected in the studied tissues, although the intensity of the signal was greater in tumors treated with GD2-targeted NPs (Figure 7A). The tumor-to-liver region of interest (ROI) intensity ratio was 3.4-fold higher for the mouse receiving NPs-3F8, as compared to the mouse receiving NPs-IgG3. Microscopic images from cryosections showed preferential accumulation of NPs-3F8 for the tumor tissue, as compared to other organs (Figure 7B).

In vivo **antitumor activity.** We evaluated the activity of the new NP formulations, administered intravenously twice a week, for 3 weeks, as compared to equimolar irinotecan (same schedule) and the published protracted regimen of irinotecan,[54] in mice bearing the PDX model HSJD-NB-007 (Figure 8A). Treatments were well tolerated by the animals, as shown by their weight curves (Figure 8B). Median survival of the animals receiving 5 days per week for 2 consecutive weeks (n=5), irinotecan 10 mg/kg at days 1 and 4 each week for 3 weeks (n=5), 4 mg/kg SN-38 in NPs-IgG3 at days 1 and 4 each week for 3 weeks (n=5), 4 mg/kg SN-38 in NPs-3F8 at days 1 and 4 each week for 3 weeks (n=5), or control treatment (n=5) was 44, 27.5, 45, 55 and 30 days, respectively (Figure 8C). Mice treated with NPs-3F8 survived significantly longer than control mice (P=0.0064) and both groups of mice treated with irinotecan (P = 0.0067). Difference in survival between NPs-3F8 and NPs-IgG3 was not statistically significant upon application of the Bonferroni correction for comparison of multiple groups (P = 0.0409). NPs-IgG3-treated mice improved

survival versus control mice (P=0064) but not as compared to irinotecan groups (P>0.05).

While irinotecan has shown promising results in preclinical research in mice with neuroblastoma,[58,59] this activity has not been translated to the bedside, probably because of the reduced activity of human carboxylesterases.[60] In this context, SN-38-loaded NK012 NPs have improved the activity of irinotecan in several tumor models, likely because of the better safety/activity profile of SN-38 released by this formulation.[49] Our current work adds relevant evidence that SN-38 delivery can be targeted to antigens expressed by pediatric solid tumors, resulting in improved accumulation and efficacy as compared to non-targeted formulations.

METHODS

Materials. SN-38 was obtained from Seqchem (Pangbourne, UK). Irinotecan for *in vivo* studies was purchased from Hospira (Lake City, IL). Clinical grade mouse monoclonal antibody 3F8 was supplied by Dr. Nai-Kong Cheung at Memorial Sloan Kettering Cancer Center (New York, NY). Murine IgG3 (purified immunoglobulin from murine myeloma, clone DX), HPBCD, polyvinyl alcohol (PVA, Mw 30-70 kDa), 2-(*N*-morpholino)ethanesulfonic acid (MES) buffer, N-hydroxysulfosuccinimide (NHS), 1-Ethyl-3-[3-dimethylaminopropyl]carbodiimide hydrochloride (EDC), 3,6-Dimethyl-1,4-dioxane-2,5-dione (D,L-lactide), stannous octoate (tin(II) octanoate), fluorescein 5(6)-isothiocyanate (FITC, anhydrous acetate, phosphate buffered saline (PBS) tablets, sodium hydroxide (NaOH) and dimethyl sulfoxide (DMSO) were purchased from Sigma-Aldrich

(St. Louis, MO). Tetrahydrofuran (THF) was from Chen Samuel Chemicals (Haifa, Israel). Glacial acetic acid, triethylamine (TEA), ethyl acetate (EtOAc) and di-sodium tetra-borate 10-hydrate were from Panreac (Barcelona, Spain). Water was from Milli-Q water purification system (Millipore, Beldford, MA). Heterobifunctional polyethylene glycol (HO-PEG-COOH, Mw 3,400) was from Laysanbio (Arab, AL, USA). Reagents for cell culture were from Life Technologies (Grand Island, NY, USA).

Preparation of SN-38-loaded NPs targeting GD2. NPs were prepared by a single emulsion method.[39] NP matrix was composed of a mixture of acid-terminated PLGA (Mw 7-17 kDa, Evonik, Germany) and PLA-PEG-COOH (5%:95%). PLA-PEG-COOH was synthetized by the ring-opening polymerization of D,L-lactide by the terminal -OH moieties of HO-PEG-COOH in presence of tin(II) octanoate as catalyst at 145 ºC under magnetic stirring (2.5 h). For the preparation of 200 mg batches of the reference nanoparticle formulation (R-NPs), 9 mg PLA-PEG-COOH were dissolved in 3.6 mL ethyl acetate and added to 171 mg of PLGA. Alternatively, the proportion of PLA-PEG-COOH was increased to 10% and 20% in additional test formulations. Each of the polymer blend solutions was then added to 3.6 mL DMSO containing 20 mg SN-38 (to achieve 10% theoretical load in the final formulation). Blank nanoparticles (without SN-38) were manufactured as controls. The resulting mixture was added to 20 mL of PVA 1% in water (w/v) and sonicated for 30” (2” on – 1” off cycles) in an ice bath. The oil-in-water (o/w) emulsion was immediately added to 240 mL of acetate buffer (pH 4.8) and stirred for 24 h away from light for solvent diffusion and evaporation. The

dispersion of hardened NPs was then centrifuged in 25 mL tubes for 1 h at 60,000 *g*. R-NPs pellets were washed twice in water followed by 30 min 60,000 g centrifugation after each wash. The final pellet was dispersed in 10 mL water containing cryopreservant (100 mg HPBCD), and frozen in liquid nitrogen until lyophilization.

To obtain NPs-3F8 (100 mg), we followed the same steps until the first wash of the hardened R-NPs. Then, the pellet was resuspended in 20 mL MES buffer 0.01 M (pH 5.5) together with 1 mL of NHS and 0.5 mL of EDC, as previously described.[61] EDC and NHS were used to activate the carboxyl groups of PLA-PEG-COOH on the NP surface to form an intermediate that can react with primary amine groups on the antibodies.[61] This solution was stirred for 15 min and washed with 200 mL of MES buffer, followed by 30 min centrifugation at 60,000 g. The pellet was then resuspended in 16 mL PBS 10x, and 3.5 mL MES buffer and 500 µL (100 µg) of 3F8 murine monoclonal antibody in MES buffer were added to the suspension of activated nanoparticles. The solution containing the antibody and the activated nanoparticles was stirred for 3 h away from light. Three final washes with water were performed to remove the excess of antibody, MES buffer and PBS. Finally, the pellet was resuspended in 5 mL of water containing 50 mg HPBCD, frozen and freeze-dried for 72 h. Additionally, NPs conjugated with murine IgG3 (NPs-IgG3; same subclass as 3F8 antibody) were manufactured as control NPs.

To produce fluorescently-labeled polymer, 500 mg PLA-PEG-COOH in 25 mL dimethylformamide reacted with 9.5 mg FITC at RT for 18 h. After 48 h dialysis through 300 kDa MWCO the polymer was freeze-dried. The new FITC-PLA-

PEG-COOH polymer replaced PLA-PEG-COOH in the nanoparticles previously described, to produce FITC-NPs-IgG3 and FITC-NPs-3F8.

Characterization of NPs. Particle size (z-average), polydispersity index (PDI) and zeta potential were determined by DLS with a Zetasizer Nano ZS from Malvern Instruments (Malvern, UK).

SN-38 load in NPs was quantified upon hydrolysis of the polymers in NaOH 0.1 M. To produce working solutions for the calibration curve, SN-38 (stock in DMSO) was diluted in NaOH 0.1 containing hydrolyzed blank nanoparticles (without drug). Appropriate volumes of the working solutions were added to pH 7,4 PBS containing 10% HPBCD (w/v) to build the final calibration curve. HPLC analysis of SN-38 was performed as previously described.[34]

Polymer characterization. PLA-PEG-COOH copolymer Mw and PDI were determined by gel permeation chromatography (GPC, Alliance HPLC system, Waters, Milford, MA) using a refractive index detector and 4 styragel HR (1-4) columns (7.8 x 300 mm, packed with 5 µm particles). Previous to injection, samples were dissolved in THF at a concentration of 1 % (w/v) and filtered through 0.45 µm filters. Runs were conducted at a flow rate of 1 mL/min, at 40℃. Poly(methyl methacrylate) standards (PSS polymer standards service, Mainz, Germany) with Mw 2,260-171,000 Da were used for Mw calibration.

SN-38 release from NPs. To determine the release profile of SN-38 from the nanoparticles, formulations containing 100 µg of encapsulated SN-38 were resuspended in 3 mL of pH 7.4 PBS (10% HPBCD) and loaded into a 40 kDa cutoff Slide-A-Lyzer G2 dialysis cassettes from Thermo Fisher (Waltham, MA). The cassettes were placed individually in hermetic plastic bags with 10 mL of pH 7.4 PBS (10% HPBCD), at 37ºC, in continuous stirring for 96 h. At sampling times 0.5, 1, 2, 4, 6, 8, 12, 24, 48, 72, 96 h, buffer from the airtight plastic bags was completely removed and replaced with fresh buffer. 100 µL of the removed buffer were processed as previously described to analyze SN-38.[34]

Tumor models. Neuroblastomas (LAN-1, SK-N-AS, IMR-5, SK-N-JD, SK-N-LP, SH-EP1 and SH-SY5Y) and HeLa cell lines were obtained from the repository maintained at Hospital Sant Joan de Deu, (HSJD, Barcelona) and cultured as previously described.[34]

Neuroblastoma, Ewing sarcoma and rhabdomyosarcoma PDX models were established from patient biopsies at HSJD under an IRB-approved protocol. HSJD-NB-007 (neuroblastoma) was established from a 5 year old male with progressive stage 4 disease, MYCN-amplified. For *in vivo* studies, fresh tumor fragments (10-50 mm^3) were subcutaneously transplanted to the flank of nude mice. The research conducted with mice adhered to the European regulations and it was approved by the local animal care and use committee (135/11).

Expression of GD2 in tumor models. Selected tumor models were characterized for GD2 antigen expression in cultured cells by an immunological

method.[62] All models were analyzed for relative mRNA expression of *GD2 synthase* by RT-qPCR, as previously described.[62]

***In vitro* binding of 3F8 to GD2.** To determine whether 3F8 monoclonal antibodies were functional upon conjugation to NPs, a competitive binding immunofluorescence assay was performed. The surface of 8-well EMD Millipore Millicell EZ Slides (Millipore, Billerica, MA) was coated with 100,000 LAN-1 ($GD2^+$) or HeLa ($GD2^-$) cells in culture. After 24 h at 37ºC and 5% CO_2, the medium was removed, cells were fixed in paraformaldehyde (4%) for 15 min at 4ºC, washed 3 times (PBS-Tween 0.05%) and blocked with BSA (3% in PBS) for 1 h. Then, either NPs-IgG3 (10,000 µg/mL) or NPs-3F8 (0, 1, 10, 100, 1,000 and 10,000 µg/mL) suspended in fresh culture medium were added to the wells, in triplicate, and incubated for 1 h at RT. Consecutively, a fixed amount of free 3F8 (5 µg in 500 µL) was added to the wells and incubated for 1 h to compete for free GD2 antigens on the cell surfaces. After 3 washes, wells were incubated with FITC-labeled secondary rabbit anti-mouse antibody (1:5,000) and DAPI (to stain nuclei) for 1h at RT. Finally, fluorescence microscopy pictures were obtained (Leica DM 5000 B, Wetzlar, Germany) and quantified by ImageJ (NIH, Bethesda, USA).

In vitro activity of NPs. To study the antiproliferative activity of SN-38, either free (from a stock in DMSO) or carried by R-NPs, NPs-IgG3 or NPs-3F8, 10,000 LAN-1 or HeLa cells were plated in 96-well plates, cultured overnight, and treated with serial dilutions of each formulation. The MTS assay (Promega,

Fitchburg, WI) was used to determine cell viability after 72 h of incubation. IC50 values, defined as the concentrations of drug required to cause a reduction of 50% in cell viability, were calculated with Graphpad Prism 5 software (La Jolla, CA).

Pharmacokinetics of SN-38 in mice with neuroblastoma. To characterize plasma and tECF concentration-time profiles of lactone SN-38 after the intravenous administration of each formulation, 62 mice bearing HSJD-NB-007 tumors received one dose of 4 mg/kg SN-38 in NPs (NP-IgG3 or NPs-3F8), intravenously (i.v.). As reference, a group of mice received 10 mg/kg irinotecan i.v. (equimolar SN-38 dose upon i.v. irinotecan metabolization to SN-38 in mice).[63] Plasma samples were obtained at different time points until 24 h and total lactone SN-38 was quantified after protein precipitation in cold methanol, as described previously.[34] In mice receiving irinotecan, such total SN-38 concentration was the summation of the plasma protein bound and unbound fractions. In this group, the unbound plasma SN-38 concentration was calculated by the application of the plasma protein binding factor (81.4%) calculated in a previous work by the ultrafiltration method.[34] In mice receiving NPs, total SN-38 concentration was the summation of the fraction still encapsulated in NPs and the fraction already released from NPs (either bound or unbound to proteins). In these two groups, one aliquot of each plasma sample was processed also as ultrafiltrate to determine the free fraction (protein unbound) of the released SN-38. Total (bound + unbound) released SN-38 was calculated upon the application of the protein binding factor to the ultrafiltrate (81.4%).

SN-38 plasma levels were fitted to a two compartment model. The maximum concentration achieved in plasma (C_{max}) was calculated by extrapolation at time 0 of the initial fast exponential decay curve.

Long-term delivery of SN-38 in tumor extracellular fluid (tECF) was studied *in vivo* in tumor-bearing mice using intratumoral microdialysis.[34,37] Briefly, 20 kDa cutoff, 4 mm-length microdialysis probes (CMA, Kista, Sweden) were inserted into subcutaneous HSJD-NB-007 tumors implanted in 13 mice under isoflurane anesthesia, and fixed with sutures to the skin. PBS with HPBCD 10% (w/v) was used as perfusion fluid at a flow rate of 0.5 µL/min. After 90 min equilibration, mice received either irinotecan 10 mg/kg, or SN-38 4 mg/kg in NPs-IgG3 or NPs-3F8, and 1.5 h dialysate samples (45 µL) were collected in a CMA 470 refrigerated fraction collector (CMA, Kista, Sweden) as previously described, and stored at -80 ºC until HPLC analysis.[34]

Microdialysis probes were calibrated using the mean recovery value (70%) previously determined *in vivo* at steady state SN-38 plasma levels.[34] AUCs of SN-38 in plasma and tECF dialysates were calculated with the trapezoid method.

Accumulation of NPs in tissues. To explore whether GD2-targeted NPs were preferentially distributed to GD2-positive tumors over non-targeted ones, both FITC-NPs-IgG3 and FITC-NPs-3F8 were intravenously administered via the tail vein in mice bearing HSJD-NB-007 tumors. After 2 h, mice were sacrificed, organs and tumors were immediately collected and macroscopic fluorescence images were taken with a commercial unit (Hamamatsu Photonics, Hamamatsu

City, Japan) with a high sensitivity cooled CCD camera and analyzed with Hokawo imaging software. After imaging, tissues were transferred to a PBS solution with sucrose 30% (w/v) for 48 h away from light. Then, they were frozen in methylbutane and 7 µm cryosections were stained with DAPI and observed under fluorescence microscopy. Results were expressed as the tumor-to-liver intensity ratio in a region of interest (ROI), i.e., the intensity of the signal of tumor ROI was normalized to the intensity of an area-equivalent ROI in the liver of the same mouse.

***In vivo* activity of NPs.** For activity assays in mice we selected the PDX model HSJD-NB-007 upon confirmation of intense expression of *GD2 synthase* by real-time qPCR (Figure 3). Freshly excised tumors from one mouse bearing the second generation of the PDX were fragmented and implanted in 25 nude mice. When the tumors reached 100-300 mm^3, mice were treated with either irinotecan 10 mg/kg per day for 5 days per week for 2 consecutive weeks [(dx5)x2] (n=5 mice),[54] irinotecan 10 mg/kg at days 1 and 4 each week for 3 weeks (n=5), 4 mg/kg SN-38 in NPs-IgG3 at days 1 and 4 each week for 3 weeks (n=5) or 4 mg/kg SN-38 in NPs-3F8 at days 1 and 4 each week for 3 weeks (n=5). The regimen of irinotecan (dx5)x2 has been previously shown active against neuroblastoma,[54] while the regimens in the other groups reduced the dose by 40% as compared to the one of (dx5)x2, and provided equimolar dosages of SN-38. Control mice (n=5) were treated with saline for 3 weeks following the same schedule of these 3 groups. By the end of treatment (day 21), 1 mouse of each group was euthanized and tumors were processed for

IHC analysis of proliferation and cell viability. Tumor growth was measured with an electronic caliper. When tumors reached 2,000 mm^3 mice were euthanized.

Statistics. GraphPad Prism 5 was used to perform the statistical analyses. One-way ANOVA test using the Bonferroni's post test to compare multiple groups was used to determine the differences in the mean tECF AUCs and tECF AUC–to-plasma ratios between treatments. For comparison of multiple survival curves, median survivals (calculated by the Kaplan-Meier method) were compared with the log-rank test with Bonferroni-corrected threshold.

References

1 London, W. B. *et al.* Evidence for an age cutoff greater than 365 days for neuroblastoma risk group stratification in the Children's Oncology Group. *Journal of clinical oncology : official journal of the American Society of Clinical Oncology* **23**, 6459-6465, doi:10.1200/JCO.2005.05.571 (2005).

2 Maris, J. M., Hogarty, M. D., Bagatell, R. & Cohn, S. L. Neuroblastoma. *Lancet* **369**, 2106-2120, doi:S0140-6736(07)60983-0 [pii]

10.1016/S0140-6736(07)60983-0 (2007).

3 Franks, L. M., Bollen, A., Seeger, R. C., Stram, D. O. & Matthay, K. K. Neuroblastoma in adults and adolescents: an indolent course with poor survival. *Cancer* **79**, 2028-2035 (1997).

4 Minchinton, A. I. & Tannock, I. F. Drug penetration in solid tumours. *Nat Rev Cancer* **6**, 583-592, doi:nrc1893 [pii]

10.1038/nrc1893 (2006).

5 Zamboni, W. C. *et al.* Relationship between tumor extracellular fluid exposure to topotecan and tumor response in human neuroblastoma xenograft and cell lines. *Cancer chemotherapy and pharmacology* **43**, 269-276 (1999).

6 Zamboni, W. C. *et al.* Relationship between topotecan systemic exposure and tumor response in human neuroblastoma xenografts. *J Natl Cancer Inst* **90**, 505-511 (1998).

7 Patel, K. J., Tredan, O. & Tannock, I. F. Distribution of the anticancer drugs doxorubicin, mitoxantrone and topotecan in tumors and normal tissues. *Cancer chemotherapy and pharmacology* **72**, 127-138, doi:10.1007/s00280-013-2176-z (2013).

8 Tredan, O., Galmarini, C. M., Patel, K. & Tannock, I. F. Drug resistance and the solid tumor microenvironment. *J Natl Cancer Inst* **99**, 1441-1454, doi:djm135 [pii]

10.1093/jnci/djm135 (2007).

9 Matsumura, Y. Poly (amino acid) micelle nanocarriers in preclinical and clinical studies. *Adv Drug Deliv Rev* **60**, 899-914, doi:S0169-409X(08)00044-6 [pii]

10.1016/j.addr.2007.11.010 (2008).

10 Saunders, L. R. *et al.* A DLL3-targeted antibody-drug conjugate eradicates high-grade pulmonary neuroendocrine tumor-initiating cells in vivo. *Science translational medicine* **7**, 302ra136, doi:10.1126/scitranslmed.aac9459 (2015).

11 Shochat, S. J., Abt, A. B. & Schengrund, C. L. VCN-releasable sialic acid and gangliosides in human neuroblastomas. *J Pediatr Surg* **12**, 413-418 (1977).

12 Kailayangiri, S. *et al.* The ganglioside antigen G(D2) is surface-expressed in Ewing sarcoma and allows for MHC-independent immune targeting. *British journal of cancer* **106**, 1123-1133, doi:10.1038/bjc.2012.57 (2012).

13 Portoukalian, J., David, M. J., Gain, P. & Richard, M. Shedding of GD2 ganglioside in patients with retinoblastoma. *International journal of cancer. Journal international du cancer* **53**, 948-951 (1993).

14 Chang, H. R., Cordon-Cardo, C., Houghton, A. N., Cheung, N. K. & Brennan, M. F. Expression of disialogangliosides GD2 and GD3 on human soft tissue sarcomas. *Cancer* **70**, 633-638 (1992).

15 Heiner, J. P. *et al.* Localization of GD2-specific monoclonal antibody 3F8 in human osteosarcoma. *Cancer research* **47**, 5377-5381 (1987).

16 Modak, S., Gerald, W. & Cheung, N. K. Disialoganglioside GD2 and a novel tumor antigen: potential targets for immunotherapy of desmoplastic small round cell tumor. *Medical and pediatric oncology* **39**, 547-551, doi:10.1002/mpo.10151 (2002).

17 Grant, S. C. *et al.* Targeting of small-cell lung cancer using the anti-GD2 ganglioside monoclonal antibody 3F8: a pilot trial. *European journal of nuclear medicine* **23**, 145-149 (1996).
18 Hamilton, W. B., Helling, F., Lloyd, K. O. & Livingston, P. O. Ganglioside expression on human malignant melanoma assessed by quantitative immune thin-layer chromatography. *International journal of cancer. Journal international du cancer* **53**, 566-573 (1993).
19 Tsuchida, T., Saxton, R. E., Morton, D. L. & Irie, R. F. Gangliosides of human melanoma. *Cancer* **63**, 1166-1174 (1989).
20 Lammie, G., Cheung, N., Gerald, W., Rosenblum, M. & Cordoncardo, C. Ganglioside gd(2) expression in the human nervous-system and in neuroblastomas - an immunohistochemical study. *International journal of oncology* **3**, 909-915 (1993).
21 Dinutuximab approved for high-risk neuroblastoma. *Cancer discovery* **5**, OF5, doi:10.1158/2159-8290.CD-NB2015-044 (2015).
22 Jiao, P. *et al.* Leading neuroblastoma cells to die by multiple premeditated attacks from a multifunctionalized nanoconstruct. *J Am Chem Soc* **133**, 13918-13921, doi:10.1021/ja206118a (2011).
23 Allen, T. M., Brandeis, E., Hansen, C. B., Kao, G. Y. & Zalipsky, S. A new strategy for attachment of antibodies to sterically stabilized liposomes resulting in efficient targeting to cancer cells. *Biochimica et biophysica acta* **1237**, 99-108 (1995).
24 Huwyler, J., Wu, D. & Pardridge, W. M. Brain drug delivery of small molecules using immunoliposomes. *Proceedings of the National Academy of Sciences of the United States of America* **93**, 14164-14169 (1996).
25 Spragg, D. D. *et al.* Immunotargeting of liposomes to activated vascular endothelial cells: a strategy for site-selective delivery in the cardiovascular system. *Proceedings of the National Academy of Sciences of the United States of America* **94**, 8795-8800 (1997).
26 Lopes de Menezes, D. E., Pilarski, L. M. & Allen, T. M. In vitro and in vivo targeting of immunoliposomal doxorubicin to human B-cell lymphoma. *Cancer research* **58**, 3320-3330 (1998).
27 Kirpotin, D. *et al.* Sterically stabilized anti-HER2 immunoliposomes: design and targeting to human breast cancer cells in vitro. *Biochemistry* **36**, 66-75, doi:10.1021/bi962148u (1997).
28 Allen, T. M., Ahmad, I., Lopes de Menezes, D. E. & Moase, E. H. Immunoliposome-mediated targeting of anti-cancer drugs in vivo. *Biochemical Society transactions* **23**, 1073-1079 (1995).
29 Brown, B. S. *et al.* Etoposide-loaded immunoliposomes as active targeting agents for GD2-positive malignancies. *Cancer biology & therapy* **15**, 851-861, doi:10.4161/cbt.28875 (2014).
30 Maeda, H., Wu, J., Sawa, T., Matsumura, Y. & Hori, K. Tumor vascular permeability and the EPR effect in macromolecular therapeutics: a review. *J Control Release* **65**, 271-284, doi:S0168-3659(99)00248-5 [pii] (2000).
31 Carcaboso, A. M. *et al.* Tyrosine kinase inhibitor gefitinib enhances topotecan penetration of gliomas. *Cancer research* **70**, 4499-4508, doi:10.1158/0008-5472.CAN-09-4264

0008-5472.CAN-09-4264 [pii] (2010).
32 de Lange, E. C. *et al.* The use of intracerebral microdialysis for the determination of pharmacokinetic profiles of anticancer drugs in tumor-bearing rat brain. *Pharmaceutical research* **12**, 1924-1931 (1995).
33 Araujo, B. V., Silva, C. F., Haas, S. E. & Dalla Costa, T. Microdialysis as a tool to determine free kidney levels of voriconazole in rodents: a model to study the

technique feasibility for a moderately lipophilic drug. *J Pharm Biomed Anal* **47**, 876-881, doi:10.1016/j.jpba.2008.02.025

S0731-7085(08)00124-6 [pii] (2008).

34 Monterrubio, C. *et al.* Combined Microdialysis-Tumor Homogenate Method for the Study of the Steady State Compartmental Distribution of a Hydrophobic Anticancer Drug in Patient-Derived Xenografts. *Pharmaceutical research*, doi:10.1007/s11095-015-1671-9 (2015).

35 Zamboni, W. C. *et al.* Plasma, tumor, and tissue disposition of STEALTH liposomal CKD-602 (S-CKD602) and nonliposomal CKD-602 in mice bearing A375 human melanoma xenografts. *Clinical cancer research : an official journal of the American Association for Cancer Research* **13**, 7217-7223, doi:13/23/7217 [pii]

10.1158/1078-0432.CCR-07-1035 (2007).

36 Zamboni, W. C. *et al.* Systemic and tumor disposition of platinum after administration of cisplatin or STEALTH liposomal-cisplatin formulations (SPI-077 and SPI-077 B103) in a preclinical tumor model of melanoma. *Cancer chemotherapy and pharmacology* **53**, 329-336, doi:10.1007/s00280-003-0719-4 (2004).

37 Monterrubio, C. *et al.* SN-38-loaded nanofiber matrices for local control of pediatric solid tumors after subtotal resection surgery. *Biomaterials* **79**, 69-78, doi:10.1016/j.biomaterials.2015.11.055 (2016).

38 Suzuki, M. & Cheung, N. K. Disialoganglioside GD2 as a therapeutic target for human diseases. *Expert Opin Ther Targets* **19**, 349-362, doi:10.1517/14728222.2014.986459 (2015).

39 Hrkach, J. *et al.* Preclinical development and clinical translation of a PSMA-targeted docetaxel nanoparticle with a differentiated pharmacological profile. *Science translational medicine* **4**, 128ra139, doi:10.1126/scitranslmed.3003651 (2012).

40 Iyer, A. K., Khaled, G., Fang, J. & Maeda, H. Exploiting the enhanced permeability and retention effect for tumor targeting. *Drug discovery today* **11**, 812-818, doi:10.1016/j.drudis.2006.07.005 (2006).

41 Li, Y., Wang, J., Wientjes, M. G. & Au, J. L. Delivery of nanomedicines to extracellular and intracellular compartments of a solid tumor. *Adv Drug Deliv Rev* **64**, 29-39, doi:10.1016/j.addr.2011.04.006 (2012).

42 Bhakta, S., Seraji, M. S., Suib, S. L. & Rusling, J. F. Antibody-like Biorecognition Sites for Proteins from Surface Imprinting on Nanoparticles. *ACS Appl Mater Interfaces* **7**, 28197-28206, doi:10.1021/acsami.5b11650 (2015).

43 Tan, Y. H. *et al.* A nanoengineering approach for investigation and regulation of protein immobilization. *ACS Nano* **2**, 2374-2384, doi:10.1021/nn800508f (2008).

44 Craddock, J. A. *et al.* Enhanced tumor trafficking of GD2 chimeric antigen receptor T cells by expression of the chemokine receptor CCR2b. *J Immunother* **33**, 780-788, doi:10.1097/CJI.0b013e3181ee6675 (2010).

45 Prapa, M. *et al.* A novel anti-GD2/4-1BB chimeric antigen receptor triggers neuroblastoma cell killing. *Oncotarget* **6**, 24884-24894, doi:10.18632/oncotarget.4670 (2015).

46 DeRose, Y. S. *et al.* Tumor grafts derived from women with breast cancer authentically reflect tumor pathology, growth, metastasis and disease outcomes. *Nat Med* **17**, 1514-1520, doi:10.1038/nm.2454 (2011).

47 Koizumi, F. *et al.* Novel SN-38-incorporating polymeric micelles, NK012, eradicate vascular endothelial growth factor-secreting bulky tumors. *Cancer research* **66**, 10048-10056, doi:66/20/10048 [pii]

10.1158/0008-5472.CAN-06-1605 (2006).

48 Cheung, N.-K. V., Guo, H., Hu, J., Tassev, D. V. & Cheung, I. Y. Humanizing murine IgG3 anti-GD2 antibody m3F8 substantially improves antibody-dependent cell-mediated cytotoxicity while retaining targeting in vivo. *Oncoimmunology* **1**, 477-486 (2012).
49 Matsumura, Y. Preclinical and clinical studies of NK012, an SN-38-incorporating polymeric micelles, which is designed based on EPR effect. *Adv Drug Deliv Rev* **63**, 184-192, doi:10.1016/j.addr.2010.05.008 (2011).
50 Nagano, T. *et al.* Antitumor activity of NK012 combined with cisplatin against small cell lung cancer and intestinal mucosal changes in tumor-bearing mouse after treatment. *Clinical cancer research : an official journal of the American Association for Cancer Research* **15**, 4348-4355, doi:10.1158/1078-0432.CCR-08-3334

1078-0432.CCR-08-3334 [pii] (2009).
51 Daryani, V. M. *et al.* Translational Pharmacokinetic-Pharmacodynamic Modeling and Simulation: Optimizing 5-Fluorouracil Dosing in Children With Pediatric Ependymoma. *CPT Pharmacometrics Syst Pharmacol*, doi:10.1002/psp4.12075 (2016).
52 Atkinson, J. M. *et al.* An integrated in vitro and in vivo high-throughput screen identifies treatment leads for ependymoma. *Cancer Cell* **20**, 384-399, doi:10.1016/j.ccr.2011.08.013

S1535-6108(11)00310-2 [pii] (2011).
53 Morfouace, M. *et al.* Pemetrexed and gemcitabine as combination therapy for the treatment of Group3 medulloblastoma. *Cancer Cell* **25**, 516-529, doi:10.1016/j.ccr.2014.02.009 (2014).
54 Thompson, J. *et al.* Efficacy of systemic administration of irinotecan against neuroblastoma xenografts. *Clinical cancer research : an official journal of the American Association for Cancer Research* **3**, 423-431 (1997).
55 Santana, V. M. *et al.* Improved response in high-risk neuroblastoma with protracted topotecan administration using a pharmacokinetically guided dosing approach. *Journal of clinical oncology : official journal of the American Society of Clinical Oncology* **23**, 4039-4047, doi:23/18/4039 [pii]

10.1200/JCO.2005.02.097 (2005).
56 Houghton, P. J. *et al.* Efficacy of topoisomerase I inhibitors, topotecan and irinotecan, administered at low dose levels in protracted schedules to mice bearing xenografts of human tumors. *Cancer Chemother.Pharmacol* **36**, 393-403 (1995).
57 Furman, W. L. *et al.* Direct translation of a protracted irinotecan schedule from a xenograft model to a phase I trial in children. *Journal of clinical oncology : official journal of the American Society of Clinical Oncology* **17**, 1815-1824 (1999).
58 Santos, A. *et al.* In vivo treatment with CPT-11 leads to differentiation of neuroblastoma xenografts and topoisomerase I alterations. *Cancer research* **64**, 3223-3229 (2004).
59 Choi, S. H., Tsuchida, Y. & Yang, H. W. Oral versus intraperitoneal administration of irinotecan in the treatment of human neuroblastoma in nude mice. *Cancer Lett* **124**, 15-21 (1998).
60 Xie, M., Yang, D., Wu, M., Xue, B. & Yan, B. Mouse liver and kidney carboxylesterase (M-LK) rapidly hydrolyzes antitumor prodrug irinotecan and the N-terminal three quarter sequence determines substrate selectivity. *Drug metabolism and disposition: the biological fate of chemicals* **31**, 21-27 (2003).
61 Betancourt, T. *et al.* PEGylation strategies for active targeting of PLA/PLGA nanoparticles. *J Biomed Mater Res A* **91**, 263-276, doi:10.1002/jbm.a.32247 (2009).

62 Pascual-Pasto, G. *et al.* Preclinical platform of retinoblastoma xenografts recapitulating human disease and molecular markers of dissemination. *Cancer Lett* **380**, 10-19, doi:10.1016/j.canlet.2016.06.012 (2016).

63 Stewart, C. F., Zamboni, W. C., Crom, W. R. & Houghton, P. J. Disposition of irinotecan and SN-38 following oral and intravenous irinotecan dosing in mice. *Cancer chemotherapy and pharmacology* **40**, 259-265 (1997).

Figures

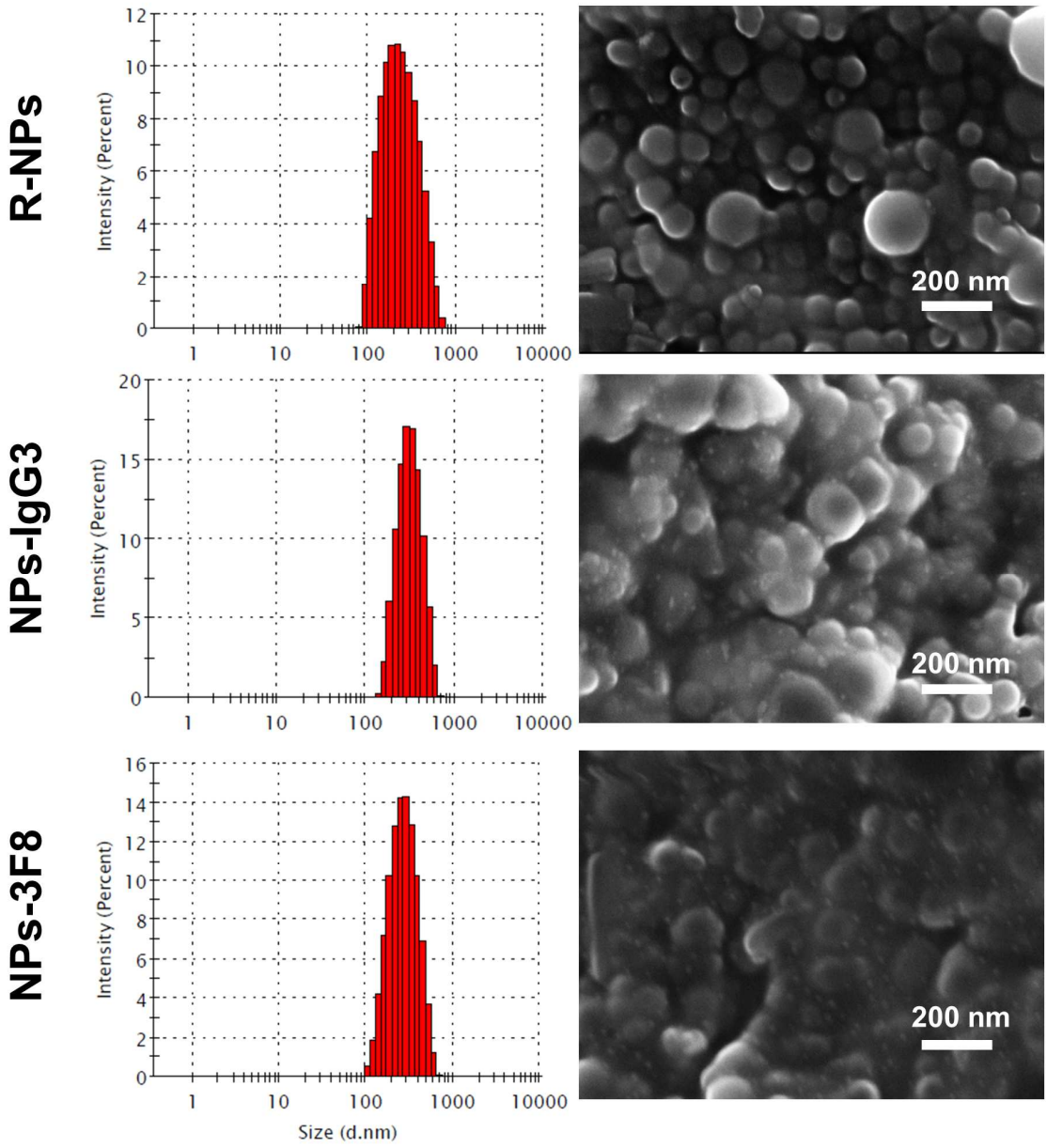

Figure 1. Characterization of the new NP formulations by DLS and SEM.

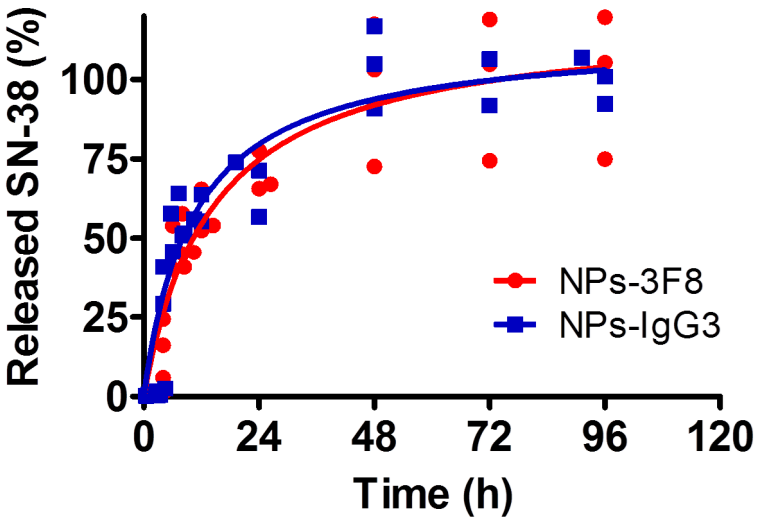

Figure 2. Cumulative release of SN-38 from NPs-IgG3 and NPs-3F8. Dots are individual data at each sampling time, obtained from triplicate samples of each formulation.

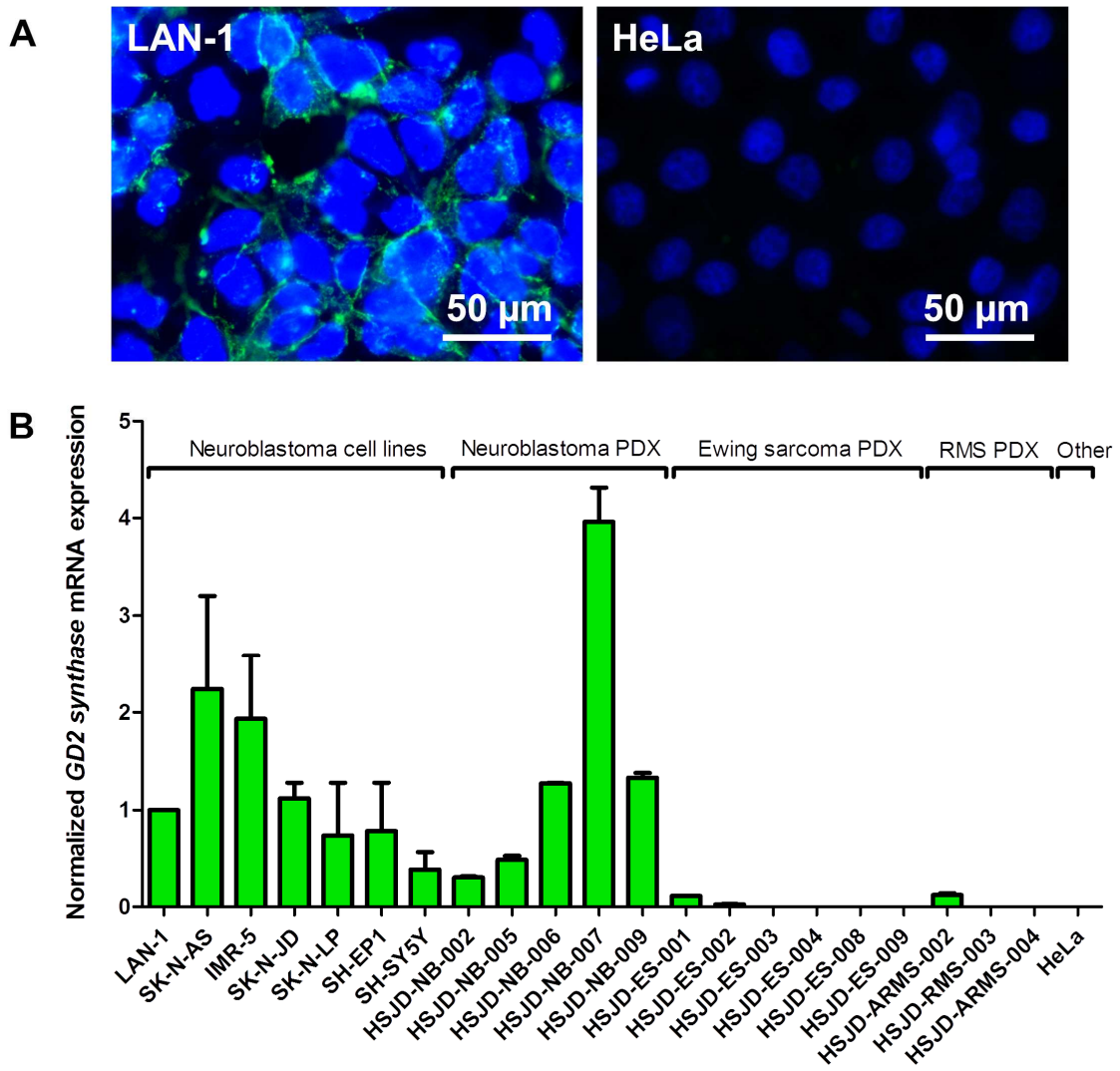

Figure 3. Expression of GD2 in tumor models. A. Immunocytochemistry of a GD2-positive neuroblastoma, LAN-1, and a GD2-negative model, HeLa. B. Relative expression of *GD2 synthase* in neuroblastoma cell lines and patient-derived xenografts of neuroblastoma, Ewing sarcoma and rhabdomyosarcoma. Values (mean and SD from triplicates) were normalized to *GD2 synthase* expression in LAN-1 cells.

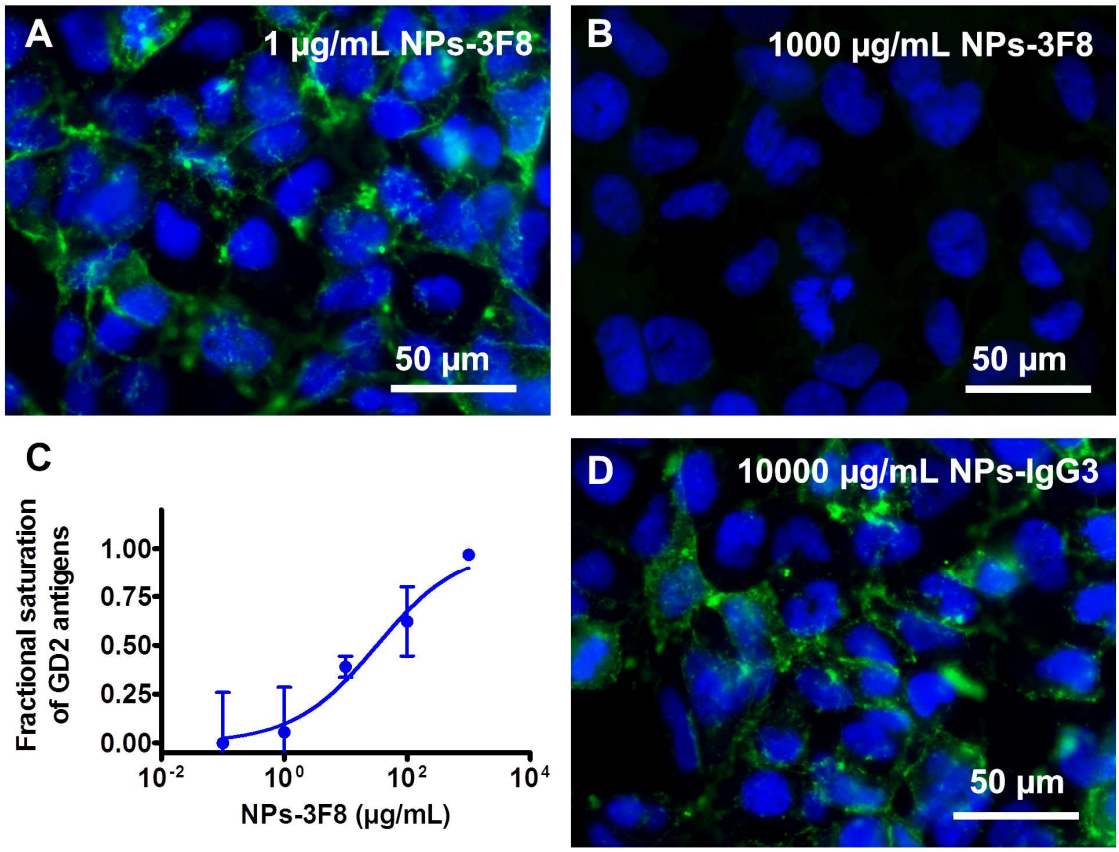

Figure 4. Competitive immunofluorescence assay. A. GD2 labeling in LAN-1 cells exposed to 1 µg/mL of NPs-3F8. This concentration of NPs did not saturate GD2 antigens in the plate. B. GD2 labeling in LAN-1 cells exposed to 1000 µg/mL of NPs-3F8. This concentration of NPs blocked the subsequent binding of free 3F8 antibody. C. Dose-response curve of the saturation of GD2 antingens exposed to increasing concentrations of NPs-3F8. D. NPs-IgG3 at high concentration (10000 µg/mL) did not compete for GD2 sites on LAN-1 cells.

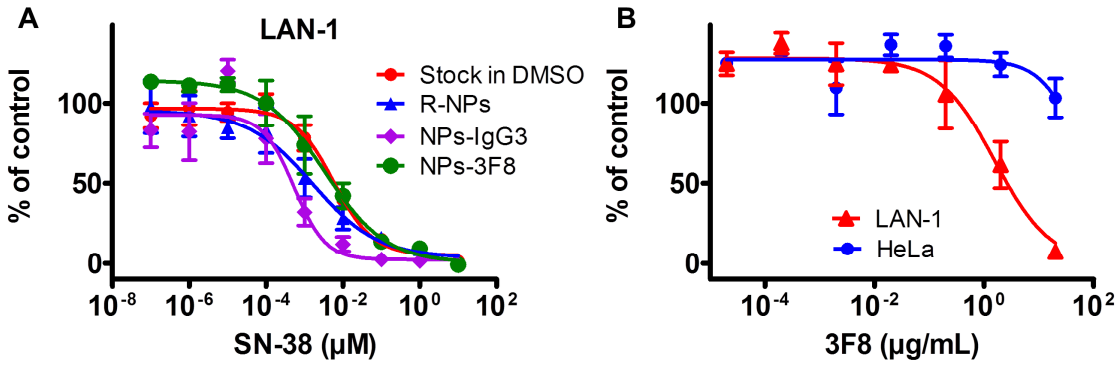

Figure 5. In vitro antiproliferative activity of SN-38 formulations (A) and 3F8 antibody (B). A. Antiproliferative activity of the formulations against LAN-1 cells. Values are expressed as % of MTS signal as compared to control untreated cells that were considered 100%. B. Antiproliferative activity of 3F8 against LAN-1 and HeLa cells.

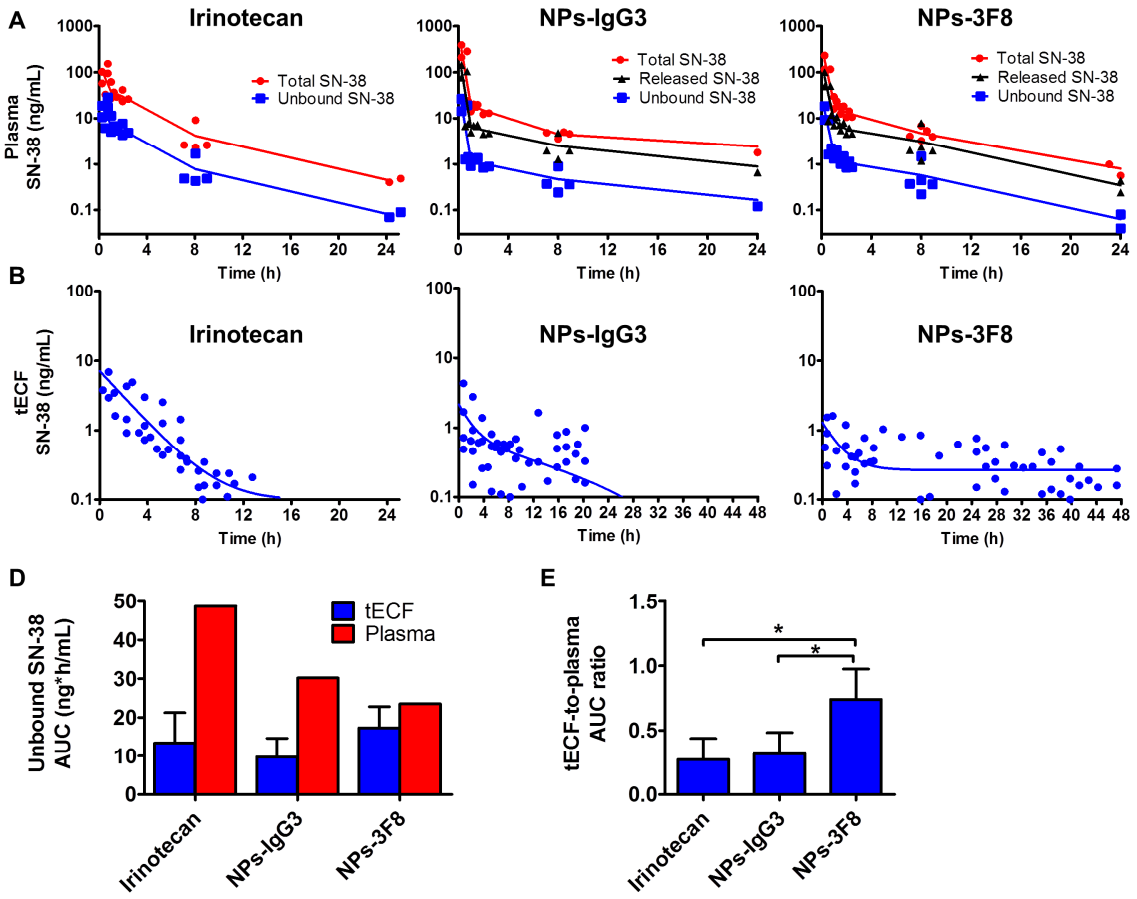

Figure 6. Plasma and tECF pharmacokinetics of SN-38. A. Plasma SN-38 concentration-time curves. Dots represent individual data. B. tECF SN-38 concentration-time curves. Dots represent individual data from 3-5 pooled experiments. C) Plasma and tECF exposure to unbound SN-38, represented as calculated AUCs. D) tECF-to-plasma AUC ratios. Mean and SD of 3-5 experiments are represented. * $P < 0.05$ (ANOVA).

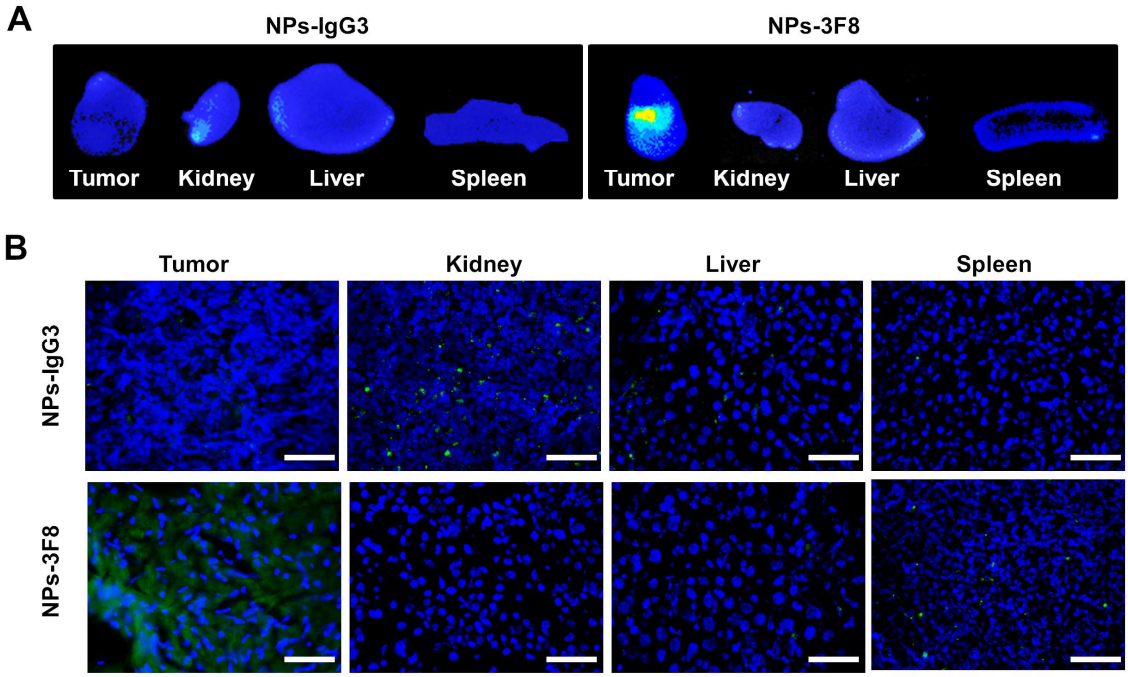

Figure 7. Accumulation of FITC-labeled NPs in vivo. A. *Ex vivo* fluorescence macroscopic images taken 2 h after a single intravenous administration of 4 mg/kg SN-38 B. DAPI-stained microscopic images derived from tissues shown in A. Bars are 100 µm.

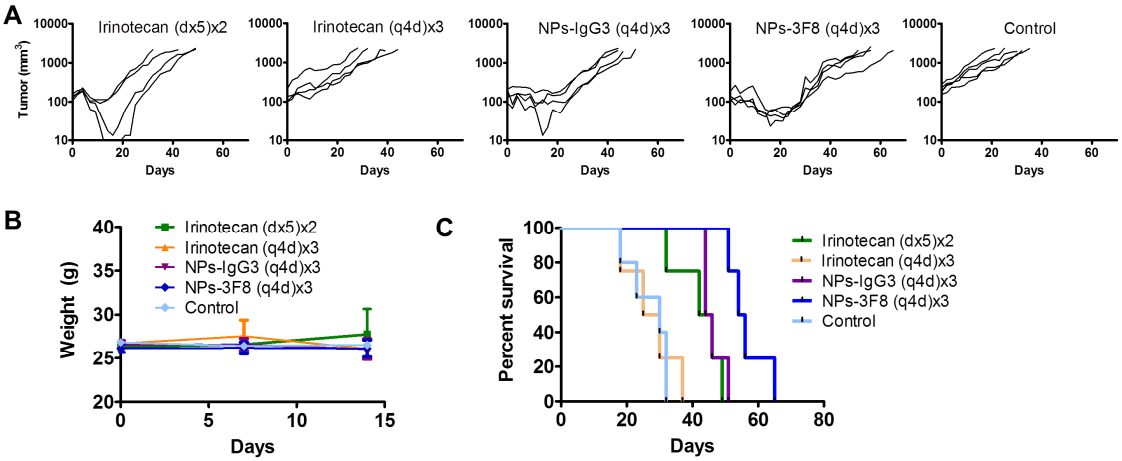

Figure 8. *In vivo* efficacy of SN-38 formulations. A. Antitumor activity of irinotecan 10 mg/kg for 5 days, repeated 2 weeks [(dx5)x2], irinotecan 10 mg/kg once every 4 days, repeated 3 weeks [(q4d)x3], NPs-IgG3 and NPs-3F8 at equimolar dosages and schedules [(q4d)x3]. Graphs show growth of individual tumors in nude mice. B. Weight of mice during treatment (mean and SD). C. Survival curves.

Tables

Table 1. Characterization of the new NP formulations. Data are means of 3 different batches.

Formulation	% of PLA-PEG-COOH (w/w)	FITC	mAb[a]	Load efficiency (%) ± SD	Particle size (nm) ± SD	PDI[b] ± SD	Zeta potential ± SD
R-NPs	20		N/A	216.1 ± 16.5	328.3 ± 39.5	0.346 ± 0.069	-28.3 ± 0.99
R-NPs	10		N/A	230.2 ± 40.5	296.9 ± 26.6	0.370 ± 0.040	-24.1 ± .56
R-NPs	5		N/A	113.5 ± 7.8	276.1 ± 1.3	0.277 ± 0.025	-26.4 ± 1.55
NPs-IgG3	5		IgG3	83.1 ± 17.4	269.1 ± 4.7	0.259 ± 0.036	-20.0 ± 1.37
NPs-3F8	5		3F8	90.7 ± 17.7	272.4 ± 19.2	0.282 ± 0.015	-22.8 ± 1.04
FITC-NPs-IgG3	5	✓	IgG3	105.7 ± 8.7	299.4 ± 20.3	0.277 ± 0.023	
FITC-NPs-3F8	5	✓	3F8	96.4 ± 16.0	299.6 ± 20.0	0.284 ± 0.023	

[a]Monoclonal antibody. [b]Polydispersity index.

DISCUSSION

Discussion

The average survival of pediatric patients with high-risk neuroblastoma, metastatic Ewing sarcoma and alveolar rhabdomyosarcoma is still poor (less than 50%) because of the rapid acquisition of chemoresistance to conventional treatments. A mechanism that could be involved in tumor chemoresistance is the inadequate drug distribution, but its role has not been thoroughly studied. Some previous works have shown the potential of using microdialysis combined with tumor homogenates to assess the preclinical intratumor drug distribution in xenograft models [127]. The authors found that the administration of gefitinib significantly improved TPT penetration into glioma orthotopic xenografts in mice and they characterized the compartmental drug distribution of TPT in the tumor extracellular fluid as well as in the vascular and intracellular compartments though the combined microdialysis-tumor homogenate method [127]. However, the implementation of microdialysis when applied to hydrophobic compounds can lead to misinterpreted results because these compounds bind to the internal surfaces of the tubing and to the membrane of the microdialysis probe as it was previously determined for other lipophilic molecules such as docetaxel [147, 157]. Loos *et al*. attempted to microdialyze docetaxel unsuccessfully even after the addition of polysorbate 80 or albumin as solubilizer agents [157]. An interesting work visually revealed also the non-specific binding of doxorubicin to the internal surfaces of plastic tubes [162] (see Figure 10 in the Introduction). The group of Julie A. Stenken successfully improved the RR of lipophilic molecules such as prostaglandins and leukotrienes upon the addition of cyclodextrins to the perfusion fluid [153]. In fact, the use of cyclodextrins as a solubilizer agent added to the perfusate has produced several works [141, 158]. Different lipophilic molecules including glucose, lactate and pyruvate were microdialyzed in human individuals from subcutaneous abdominal tissue by adding 2-hydroxypropyl-β-cyclodetrin (HPBCD) to the perfusate solution and the method was safe for its use in patients [158]. The authors determined an enhancement effect of the cyclodextrins on the uptake of lipophilic compounds from the subcutaneous adipose tissue because of the formation of a complex between the

hydrophobic compounds and the hydrophobic core of the cyclodextrins. In contrast with previous results where SN-38 was microdialyzed without the addition of solubilizer agents [202, 203], we observed the necessity of using a solubilizer to successfully microdialyze SN-38, especially the SN-38L counterpart. Dodds *et al*. studied SN-38 distribution in NB1691 neuroblastoma xenografts [203]. The authors claimed to be able to determine the concentration of both lactone and carboxylate forms of SN-38 in dialysates obtained by perfusing Ringer's solution through the microdialysis device, but here we have demonstrated that SN-38L is extremely lipophilic and thus it cannot be reproducibly dialyzed without adding a solubilizer agent in the perfusate solution. Encouraged by previous studies using cyclodextrins, we decided to use HPBCD in our microdialysis studies with SN-38. Despite it was described before that the addition of HPBCD at the concentration of 10% (w/v) does not cause significant tissue alteration in humans [158], we had some concerns regarding how HPBCD could affect SN-38 cellular uptake and tissue integrity. We determined that extravasation of HPBCD from inside of the microdialysis probe to the surrounding tissue was negligible (<1%). Moreover, it has been determined that drug release from cyclodextrins as a delivery agent is almost immediate [204], so we did not expect much affinity of the few extravasated HPBCD for the free SN-38. According to May *et al*. [158], who observed an enhanced relative recovery of endogenous analytes by adding HPBCD to the perfusion fluid (figure 11), we observed enhanced recovery of SN-38L as a result of the use of HPBCD in the perfusate solution, resulting in a complex between the hydrophobic core of the cyclodextrin and the hydrophobic SN-38L. Fortunately this complex is not irreversible because methanol and acetonitrile compete with the cyclodextrin hydrophobic core and HPBCD did not affect to the peak retention times of SN-38 in HPLC chromatograms. Thus, while others may have been concerned about the injection of HPBCD in the chromatographic columns because of the possibility of the formation of complexes inside, we determined that our method was safe and reproducible when injecting dialysate samples into our chromatographic system repeatedly. Currently, we use HPBCD in all HPLC methods developed for SN-38 in our laboratory, because it greatly improves their linearity and reproducibility. The new

microdialysis method developed in this work showed to be a useful and reproducible method to sample SN-38 from the extracellular fluid avoiding the problems of non-specific binding of the drug to the tubes or the membrane of the probe and allowing chromatographic analysis. Dialysate samples, together with tumor homogenates, provided full information about compartmental SN-38 distribution in pediatric PDX models.

Disposition of other camptothecins have been studied using microdialysis. Zamboni *et al.* used a microdialysis probe with a molecular cutoff of 20 kDa to study the distribution of topotecan, an analogue of camptothecins, in mice bearing sensitive NB1643 and resistant NB1691 human neuroblastoma xenografts [165]. In a previous study the authors described antitumor activity as directly related to topotecan dose and systemic exposure [112]. In this new study they found that the sensitive model NB1643 showed 3.5-fold higher tumor penetration than the resistant NB1691 suggesting that tumor penetration of topotecan could be associated with antitumor response in neuroblastoma. Figure 12 depicts topotecan plasma and tECF concentrations in sensitive and chemoresistant models. In our opinion, however, their study was not complete because microdialysis alone is only partially informative in tumor drug penetration studies. We would expect high drug concentrations in tECF of most tumors, given the EPR effect. In addition, only drugs in the tECF are analyzed by microdialysis alone, whereas most chemotherapy agents have intracellular targets. Lastly, it is risky to compare drug efficacy in tumors from different patients, as in the Zamboni study, and to correlate treatment failure only with drug distribution in the tECF of each model. Thus, in our work on drug delivery in tumors derived from pediatric patients, we addressed these concerns by implementing (1) the microdialysis – tumor homogenate technique to characterize compartmental drug distribution within the tumors, and (2) paired tumor models from the same patient to correct for the interpatient variability. We applied this approach to study tumor evolution as a result of therapy pressure in neuroblastoma, Ewing sarcoma and rhabdomyosarcoma PDX models. Each model was obtained from the same patient at different stages of the malignancy. Results showed that the late (resistant) models from each patient were associated with worse distribution of the drug (SN-38L) in the

intracellular space. To our knowledge, we are the first to accomplish this challenging experimental setup including functional studies *in vivo* in paired models from pediatric solid tumor patients.

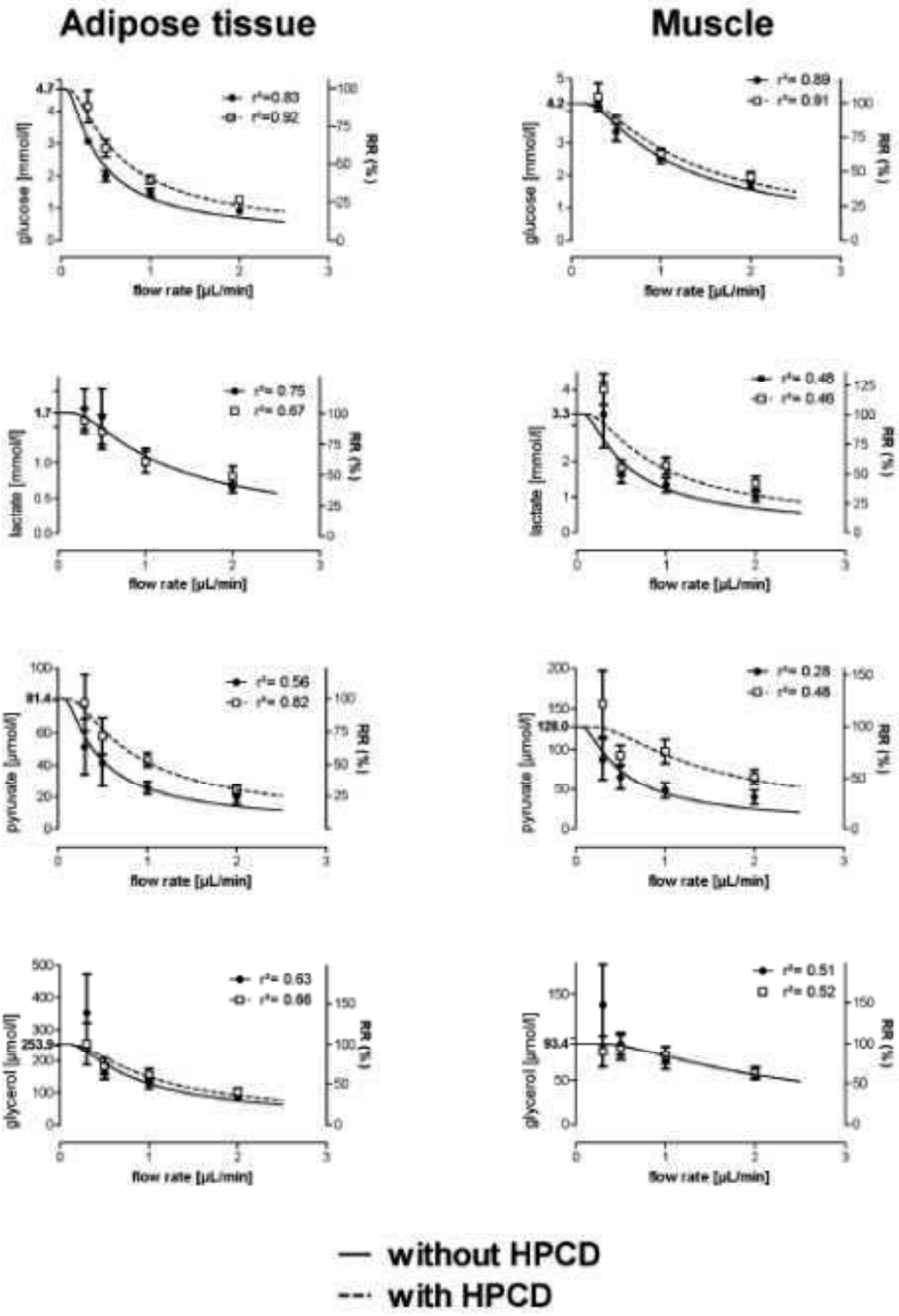

Figure 11. Metabolite recovery in adipose and skeletal muscle tissue at different flow rates. Slight enhanced relative recovery (RR) with the use of HPBCD is evidenced in most cases. Extracted from May *et al.* [158].

Because SN-38 is a highly lipophilic drug, microdialysis was conducted as previously described, using HPBCD as solubilizer agent to avoid non-specific adsorption of the drug to the internal surfaces of the microdialysis device. The results presented in this thesis show the reduced penetration of the drug SN-38L in late-stage tumors compared to the early-stage tumor models from the same patient. However, the neuroblastoma model HSJD-NB-005 did not show reduced penetration compared to the earlier-stage HSJD-NB-004, like the other paired xenograft models. Originally in the patient, this neuroblastoma was chemoresistant from the beginning (HSJD-NB-004) and never responded to any treatment received. Moreover, these two models were MYCN amplified and p53 mutated, conferring high chemoresistance.

The results of the efficacy study comparing the efficacy of irinotecan in paired Ewing sarcoma models suggest that hindered drug penetration to the intracellular compartment might play an important role in tumor chemoresistance, as previously described for topotecan [165]. Thus, we reasoned that new DDS improving drug delivery might overcome this acquired pharmacokinetic limitation of late stage tumors, and might lead to improved drug delivery and efficacy.

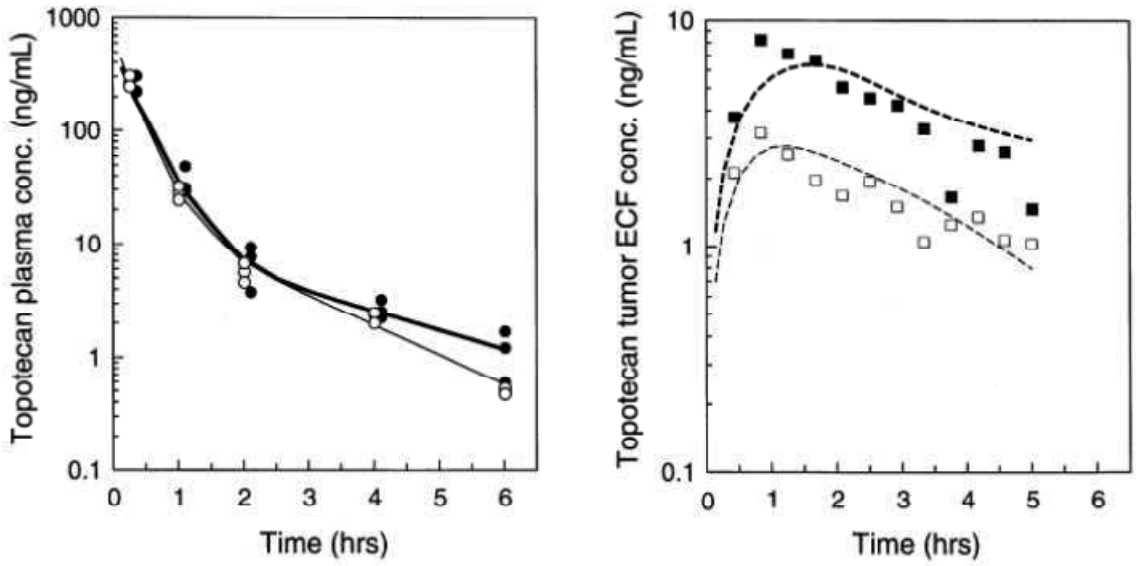

Figura 12. Concentration-time profiles of topotecan in plasma and tECF for NB1643 (●,■) sensitive and NB1691 (○,□) chemoresistant neuroblastoma models. Extracted from Zamboni *et al*. [112].

Accordingly, we designed two different SN-38-delivery systems, one for local delivery and the other for systemic administration. We characterized preclinically the release, tumor delivery and efficacy of camptothecins loaded into the new polymeric nanocarriers.

The use of polymeric matrices for local drug release, commonly designed as nanofibers or films, is reaching increasing interest lately. Since current local control of pediatric solid tumors is inefficient [205-207] and the use of radiotherapy is usually associated to second malignances [208] the use of polymeric matrices at the tumor site following debulking surgery may be useful to replace or delay radiotherapy and to control the re-growth of tumor residues in the surgical bed. Here, in collaboration with Dr J.A. Tornero at the Universidad Politecnica de Cataluña, we developed a new DDS for local release of SN-38 microcrystals previously incorporated to the polymeric nanofiber matrices generated by electrospinning. Electrospun polymeric nanofibers were chosen because of their malleability, which allows them to be applied over different surfaces, and because of their high surface and porosity that allow body fluids to get through facilitating drug release at the target tissue. Microdialysis probes implanted in the tumor bulk at different distances from the matrices showed that SN-38 concentration dropped dramatically at distances greater than 2 mm from the nanofiber matrices in contact with the subcutaneous tumor xenograft [209] and it was not quantifiable when the distance between the microdialysis probe and the matrix was greater than 5 mm. These results confirmed that local penetration of the drug is limited in tissues, and they could explain the failure of previous studies with local DDS implanted on top of bulky tumors [210, 211]. Our microdialysis method conferred several advantages to study local tissue penetration by local DDS. Methods like the use of radiolabeled drugs for diffusion studies are not suitable for its use in most laboratories [212] while other methods such as *ex vivo* tumor homogenates might not be the ideal platform since it is relatively easy to overestimate the real drug penetration [213]. Using terminal sampling to determine the extent of penetration of a locally administered drug to the tumor bulk might lead to an overestimation probably because of the maintained drug release of the DDS until sample

collection, while in the *ex vivo* tissue there is no longer the capacity of drug elimination [214]. Our complete study led us to propose that the use of local DDS systems in oncology should be limited to those patients that underwent macroscopic total resection of the tumor or patients with minimal tumor residues after surgery.

The next main goal of this thesis was to develop, characterize and evaluate a polymeric nanoparticulate formulation of SN-38 for its systemic administration in aggressive stage 4 neuroblastoma-bearing mice. To perform this project we collaborated with Dr Sosnik at Technion (Haifa, Israel), who provided newly synthesized polymers and resources for the characterization of the DDS. Our rationale to propose this DDS was that nanoparticulate SN-38 would overcome the limitation of the poor conversion rate from IRN to SN-38 in humans [110]. Hydrophobic SN-38 was successfully encapsulated into polymeric poly(lactic-co-glycolic) acid (PLGA) + PLA-PEG (5% w/w) nanoparticles. Several works using nanoparticulate formulations of SN-38 have been published [172-175]. Some of them have shown remarkable activity of the NK012 NPs over different tumor models in preclinical experiments [215-217]. Also, tocopherol-conjugated SN-38 has shown improved efficacy at lower doses than standard IRN in neuroblastoma xenografts [218, 219]. Here, polymeric NPs decorated with 3F8 monoclonal antibody against GD2 ganglioside, highly expressed on the membrane of neuroblastoma cells [220] and in other pediatric tumors [221-228] were proposed as a polymeric platform for the systemic administration of SN-38. GD2 expression is restricted to central nervous system in healthy tissues and in less proportion in peripheral neurons and skin melanocytes [229], thus it is a good candidate molecule for targeted therapy. We expected active targeting with the murine monoclonal antibody 3F8 (a clinical-grade antibody that reached clinical trials in children with neuroblastoma). Microdialysis results demonstrated that longer SN-38 exposure in the tECF, provided by the targeted formulation, correlated with improved antitumor activity. We suggest that, while polymeric nanofibers would be advantageous for the local control of the disease, SN-38 – loaded polymeric NPs would be a platform more oriented to the systemic administration and control of the disseminated

tumor. Next projects in the laboratory should address whether neuroblastoma metastases are controlled better with the GD2-targeted formulation, although we currently do not have the adequate metastatic patient-derived neuroblastoma xenograft model to address such question. To our knowledge, this is the first demonstration of improved intratumor drug distribution upon administration of a polymer NP formulation with active targeting of the ganglioside GD2 in neuroblastoma. Few previous studies have used microdialysis to assess drug distribution in solid tumors, and no study has addressed before tECF drug delivery by microdialysis upon the administration of systemic polymer nanoparticles [61, 127].

In summary, our results contributed to the field of pediatric oncology in several ways. First, we were able to validate a unique method to study drug distribution in clinically relevant tumor models. Second, we applied such method to find for the first time how tumors evolve towards a “drug impenetrable” phenotype under treatment pressure. Third, once identified the new unmet medical need, we developed two novel DDS to improve drug delivery and efficacy in our tumor models.

CONCLUSIONS

Conclusions

The results of this work characterized the delivery of the model anticancer agent SN-38 in pediatric solid tumors. The main conclusions are:

1) It was possible to microdialyze the highly lipophilic SN-38 by adding HPBCD at the concentration of 10% (w/v) to PBS (pH 7.4) as perfusion fluid, successfully avoiding the non-specific adsorption of the drug to the microdialysis device. We were able to calibrate the microdialysis probes by the ZFR method.

2) Inadequate drug distribution may have an important role in tumor chemoresistance acquired due to treatment pressure, as elucidated from the study of drug distribution in paired xenograft models of pediatric solid tumors by using the combined microdialysis – tumor homogenate technique. Thus, new drug delivery approaches might be needed to overcome this newly identified unmet medical need.

3) The use of locally implanted electrospun polymeric nanofiber matrices in the surgical bed upon tumor resection surgery allowed achieving high local concentration of SN-38 while keeping low systemic exposure. The matrices delayed tumor growth in neuroblastoma and Ewing sarcoma PDX models upon subtotal resection surgery. The distribution of the SN-38 was mostly limited to the site of implantation as shown from the microdialysis experiments as well as it was the efficacy, not affecting the contralateral untreated tumor in mice. Thus, we suggest that the patients that would benefit from this new DDS would be the ones with minimal or microscopic tumor rests after resection surgery.

4) GD2-targeted SN-38 nanoparticles achieved selective targeting of the GD2-expressing tumor neuroblastoma. The targeted formulation prolonged drug exposure in tumors, which was translated into improved treatment efficacy even with fewer dosages than the prodrug IRN.

REFERENCES

References

1. Mora, J., *What is a pediatric tumor?* Clinical Oncology in Adolescents and Young Adults, 2012. **2**: p. 7-15.
2. Khanna, K.K. and S.P. Jackson, *DNA double-strand breaks: signaling, repair and the cancer connection.* Nat Genet, 2001. **27**(3): p. 247-54.
3. Vilenchik, M.M. and A.G. Knudson, *Endogenous DNA double-strand breaks: production, fidelity of repair, and induction of cancer.* Proc Natl Acad Sci U S A, 2003. **100**(22): p. 12871-6.
4. Mora, J. and W.L. Gerald, *Origin of neuroblastic tumors: clues for future therapeutics.* Expert Rev Mol Diagn, 2004. **4**(3): p. 293-302.
5. Ora, I. and A. Eggert, *Progress in treatment and risk stratification of neuroblastoma: impact on future clinical and basic research.* Semin Cancer Biol, 2011. **21**(4): p. 217-28.
6. Mora J, C.O., Morales L, *Tumores neuroblásticos. Neuroblastoma. Ed M Cruz: Tratado de pediatría 9ª ed 2006 Ergon, Madrid.*
7. PerisBonet R, P.R.E., Ríos Martín I, Sayas Sánchez N, Valero Poveda S., *Cáncer infantil en España. Estadísticas1980-2015. Registro Español de Tumores Infantiles (RETI-SEHOP). Valencia: UniversitatdeValència, 2016.*
8. Maris, J.M., et al., *Neuroblastoma.* Lancet, 2007. **369**(9579): p. 2106-20.
9. Mora, J., N. Fernández, and A.M. Sánches. *Neuroblastic Tumors*. Oncopedia 2010 03/11/2010]; Available from: www.cure4kids.org/oncopedia.
10. Brodeur, G.M., et al., *Revisions of the international criteria for neuroblastoma diagnosis, staging, and response to treatment.* J Clin Oncol, 1993. **11**(8): p. 1466-77.
11. Cooper, M.J., G.M. Hutchins, and M.A. Israel, *Histogenesis of the human adrenal medulla. An evaluation of the ontogeny of chromaffin and nonchromaffin lineages.* Am J Pathol, 1990. **137**(3): p. 605-15.
12. Vaux, D.L., *Toward an understanding of the molecular mechanisms of physiological cell death.* Proc Natl Acad Sci U S A, 1993. **90**(3): p. 786-9.
13. Kushner, B.H. and N.K. Cheung, *What factors predict a favorable outcome in young children with disseminated neuroblastoma?* Nat Clin Pract Oncol, 2006. **3**(5): p. 242-3.
14. Kushner, B.H., *Neuroblastoma: a disease requiring a multitude of imaging studies.* J Nucl Med, 2004. **45**(7): p. 1172-88.
15. David, R., et al., *The many faces of neuroblastoma.* Radiographics, 1989. **9**(5): p. 859-82.
16. Baker, D.L., et al., *Outcome after reduced chemotherapy for intermediate-risk neuroblastoma.* N Engl J Med, 2010. **363**(14): p. 1313-23.
17. Rubie, H., et al., *Excellent outcome with reduced treatment in infants with nonmetastatic and unresectable neuroblastoma without MYCN amplification: results of the prospective INES 99.1.* J Clin Oncol, 2011. **29**(4): p. 449-55.
18. Corvi, R., et al., *Non-syntenic amplification of MDM2 and MYCN in human neuroblastoma.* Oncogene, 1995. **10**(6): p. 1081-6.
19. Canete, A., et al., *Poor survival for infants with MYCN-amplified metastatic neuroblastoma despite intensified treatment: the International Society of Paediatric Oncology European Neuroblastoma Experience.* J Clin Oncol, 2009. **27**(7): p. 1014-9.
20. Cheung, N.K., et al., *N7: a novel multi-modality therapy of high risk neuroblastoma (NB) in children diagnosed over 1 year of age.* Med Pediatr Oncol, 2001. **36**(1): p. 227-30.
21. Bagatell, R., et al., *Phase II Study of Irinotecan and Temozolomide in Children With Relapsed or Refractory Neuroblastoma: A Children's Oncology Group Study.* J Clin Oncol, 2011. **29**(2): p. 208-13.
22. London, W.B., et al., *Phase II randomized comparison of topotecan plus cyclophosphamide versus topotecan alone in children with recurrent or refractory neuroblastoma: a Children's Oncology Group study.* J Clin Oncol, 2010. **28**(24): p. 3808-15.
23. Saylors, R.L., 3rd, et al., *Cyclophosphamide plus topotecan in children with recurrent or refractory solid tumors: a Pediatric Oncology Group phase II study.* J Clin Oncol, 2001. **19**(15): p. 3463-9.
24. Kushner, B.H., et al., *Pilot study of topotecan and high-dose cyclophosphamide for resistant pediatric solid tumors.* Med Pediatr Oncol, 2000. **35**(5): p. 468-74.

25. Sato, Y., et al., *Usefulness of 18F-Fluorodeoxyglucose Positron Emission Tomography for Follow-Up of 13-cis-Retinoic Acid Treatment for Residual Neuroblastoma After Myeloablative Chemotherapy.* Medicine (Baltimore), 2015. **94**(31): p. e1290.
26. Mora, J., *Dinutuximab for the treatment of pediatric patients with high-risk neuroblastoma.* Expert Rev Clin Pharmacol, 2016: p. 1-7.
27. Gilman, A.L., et al., *Phase I study of ch14.18 with granulocyte-macrophage colony-stimulating factor and interleukin-2 in children with neuroblastoma after autologous bone marrow transplantation or stem-cell rescue: a report from the Children's Oncology Group.* J Clin Oncol, 2009. **27**(1): p. 85-91.
28. Bordow, S.B., et al., *Prognostic significance of MYCN oncogene expression in childhood neuroblastoma.* J Clin Oncol, 1998. **16**(10): p. 3286-94.
29. Komotar, R.J., et al., *Chromosome 1p and 11q deletions and outcome in neuroblastoma-a critical review.* Clin Med Oncol, 2008. **2**: p. 419-20.
30. Tweddle, D.A., et al., *The p53 pathway and its inactivation in neuroblastoma.* Cancer Lett, 2003. **197**(1-2): p. 93-8.
31. Norris, M.D., et al., *Expression of the gene for multidrug-resistance-associated protein and outcome in patients with neuroblastoma.* N Engl J Med, 1996. **334**(4): p. 231-8.
32. Van Maerken, T., et al., *Antitumor activity of the selective MDM2 antagonist nutlin-3 against chemoresistant neuroblastoma with wild-type p53.* J Natl Cancer Inst, 2009. **101**(22): p. 1562-74.
33. Beaudry, P., et al., *Potent antitumor effects of ZD6474 on neuroblastoma via dual targeting of tumor cells and tumor endothelium.* Mol Cancer Ther, 2008. **7**(2): p. 418-24.
34. Li, Z., et al., *In vitro and in vivo inhibition of neuroblastoma tumor cell growth by AKT inhibitor perifosine.* J Natl Cancer Inst, 2010. **102**(11): p. 758-70.
35. Brignole, C., et al., *Effect of bortezomib on human neuroblastoma cell growth, apoptosis, and angiogenesis.* J Natl Cancer Inst, 2006. **98**(16): p. 1142-57.
36. University of Michigan Cancer Center; Millennium Pharmaceuticals, I., *A Phase One Study of Intravenous Irinotecan and Bortezomib in Children With Recurrent/Refractory High-Risk Neuroblastoma. Bethesda (MD): National Library of Medicine (US). 2000 - [Last accessed on 2016 Mar 29]. Available from: https://clinicaltrials.gov/ct2/show/NCT00644696 Identifier : NCT00644696.*
37. (NCI)., P.B.T.C.N.C.I., *Phase I and Pharmacokinetic Study of Enzastaurin (LY317615) in Children and Adolescents With Refractory Primary CNS Tumors. Bethesda (MD): National Library of Medicine (US). 2000 - [Last accessed on 2016 Mar 29]. Available from: https://clinicaltrials.gov/ct2/show/NCT00503724 Identifier : NCT00503724.*
38. Carr, J., et al., *Increased frequency of aberrations in the p53/MDM2/p14(ARF) pathway in neuroblastoma cell lines established at relapse.* Cancer Res, 2006. **66**(4): p. 2138-45.
39. George, R.E., et al., *Activating mutations in ALK provide a therapeutic target in neuroblastoma.* Nature, 2008. **455**(7215): p. 975-8.
40. Peterson, S. and E. Bogenmann, *The RET and TRKA pathways collaborate to regulate neuroblastoma differentiation.* Oncogene, 2004. **23**(1): p. 213-25.
41. Minchinton, A.I. and I.F. Tannock, *Drug penetration in solid tumours.* Nat Rev Cancer, 2006. **6**(8): p. 583-92.
42. Olive, K.P., et al., *Inhibition of Hedgehog signaling enhances delivery of chemotherapy in a mouse model of pancreatic cancer.* Science, 2009. **324**(5933): p. 1457-61.
43. Ewing, J., *Classics in oncology. Diffuse endothelioma of bone. James Ewing. Proceedings of the New York Pathological Society, 1921.* CA Cancer J Clin, 1972. **22**(2): p. 95-8.
44. Paulussen, M., et al., *Results of the EICESS-92 Study: two randomized trials of Ewing's sarcoma treatment--cyclophosphamide compared with ifosfamide in standard-risk patients and assessment of benefit of etoposide added to standard treatment in high-risk patients.* J Clin Oncol, 2008. **26**(27): p. 4385-93.
45. Esiashvili, N., M. Goodman, and R.B. Marcus, Jr., *Changes in incidence and survival of Ewing sarcoma patients over the past 3 decades: Surveillance Epidemiology and End Results data.* J Pediatr Hematol Oncol, 2008. **30**(6): p. 425-30.
46. Lin, P.P., Y. Wang, and G. Lozano, *Mesenchymal Stem Cells and the Origin of Ewing's Sarcoma.* Sarcoma, 2011. **2011**.
47. Ordonez, J.L., et al., *Advances in Ewing's sarcoma research: where are we now and what lies ahead?* Cancer Res, 2009. **69**(18): p. 7140-50.

48. Jawad, M.U., et al., *Ewing sarcoma demonstrates racial disparities in incidence-related and sex-related differences in outcome: an analysis of 1631 cases from the SEER database, 1973-2005.* Cancer, 2009. **115**(15): p. 3526-36.
49. SJ., V.S.K., *Ewing Sarcoma: Focus on Medical Management. Journal of Bone and Soft Tissue Tumors May-Aug 2015;1(1):8-17.*
50. Gaspar, N., et al., *Ewing Sarcoma: Current Management and Future Approaches Through Collaboration.* J Clin Oncol, 2015. **33**(27): p. 3036-46.
51. Nesbit, M.E., Jr., et al., *Multimodal therapy for the management of primary, nonmetastatic Ewing's sarcoma of bone: a long-term follow-up of the First Intergroup study.* J Clin Oncol, 1990. **8**(10): p. 1664-74.
52. Jain, S. and G. Kapoor, *Chemotherapy in Ewing's sarcoma.* Indian J Orthop, 2010. **44**(4): p. 369-77.
53. Juergens, C., et al., *Safety assessment of intensive induction with vincristine, ifosfamide, doxorubicin, and etoposide (VIDE) in the treatment of Ewing tumors in the EURO-E.W.I.N.G. 99 clinical trial.* Pediatr Blood Cancer, 2006. **47**(1): p. 22-9.
54. Granowetter, L., et al., *Dose-intensified compared with standard chemotherapy for nonmetastatic Ewing sarcoma family of tumors: a Children's Oncology Group Study.* J Clin Oncol, 2009. **27**(15): p. 2536-41.
55. Kramer, S., et al., *Incidence of childhood cancer: experience of a decade in a population-based registry.* J Natl Cancer Inst, 1983. **70**(1): p. 49-55.
56. Crist, W., et al., *The Third Intergroup Rhabdomyosarcoma Study.* J Clin Oncol, 1995. **13**(3): p. 610-30.
57. Dagher, R. and L. Helman, *Rhabdomyosarcoma: an overview.* Oncologist, 1999. **4**(1): p. 34-44.
58. Healey, E.A., et al., *A 10-year experience of pediatric brachytherapy.* Int J Radiat Oncol Biol Phys, 1995. **32**(2): p. 451-5.
59. Gerbaulet, A.P., et al., *Conservative treatment for lower gynecological tract malignancies in children and adolescents: the Institut Gustave-Roussy experience.* Int J Radiat Oncol Biol Phys, 1989. **17**(3): p. 655-8.
60. Casanovas, O., et al., *Drug resistance by evasion of antiangiogenic targeting of VEGF signaling in late-stage pancreatic islet tumors.* Cancer Cell, 2005. **8**(4): p. 299-309.
61. Zhou, Q., et al., *Activation of alternate prosurvival pathways accounts for acquired sunitinib resistance in U87MG glioma xenografts.* J Pharmacol Exp Ther, 2012. **343**(2): p. 509-19.
62. Gottesman, M.M., T. Fojo, and S.E. Bates, *Multidrug resistance in cancer: role of ATP-dependent transporters.* Nat Rev Cancer, 2002. **2**(1): p. 48-58.
63. Shapiro, D.N., et al., *Fusion of PAX3 to a member of the forkhead family of transcription factors in human alveolar rhabdomyosarcoma.* Cancer Res, 1993. **53**(21): p. 5108-12.
64. Komdeur, R., et al., *Multidrug resistance proteins in rhabdomyosarcomas: comparison between children and adults.* Cancer, 2003. **97**(8): p. 1999-2005.
65. Chan, H.S., et al., *Immunohistochemical detection of P-glycoprotein: prognostic correlation in soft tissue sarcoma of childhood.* J Clin Oncol, 1990. **8**(4): p. 689-704.
66. de Cremoux, P., et al., *Role of chemotherapy resistance genes in outcome of neuroblastoma.* Pediatr Blood Cancer, 2007. **48**(3): p. 311-7.
67. Nakanishi, H., et al., *P-glycoprotein expression in soft-tissue sarcomas.* J Cancer Res Clin Oncol, 1997. **123**(6): p. 352-6.
68. Kuttesch, J.F., et al., *P-glycoprotein expression at diagnosis may not be a primary mechanism of therapeutic failure in childhood rhabdomyosarcoma.* J Clin Oncol, 1996. **14**(3): p. 886-900.
69. Oda, Y., et al., *Reverse transcriptase-polymerase chain reaction amplification of MDR1 gene expression in adult soft tissue sarcomas.* Diagn Mol Pathol, 1996. **5**(2): p. 98-106.
70. Citti, A., et al., *Expression of multidrug resistance-associated proteins in paediatric soft tissue sarcomas before and after chemotherapy.* Int J Oncol, 2012. **41**(1): p. 117-24.
71. Johnson, J.I., et al., *Relationships between drug activity in NCI preclinical in vitro and in vivo models and early clinical trials.* Br J Cancer, 2001. **84**(10): p. 1424-31.
72. Li, A., et al., *Genomic changes and gene expression profiles reveal that established glioma cell lines are poorly representative of primary human gliomas.* Mol Cancer Res, 2008. **6**(1): p. 21-30.
73. Houghton, P.J., et al., *The pediatric preclinical testing program: description of models and early testing results.* Pediatr Blood Cancer, 2007. **49**(7): p. 928-40.
74. Daniel, V.C., et al., *A primary xenograft model of small-cell lung cancer reveals irreversible changes in gene expression imposed by culture in vitro.* Cancer Res, 2009. **69**(8): p. 3364-73.

75. Voskoglou-Nomikos, T., J.L. Pater, and L. Seymour, *Clinical predictive value of the in vitro cell line, human xenograft, and mouse allograft preclinical cancer models.* Clin Cancer Res, 2003. **9**(11): p. 4227-39.
76. Morton, C.L. and P.J. Houghton, *Establishment of human tumor xenografts in immunodeficient mice.* Nat Protoc, 2007. **2**(2): p. 247-50.
77. Rubio-Viqueira, B., et al., *An in vivo platform for translational drug development in pancreatic cancer.* Clin Cancer Res, 2006. **12**(15): p. 4652-61.
78. Verschraegen, C.F., et al., *Establishment and characterization of cancer cell cultures and xenografts derived from primary or metastatic Mullerian cancers.* Clin Cancer Res, 2003. **9**(2): p. 845-52.
79. Schmidt, K.F., et al., *Volume reconstruction techniques improve the correlation between histological and in vivo tumor volume measurements in mouse models of human gliomas.* J Neurooncol, 2004. **68**(3): p. 207-15.
80. Verstijnen, C.P., et al., *Culturing and xenografting of primary colorectal carcinoma cells: comparison of in vitro, and in vivo model and primary tumor.* Anticancer Res, 1988. **8**(6): p. 1193-200.
81. Fichtner, I., et al., *Establishment of patient-derived non-small cell lung cancer xenografts as models for the identification of predictive biomarkers.* Clin Cancer Res, 2008. **14**(20): p. 6456-68.
82. Neale, G., et al., *Molecular characterization of the pediatric preclinical testing panel.* Clin Cancer Res, 2008. **14**(14): p. 4572-83.
83. Jin, K., et al., *Patient-derived human tumour tissue xenografts in immunodeficient mice: a systematic review.* Clin Transl Oncol, 2010. **12**(7): p. 473-80.
84. Sausville, E.A. and A.M. Burger, *Contributions of human tumor xenografts to anticancer drug development.* Cancer Res, 2006. **66**(7): p. 3351-4, discussion 3354.
85. Shultz, L.D., et al., *Human lymphoid and myeloid cell development in NOD/LtSz-scid IL2R gamma null mice engrafted with mobilized human hemopoietic stem cells.* J Immunol, 2005. **174**(10): p. 6477-89.
86. Houghton, J.A., et al., *Biochemical determinants of responsiveness to 5-fluorouracil and its derivatives in xenografts of human colorectal adenocarcinomas in mice.* Cancer Res, 1981. **41**(1): p. 144-9.
87. Houghton, J.A. and D.M. Taylor, *Growth characteristics of human colorectal tumours during serial passage in immune-deprived mice.* Br J Cancer, 1978. **37**(2): p. 213-23.
88. N. Dey, Y.S., B. Leyland-Jones and P. De, *Evolution of Tumor Model: From Animal Model of Tumor to Tumor Model in Animal. Journal of Cancer Therapy, Vol. 4 No. 9, 2013, pp. 1411-1425. doi: 10.4236/jct.2013.49168.*
89. Wall, M.E., et al., *Plant Antitumor Agents. I. The Isolation and Structure of Camptothecin, a Novel Alkaloidal Leukemia and Tumor Inhibitor from Camptotheca acuminata1,2.* Journal of the American Chemical Society, 1966. **88**(16): p. 3888-3890.
90. Hsiang, Y.H., et al., *Camptothecin induces protein-linked DNA breaks via mammalian DNA topoisomerase I.* J Biol Chem, 1985. **260**(27): p. 14873-8.
91. Hsiang, Y.H. and L.F. Liu, *Identification of mammalian DNA topoisomerase I as an intracellular target of the anticancer drug camptothecin.* Cancer Res, 1988. **48**(7): p. 1722-6.
92. Tsao, Y.P., et al., *Interaction between replication forks and topoisomerase I-DNA cleavable complexes: studies in a cell-free SV40 DNA replication system.* Cancer Res, 1993. **53**(24): p. 5908-14.
93. Gottlieb, J.A., et al., *Preliminary pharmacologic and clinical evaluation of camptothecin sodium (NSC-100880).* Cancer Chemother Rep, 1970. **54**(6): p. 461-70.
94. Hertzberg, R.P., et al., *Modification of the hydroxy lactone ring of camptothecin: inhibition of mammalian topoisomerase I and biological activity.* J Med Chem, 1989. **32**(3): p. 715-20.
95. Creaven, P.J. and L.M. Allen, *Renal clearance of camptothecin (NSC-100880): effect of urine volume.* Cancer Chemother Rep, 1973. **57**(2): p. 175-84.
96. Fassberg, J. and V.J. Stella, *A kinetic and mechanistic study of the hydrolysis of camptothecin and some analogues.* J Pharm Sci, 1992. **81**(7): p. 676-84.
97. Burke, T.G. and Z. Mi, *The structural basis of camptothecin interactions with human serum albumin: impact on drug stability.* J Med Chem, 1994. **37**(1): p. 40-6.
98. Mi, Z. and T.G. Burke, *Marked interspecies variations concerning the interactions of camptothecin with serum albumins: a frequency-domain fluorescence spectroscopic study.* Biochemistry, 1994. **33**(42): p. 12540-5.

99. Scott, D.O., D.S. Bindra, and V.J. Stella, *Plasma pharmacokinetics of lactone and carboxylate forms of 20(S)-camptothecin in anesthetized rats.* Pharm Res, 1993. **10**(10): p. 1451-7.
100. Rosing, H., et al., *High-performance liquid chromatographic determination of the novel antitumour drug topotecan and topotecan as the total of the lactone plus carboxylate forms, in human plasma.* J Chromatogr B Biomed Appl, 1995. **668**(1): p. 107-15.
101. Supko, J.G. and L. Malspeis, *Pharmacokinetics of the 9-amino and 10,11-methylenedioxy derivatives of camptothecin in mice.* Cancer Res, 1993. **53**(13): p. 3062-9.
102. Kingsbury, W.D., et al., *Synthesis of water-soluble (aminoalkyl)camptothecin analogues: inhibition of topoisomerase I and antitumor activity.* J Med Chem, 1991. **34**(1): p. 98-107.
103. Grochow, L.B., et al., *Pharmacokinetics and pharmacodynamics of topotecan in patients with advanced cancer.* Drug Metab Dispos, 1992. **20**(5): p. 706-13.
104. van Warmerdam, L.J., et al., *Pharmacokinetics and pharmacodynamics of topotecan given on a daily-times-five schedule in phase II clinical trials using a limited-sampling procedure.* Cancer Chemother Pharmacol, 1996. **38**(3): p. 254-60.
105. Abraham, S.A., et al., *An evaluation of transmembrane ion gradient-mediated encapsulation of topotecan within liposomes.* J Control Release, 2004. **96**(3): p. 449-61.
106. Satoh, T., et al., *Metabolic activation of CPT-11, 7-ethyl-10-[4-(1-piperidino)-1-piperidino]carbonyloxycamptothecin, a novel antitumor agent, by carboxylesterase.* Biol Pharm Bull, 1994. **17**(5): p. 662-4.
107. Rothenberg, M.L., et al., *Phase I and pharmacokinetic trial of weekly CPT-11.* J Clin Oncol, 1993. **11**(11): p. 2194-204.
108. Grivicich, I., et al., *Irinotecan and oxaliplatin: an overview of the novel chemotherapeutic options for the treatment of advanced colorectal cancer.* Braz J Med Biol Res, 2001. **34**(9): p. 1087-103.
109. Sampson, V.B., et al., *Vorinostat Enhances Cytotoxicity of SN-38 and Temozolomide in Ewing Sarcoma Cells and Activates STAT3/AKT/MAPK Pathways.* PLoS One, 2015. **10**(11): p. e0142704.
110. Slatter, J.G., et al., *Pharmacokinetics, metabolism, and excretion of irinotecan (CPT-11) following I.V. infusion of [(14)C]CPT-11 in cancer patients.* Drug Metab Dispos, 2000. **28**(4): p. 423-33.
111. Furman, W.L., et al., *Cefixime allows greater dose escalation of oral irinotecan: a phase I study in pediatric patients with refractory solid tumors.* J Clin Oncol, 2006. **24**(4): p. 563-70.
112. Zamboni, W.C., et al., *Relationship between topotecan systemic exposure and tumor response in human neuroblastoma xenografts.* J Natl Cancer Inst, 1998. **90**(7): p. 505-11.
113. Blaney, S.M., et al., *Phase II trial of topotecan administered as 72-hour continuous infusion in children with refractory solid tumors: a collaborative Pediatric Branch, National Cancer Institute, and Children's Cancer Group Study.* Clin Cancer Res, 1998. **4**(2): p. 357-60.
114. Thompson, J., et al., *Efficacy of systemic administration of irinotecan against neuroblastoma xenografts.* Clin Cancer Res, 1997. **3**(3): p. 423-31.
115. Vassal, G., et al., *Therapeutic activity of CPT-11, a DNA-topoisomerase I inhibitor, against peripheral primitive neuroectodermal tumour and neuroblastoma xenografts.* Br J Cancer, 1996. **74**(4): p. 537-45.
116. Saito, Y., et al., *Antitumour activity of NK012, SN-38-incorporating polymeric micelles, in hypovascular orthotopic pancreatic tumour.* Eur J Cancer, 2009.
117. Koizumi, F., et al., *Novel SN-38-incorporating polymeric micelles, NK012, eradicate vascular endothelial growth factor-secreting bulky tumors.* Cancer Res, 2006. **66**(20): p. 10048-56.
118. Sumitomo, M., et al., *Novel SN-38-incorporated polymeric micelle, NK012, strongly suppresses renal cancer progression.* Cancer Res, 2008. **68**(6): p. 1631-5.
119. Nakajima, T.E., et al., *Antitumor effect of SN-38-releasing polymeric micelles, NK012, on spontaneous peritoneal metastases from orthotopic gastric cancer in mice compared with irinotecan.* Cancer Res, 2008. **68**(22): p. 9318-22.
120. Nagano, T., et al., *Antitumor activity of NK012 combined with cisplatin against small cell lung cancer and intestinal mucosal changes in tumor-bearing mouse after treatment.* Clin Cancer Res, 2009. **15**(13): p. 4348-55.
121. Burris III, H.A., et al., *A phase I dose-escalation study of NK012.* J Clin Oncol, 2008. **26 (May 20 Suppl; abstr 2538)**.
122. Zamboni, W.C., et al., *Plasma, tumor, and tissue disposition of STEALTH liposomal CKD-602 (S-CKD602) and nonliposomal CKD-602 in mice bearing A375 human melanoma xenografts.* Clin Cancer Res, 2007. **13**(23): p. 7217-23.

123. Furman, W.L., et al., *Direct translation of a protracted irinotecan schedule from a xenograft model to a phase I trial in children.* J Clin Oncol, 1999. **17**(6): p. 1815-24.
124. Davies, M.I. and C.E. Lunte, *Microdialysis sampling for hepatic metabolism studies. Impact of microdialysis probe design and implantation technique on liver tissue.* Drug Metab Dispos, 1995. **23**(10): p. 1072-9.
125. Ault, J.M., et al., *Dermal microdialysis sampling in vivo.* Pharm Res, 1994. **11**(11): p. 1631-9.
126. Palsmeier, R.K. and C.E. Lunte, *Microdialysis sampling in tumor and muscle: study of the disposition of 3-amino-1,2,4-benzotriazine-1,4-di-N-oxide (SR 4233).* Life Sci, 1994. **55**(10): p. 815-25.
127. Carcaboso, A.M., et al., *Tyrosine kinase inhibitor gefitinib enhances topotecan penetration of gliomas.* Cancer Res, 2010. **70**(11): p. 4499-508.
128. de Lange, E.C., A.G. de Boer, and D.D. Breimer, *Methodological issues in microdialysis sampling for pharmacokinetic studies.* Adv Drug Deliv Rev, 2000. **45**(2-3): p. 125-48.
129. Carcaboso, A.M., et al., *Episcleral implants for topotecan delivery to the posterior segment of the eye.* Invest Ophthalmol Vis Sci, 2010. **51**(4): p. 2126-34.
130. Garimella, T.S., et al., *Plasma pharmacokinetics and tissue distribution of the breast cancer resistance protein (BCRP/ABCG2) inhibitor fumitremorgin C in SCID mice bearing T8 tumors.* Cancer Chemother Pharmacol, 2005. **55**(2): p. 101-9.
131. Nguyen, L., et al., *Quantitative analysis of PD 0332991 in xenograft mouse tumor tissue by a 96-well supported liquid extraction format and liquid chromatography/mass spectrometry.* J Pharm Biomed Anal, 2010. **53**(3): p. 228-34.
132. Yang, Z., et al., *Microdialysis studies of the distribution of stavudine into the central nervous system in the freely-moving rat.* Pharm Res, 1997. **14**(7): p. 865-72.
133. Konings, I.R., et al., *Application of prolonged microdialysis sampling in carboplatin-treated cancer patients.* Cancer Chemother Pharmacol, 2009. **64**(3): p. 509-16.
134. Kostin, A., D. Stenberg, and T. Porkka-Heiskanen, *Nitric oxide modulates the discharge rate of basal forebrain neurones: a study in freely moving rats.* J Sleep Res, 2009. **18**(4): p. 447-53.
135. Neugebauer, F., V. Korz, and J.U. Frey, *Modulation of extracellular monoamine transmitter concentrations in the hippocampus after weak and strong tetanization of the perforant path in freely moving rats.* Brain Res, 2009. **1273**: p. 29-38.
136. Bito, L., et al., *The concentrations of free amino acids and other electrolytes in cerebrospinal fluid, in vivo dialysate of brain, and blood plasma of the dog.* J Neurochem, 1966. **13**(11): p. 1057-67.
137. Ungerstedt, U. and A. Hallstrom, *In vivo microdialysis--a new approach to the analysis of neurotransmitters in the brain.* Life Sci, 1987. **41**(7): p. 861-4.
138. Lindefors, N., E. Brodin, and U. Ungerstedt, *Microdialysis combined with a sensitive radioimmunoassay. A technique for studying in vivo release of neuropeptides.* J Pharmacol Methods, 1987. **17**(4): p. 305-12.
139. Brodin, E., et al., *In vivo release of substance P in cat dorsal horn studied with microdialysis.* Neurosci Lett, 1987. **76**(3): p. 357-62.
140. Guihen, E. and W.T. O'Connor, *Current separation and detection methods in microdialysis the drive towards sensitivity and speed.* Electrophoresis, 2009. **30**(12): p. 2062-75.
141. Ao, X. and J.A. Stenken, *Water-soluble cyclodextrin polymers for enhanced relative recovery of hydrophobic analytes during microdialysis sampling.* Analyst, 2003. **128**(9): p. 1143-9.
142. Chaurasia, C.S., et al., *AAPS-FDA workshop white paper: microdialysis principles, application and regulatory perspectives.* Pharm Res, 2007. **24**(5): p. 1014-25.
143. Tisdall, M.M. and M. Smith, *Cerebral microdialysis: research technique or clinical tool.* Br J Anaesth, 2006. **97**(1): p. 18-25.
144. Carneheim, C. and L. Stahle, *Microdialysis of lipophilic compounds: a methodological study.* Pharmacol Toxicol, 1991. **69**(5): p. 378-80.
145. Kjellstrom, S., et al., *On-line coupling of microdialysis sampling with liquid chromatography for the determination of peptide and non-peptide leukotrienes.* J Chromatogr A, 1998. **823**(1-2): p. 489-96.
146. Araujo, B.V., et al., *Microdialysis as a tool to determine free kidney levels of voriconazole in rodents: a model to study the technique feasibility for a moderately lipophilic drug.* J Pharm Biomed Anal, 2008. **47**(4-5): p. 876-81.
147. Schuck, V.J., I. Rinas, and H. Derendorf, *In vitro microdialysis sampling of docetaxel.* J Pharm Biomed Anal, 2004. **36**(4): p. 807-13.
148. Stahle, L., *Drug distribution studies with microdialysis: I. Tissue dependent difference in recovery between caffeine and theophylline.* Life Sci, 1991. **49**(24): p. 1835-42.

149. Chaurasia, C.S., *In vivo microdialysis sampling: theory and applications.* Biomed Chromatogr, 1999. **13**(5): p. 317-32.
150. Smith, A.D. and J.B. Justice, *The effect of inhibition of synthesis, release, metabolism and uptake on the microdialysis extraction fraction of dopamine.* J Neurosci Methods, 1994. **54**(1): p. 75-82.
151. Le Quellec, A., et al., *Microdialysis probes calibration: gradient and tissue dependent changes in no net flux and reverse dialysis methods.* J Pharmacol Toxicol Methods, 1995. **33**(1): p. 11-6.
152. Khramov, A.N. and J.A. Stenken, *Enhanced microdialysis recovery of some tricyclic antidepressants and structurally related drugs by cyclodextrin-mediated transport.* Analyst, 1999. **124**(7): p. 1027-33.
153. Sun, L. and J.A. Stenken, *Improving microdialysis extraction efficiency of lipophilic eicosanoids.* J Pharm Biomed Anal, 2003. **33**(5): p. 1059-71.
154. Kurosaki, Y., et al., *Lipo-microdialysis: a new microdialysis method for studying the pharmacokinetics of lipophilic substances.* Biol Pharm Bull, 1998. **21**(2): p. 194-6.
155. Khramov, A.N. and J.A. Stenken, *Enhanced Microdialysis Extraction Efficiency of Ibuprofen in Vitro by Facilitated Transport with beta-Cyclodextrin.* Anal Chem, 1999. **71**(7): p. 1257-64.
156. Elmeliegy, M.A., et al., *Role of ATP-Binding Cassette and Solute Carrier Transporters in Erlotinib CNS Penetration and Intracellular Accumulation.* Clin Cancer Res, 2011. **17**(1): p. 89-99.
157. Loos, W.J., et al., *Pitfalls of the application of microdialysis in clinical oncology: controversial findings with docetaxel.* J Pharm Biomed Anal, 2007. **45**(2): p. 288-94.
158. May, M., et al., *Enhanced human tissue microdialysis using hydroxypropyl-ss-cyclodextrin as molecular carrier.* PLoS One, 2013. **8**(4): p. e60628.
159. Hamrin, K., et al., *Microdialysis in human skeletal muscle: effects of adding a colloid to the perfusate.* J Appl Physiol, 2002. **92**(1): p. 385-93.
160. Rosdahl, H., U. Ungerstedt, and J. Henriksson, *Microdialysis in human skeletal muscle and adipose tissue at low flow rates is possible if dextran-70 is added to prevent loss of perfusion fluid.* Acta Physiol Scand, 1997. **159**(3): p. 261-2.
161. Dahlin, A.P., et al., *Methodological aspects on microdialysis protein sampling and quantification in biological fluids: an in vitro study on human ventricular CSF.* Anal Chem, 2010. **82**(11): p. 4376-85.
162. Whitaker, G. and C.E. Lunte, *Investigation of microdialysis sampling calibration approaches for lipophilic analytes: doxorubicin.* J Pharm Biomed Anal, 2010. **53**(3): p. 490-6.
163. Wang, Y. and D.F. Welty, *The simultaneous estimation of the influx and efflux blood-brain barrier permeabilities of gabapentin using a microdialysis-pharmacokinetic approach.* Pharm Res, 1996. **13**(3): p. 398-403.
164. Zamboni, W.C., et al., *Inter- and intratumoral disposition of platinum in solid tumors after administration of cisplatin.* Clin Cancer Res, 2002. **8**(9): p. 2992-9.
165. Zamboni, W.C., et al., *Relationship between tumor extracellular fluid exposure to topotecan and tumor response in human neuroblastoma xenograft and cell lines.* Cancer Chemother Pharmacol, 1999. **43**(4): p. 269-76.
166. Sziraki, I., et al., *The Use of Microdialysis Techniques in Mice to Study P-gp Function at the Blood-Brain Barrier.* J Biomol Screen, 2012.
167. Langer, R. and J. Folkman, *Polymers for the sustained release of proteins and other macromolecules.* Nature, 1976. **263**(5580): p. 797-800.
168. Pui, C.H., et al., *Challenging issues in pediatric oncology.* Nat Rev Clin Oncol, 2011. **8**(9): p. 540-9.
169. Orentas, R.J., D.W. Lee, and C. Mackall, *Immunotherapy targets in pediatric cancer.* Front Oncol, 2012. **2**: p. 3.
170. Khuong-Quang, D.A., et al., *K27M mutation in histone H3.3 defines clinically and biologically distinct subgroups of pediatric diffuse intrinsic pontine gliomas.* Acta Neuropathol, 2012. **124**(3): p. 439-47.
171. Pharmacia and Upjohn Company, P., Inc. , *http://labeling.pfizer.com/ShowLabeling.aspx?id=533*.
172. Zhang, Z. and S.S. Feng, *The drug encapsulation efficiency, in vitro drug release, cellular uptake and cytotoxicity of paclitaxel-loaded poly(lactide)-tocopheryl polyethylene glycol succinate nanoparticles.* Biomaterials, 2006. **27**(21): p. 4025-33.
173. Kim, S.H., et al., *Target-specific cellular uptake of PLGA nanoparticles coated with poly(L-lysine)-poly(ethylene glycol)-folate conjugate.* Langmuir, 2005. **21**(19): p. 8852-7.

174. Bharali, D.J., et al., *Novel nanoparticles for the delivery of recombinant hepatitis B vaccine.* Nanomedicine, 2008. **4**(4): p. 311-7.
175. Kunii, R., H. Onishi, and Y. Machida, *Preparation and antitumor characteristics of PLA/(PEG-PPG-PEG) nanoparticles loaded with camptothecin.* Eur J Pharm Biopharm, 2007. **67**(1): p. 9-17.
176. Ebrahimnejad, P., et al., *Preparation and in vitro evaluation of actively targetable nanoparticles for SN-38 delivery against HT-29 cell lines.* Nanomedicine, 2010. **6**(3): p. 478-85.
177. Matsumura, Y. and H. Maeda, *A new concept for macromolecular therapeutics in cancer chemotherapy: mechanism of tumoritropic accumulation of proteins and the antitumor agent smancs.* Cancer Res, 1986. **46**(12 Pt 1): p. 6387-92.
178. Ebrahimnejad, P., et al., *Characterization, blood profile and biodistribution properties of surface modified PLGA nanoparticles of SN-38.* Int J Pharm, 2011. **406**(1-2): p. 122-7.
179. Maeda, H., et al., *Tumor vascular permeability and the EPR effect in macromolecular therapeutics: a review.* J Control Release, 2000. **65**(1-2): p. 271-84.
180. Holback, H. and Y. Yeo, *Intratumoral drug delivery with nanoparticulate carriers.* Pharm Res, 2011. **28**(8): p. 1819-30.
181. Gradishar, W.J., et al., *Phase III trial of nanoparticle albumin-bound paclitaxel compared with polyethylated castor oil-based paclitaxel in women with breast cancer.* J Clin Oncol, 2005. **23**(31): p. 7794-803.
182. Sasaki, Y., et al., *Phase II trial of nanoparticle albumin-bound paclitaxel as second-line chemotherapy for unresectable or recurrent gastric cancer.* Cancer Sci, 2014. **105**(7): p. 812-7.
183. Von Hoff, D.D., et al., *Increased survival in pancreatic cancer with nab-paclitaxel plus gemcitabine.* N Engl J Med, 2013. **369**(18): p. 1691-703.
184. Zhang, L., et al., *Nab-paclitaxel is an active drug in preclinical model of pediatric solid tumors.* Clin Cancer Res, 2013. **19**(21): p. 5972-83.
185. Houghton, P.J., et al., *Initial testing (stage 1) of the tubulin binding agent nanoparticle albumin-bound (nab) paclitaxel (Abraxane((R))) by the Pediatric Preclinical Testing Program (PPTP).* Pediatr Blood Cancer, 2015. **62**(7): p. 1214-21.
186. Wagner, L.M., et al., *Preclinical evaluation of nanoparticle albumin-bound paclitaxel for treatment of pediatric bone sarcoma.* Pediatr Blood Cancer, 2014. **61**(11): p. 2096-8.
187. Corporation, C., *To Find a Safe Dose and Show Early Clinical Activity of Weekly Nab-paclitaxel in Pediatric Patients With Recurrent/ Refractory Solid Tumors. Bethesda (MD): National Library of Medicine (US). 2000 - [Last accessed on 2016 Feb 18]. Available from: https://clinicaltrials.gov/ct2/show/NCT01962103 Identifier : NCT01962103.*
188. (NCI), C.s.O.G.N.C.I., *Combination Chemotherapy in Treating Young Patients With Recurrent or Resistant Malignant Germ Cell Tumors. Bethesda (MD): National Library of Medicine (US). 2000 - [Last accessed on 2016 Feb 18]. Available from: https://clinicaltrials.gov/ct2/show/study/NCT00467051 Identifier : NCT00467051.*
189. Muggia, F.M., et al., *Phase II study of liposomal doxorubicin in refractory ovarian cancer: antitumor activity and toxicity modification by liposomal encapsulation.* J Clin Oncol, 1997. **15**(3): p. 987-93.
190. Munoz, A., et al., *Pegylated liposomal doxorubicin hydrochloride (PLD) for advanced sarcomas in children: preliminary results.* Pediatr Blood Cancer, 2004. **43**(2): p. 152-5.
191. Chidiac, T., et al., *Phase II trial of liposomal doxorubicin (Doxil) in advanced soft tissue sarcomas.* Invest New Drugs, 2000. **18**(3): p. 253-9.
192. Hsieh, P.C., et al., *Local controlled intramyocardial delivery of platelet-derived growth factor improves postinfarction ventricular function without pulmonary toxicity.* Circulation, 2006. **114**(7): p. 637-44.
193. Seong, H., et al., *BCNU-loaded poly(D, L-lactide-co-glycolide) wafer and antitumor activity against XF-498 human CNS tumor cells in vitro.* Int J Pharm, 2003. **251**(1-2): p. 1-12.
194. Xie, J. and C.H. Wang, *Electrospun micro- and nanofibers for sustained delivery of paclitaxel to treat C6 glioma in vitro.* Pharm Res, 2006. **23**(8): p. 1817-26.
195. Xu, X., et al., *BCNU-loaded PEG-PLLA ultrafine fibers and their in vitro antitumor activity against Glioma C6 cells.* J Control Release, 2006. **114**(3): p. 307-16.
196. Liu, R., et al., *Prevention of local tumor recurrence following surgery using low-dose chemotherapeutic polymer films.* Ann Surg Oncol, 2010. **17**(4): p. 1203-13.
197. Liu, R., et al., *Paclitaxel-eluting polymer film reduces locoregional recurrence and improves survival in a recurrent sarcoma model: a novel investigational therapy.* Ann Surg Oncol, 2012. **19**(1): p. 199-206.

198. Wolinsky, J.B., et al., *Prevention of in vivo lung tumor growth by prolonged local delivery of hydroxycamptothecin using poly(ester-carbonate)-collagen composites.* J Control Release, 2010. **144**(3): p. 280-7.
199. Meinel, A.J., et al., *Electrospun matrices for localized drug delivery: current technologies and selected biomedical applications.* Eur J Pharm Biopharm, 2012. **81**(1): p. 1-13.
200. Heldin, C.H., et al., *High interstitial fluid pressure - an obstacle in cancer therapy.* Nat Rev Cancer, 2004. **4**(10): p. 806-13.
201. Carmeliet, P., *Angiogenesis in life, disease and medicine.* Nature, 2005. **438**(7070): p. 932-6.
202. Metz, M.Z., et al., *Neural stem cell-mediated delivery of irinotecan-activating carboxylesterases to glioma: implications for clinical use.* Stem Cells Transl Med, 2013. **2**(12): p. 983-92.
203. Dodds, H.M., et al., *The importance of tumor glucuronidase in the activation of irinotecan in a mouse xenograft model.* J Pharmacol Exp Ther, 2002. **303**(2): p. 649-55.
204. Hirayama, F. and K. Uekama, *Cyclodextrin-based controlled drug release system.* Adv Drug Deliv Rev, 1999. **36**(1): p. 125-141.
205. Rich, B.S., et al., *Local control, survival, and operative morbidity and mortality after re-resection, and intraoperative radiation therapy for recurrent or persistent primary high-risk neuroblastoma.* J Pediatr Surg, 2011. **46**(1): p. 97-102.
206. Rodriguez-Galindo, C., et al., *Prognostic factors for local and distant control in Ewing sarcoma family of tumors.* Ann Oncol, 2008. **19**(4): p. 814-20.
207. Mazzoleni, S., et al., *Outcomes and prognostic factors after recurrence in children and adolescents with nonmetastatic rhabdomyosarcoma.* Cancer, 2005. **104**(1): p. 183-90.
208. Kumar, S., *Second malignant neoplasms following radiotherapy.* Int J Environ Res Public Health, 2012. **9**(12): p. 4744-59.
209. Arifin, D.Y., et al., *Role of convective flow in carmustine delivery to a brain tumor.* Pharm Res, 2009. **26**(10): p. 2289-302.
210. Ranganath, S.H. and C.H. Wang, *Biodegradable microfiber implants delivering paclitaxel for post-surgical chemotherapy against malignant glioma.* Biomaterials, 2008. **29**(20): p. 2996-3003.
211. Zong, S., et al., *The use of cisplatin-loaded mucoadhesive nanofibers for local chemotherapy of cervical cancers in mice.* Eur J Pharm Biopharm, 2015. **93**: p. 127-35.
212. Fung, L.K., et al., *Pharmacokinetics of interstitial delivery of carmustine, 4-hydroperoxycyclophosphamide, and paclitaxel from a biodegradable polymer implant in the monkey brain.* Cancer Res, 1998. **58**(4): p. 672-84.
213. Ranganath, S.H., et al., *The use of submicron/nanoscale PLGA implants to deliver paclitaxel with enhanced pharmacokinetics and therapeutic efficacy in intracranial glioblastoma in mice.* Biomaterials, 2010. **31**(19): p. 5199-207.
214. Carcaboso, A.M., et al., *Topotecan vitreous levels after periocular or intravenous delivery in rabbits: an alternative for retinoblastoma chemotherapy.* Invest Ophthalmol Vis Sci, 2007. **48**(8): p. 3761-7.
215. Zhang, R., et al., *Convection-enhanced delivery of SN-38-loaded polymeric micelles (NK012) enables consistent distribution of SN-38 and is effective against rodent intracranial brain tumor models.* Drug Deliv, 2015: p. 1-7.
216. Yanagihara, K., et al., *Marked antitumor effect of NK012, a SN-38-incorporating micelle formulation, in a newly developed mouse model of liver metastasis resulting from gastric cancer.* Ther Deliv, 2014. **5**(2): p. 129-38.
217. Takahashi, A., et al., *Detailed distribution of NK012, an SN-38-incorporating micelle, in the liver and its potent antitumor effects in mice bearing liver metastases.* Clin Cancer Res, 2010. **16**(19): p. 4822-31.
218. Alferiev, I.S., et al., *Nanoparticle-mediated delivery of a rapidly activatable prodrug of SN-38 for neuroblastoma therapy.* Biomaterials, 2015. **51**: p. 22-9.
219. Iyer, R., et al., *Nanoparticle delivery of an SN38 conjugate is more effective than irinotecan in a mouse model of neuroblastoma.* Cancer Lett, 2015. **360**(2): p. 205-12.
220. Shochat, S.J., A.B. Abt, and C.L. Schengrund, *VCN-releasable sialic acid and gangliosides in human neuroblastomas.* J Pediatr Surg, 1977. **12**(3): p. 413-8.
221. Kailayangiri, S., et al., *The ganglioside antigen G(D2) is surface-expressed in Ewing sarcoma and allows for MHC-independent immune targeting.* Br J Cancer, 2012. **106**(6): p. 1123-33.
222. Portoukalian, J., et al., *Shedding of GD2 ganglioside in patients with retinoblastoma.* Int J Cancer, 1993. **53**(6): p. 948-51.
223. Chang, H.R., et al., *Expression of disialogangliosides GD2 and GD3 on human soft tissue sarcomas.* Cancer, 1992. **70**(3): p. 633-8.

224. Heiner, J.P., et al., *Localization of GD2-specific monoclonal antibody 3F8 in human osteosarcoma.* Cancer Res, 1987. **47**(20): p. 5377-81.
225. Modak, S., W. Gerald, and N.K. Cheung, *Disialoganglioside GD2 and a novel tumor antigen: potential targets for immunotherapy of desmoplastic small round cell tumor.* Med Pediatr Oncol, 2002. **39**(6): p. 547-51.
226. Grant, S.C., et al., *Targeting of small-cell lung cancer using the anti-GD2 ganglioside monoclonal antibody 3F8: a pilot trial.* Eur J Nucl Med, 1996. **23**(2): p. 145-9.
227. Hamilton, W.B., et al., *Ganglioside expression on human malignant melanoma assessed by quantitative immune thin-layer chromatography.* Int J Cancer, 1993. **53**(4): p. 566-73.
228. Tsuchida, T., et al., *Gangliosides of human melanoma.* Cancer, 1989. **63**(6): p. 1166-74.
229. Lammie, G., et al., *Ganglioside gd(2) expression in the human nervous-system and in neuroblastomas - an immunohistochemical study.* Int J Oncol, 1993. **3**(5): p. 909-15.